

Fall 2000

An Ameliorated Prediction of the Empennage In-Flight Gust Loads for a General Aviation Aircraft

Philippe Marchand

Embry-Riddle Aeronautical University - Daytona Beach

Follow this and additional works at: <https://commons.erau.edu/db-theses>



Part of the [Aerospace Engineering Commons](#)

Scholarly Commons Citation

Marchand, Philippe, "An Ameliorated Prediction of the Empennage In-Flight Gust Loads for a General Aviation Aircraft" (2000). *Theses - Daytona Beach*. 261.

<https://commons.erau.edu/db-theses/261>

This thesis is brought to you for free and open access by Embry-Riddle Aeronautical University – Daytona Beach at ERAU Scholarly Commons. It has been accepted for inclusion in the Theses - Daytona Beach collection by an authorized administrator of ERAU Scholarly Commons. For more information, please contact commons@erau.edu.

**AN AMELIORATED PREDICTION
OF THE EMPENNAGE
IN-FLIGHT GUST LOADS
FOR A GENERAL AVIATION
AIRCRAFT**

By

Philippe MARCHAND

**A Thesis Submitted to the Graduate Studies Office
in Partial Fulfillment of the Requirements for the Degree of
Master of Science in Aerospace Engineering**

Embry-Riddle Aeronautical University

Daytona Beach, Florida

Fall 2000

UMI Number: EP31933

INFORMATION TO USERS

The quality of this reproduction is dependent upon the quality of the copy submitted. Broken or indistinct print, colored or poor quality illustrations and photographs, print bleed-through, substandard margins, and improper alignment can adversely affect reproduction.

In the unlikely event that the author did not send a complete manuscript and there are missing pages, these will be noted. Also, if unauthorized copyright material had to be removed, a note will indicate the deletion.

UMI[®]

UMI Microform EP31933
Copyright 2011 by ProQuest LLC
All rights reserved. This microform edition is protected against
unauthorized copying under Title 17, United States Code.

ProQuest LLC
789 East Eisenhower Parkway
P.O. Box 1346
Ann Arbor, MI 48106-1346

AN AMELIORATED PREDICTION OF THE EMPENNAGE IN-FLIGHT GUST LOADS FOR A GENERAL AVIATION AIRCRAFT

by

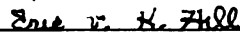
Philippe Marchand

This Thesis was prepared under the direction of the candidate's thesis committee chairman, Dr. David Kim, Department of Aerospace Engineering, and has been approved by the members of this thesis committee. It was submitted to the Office Graduate of Studies and was accepted in partial fulfillment of the requirements for the degree of Master of Science in Aerospace Engineering.

THESIS COMMITTEE:



Dr. David Kim
Chairman



Dr. Eric v. K. Hill
Member



Dr. Frank J. Radosta
Member



Dr Habib Eslami
Graduate Program Coordinator,
Aerospace Engineering

12/05/2000
Date

ACKNOWLEDGEMENTS

I would like to take the opportunity to thank the individuals who contributed in making this thesis a reality. Their unconditional help and dedication allowed me to complete this research within the established period.

I express my greatest appreciation to my thesis committee chairman, Dr. David Kim, whose critical feedbacks and assistance were crucial for the successful outcome of this thesis. I would like to express my appreciation to the contributions made by my thesis committee members Dr. Eric Hill and Dr. Frank Radosta. I am especially thankful to Mr. Maciej Marciniak whose previous studies established the guidelines for this research. A special thanks to the maintenance department for its help in keeping the airplane airworthy and making all the necessary repairs.

I would also like to thank EPF (French Engineer School) and Embry-Riddle Aeronautical University for having offered me the possibility of studying at ERAU through the Bachelor and the Master of Science in Aerospace Engineering.

This statement would be incomplete without expressing my sincere appreciation and gratitude to both my parents and my girlfriend Delphine for their faith, understanding, efforts and guidance during this challenging past year.

ABSTRACT

Author: Philippe Marchand
Title: An Ameliorated Prediction of the Empennage In-Flight Gust Loads for a General Aviation Aircraft
Institution: Embry-Riddle Aeronautical University
Degree: Master of Science in Aerospace Engineering
Year: 2000

Airplanes often operate beyond their original design load profiles. Aviation opens so many new possibilities and wide variety of possible activities that it is hard for designers to foresee all loading spectra that the airplane structure will experience throughout its life. Nevertheless, the aircraft structures are required to be designed to fail-safe or safe-life criteria to be certified by the FAA. AFS-120 provides a database of normal accelerations that can be used to derive airplane wing loads. ACE-100 describes an acceptable method for determining the fatigue life of an empennage based on the same normal acceleration data provided in AFS-120. However, this data have not been demonstrated to be applicable for empennage loads.

Earlier works have shown that maneuver induced-loads on the empennage can be predicted from motion parameters measured near the airplane center of gravity. Maneuver loads are pilot induced and do not account for weather related loads. During flight, the airplane is subjected to atmospheric turbulence and a method for determining empennage gust loads is desired. Embry-Riddle, with financial support from the FAA, has flight-tested a C-172P equipped with sensors to develop an ameliorated prediction of the empennage in-flight gust loads for a general aviation aircraft using Neural Networks. Both the power spectral density and the FAA 'two-second' methods have been applied to separate maneuvers and gusts. Findings were unexpected in that for this airplane, aircraft rotational motion appears to dampen empennage gust loads considerably and for the conditions tested, gust loads were not as significant as maneuver loads.

TABLE OF CONTENTS

ACKNOWLEDGEMENTS	iii
ABSTRACT	iv
TABLE OF CONTENTS	v
LIST OF TABLES	viii
LIST OF FIGURES	ix
NOTATIONS	xii
Chapter	
I. INTRODUCTION	1
1.1 OVERVIEW	1
1.2 PREVIOUS RESEARCH	3
1.3 CURRENT APPROACH.....	6
II. BACKGROUND THEORY	8
2.1 AERODYNAMIC LOADING	8
2.1.1 Introduction.....	8
2.1.2 Mechanism of Gust Loads Generation	8
2.1.2.a Vertical and Lateral Gust:.....	9
2.1.2.b Head-on Gust:.....	11
2.1.2.c Effect of Airplane Motions:	12
2.1.3 Characteristics of Turbulence	14
2.1.3.a Gust Profile	14
2.2 DISCRETE-GUST STATIC LOADS	16
2.2.1 Gust Idealization	16
2.2.2 FAR Static Gust Requirement	16
2.2.3 FAR Gust Load Formula	17
2.2.4 Effect of Static Aeroelastic Deformation on $C_{L\alpha}$	19

2.3	STRESSES AND STRAINS ACTING ON AN AIRCRAFT	20
2.4	POWER SPECTRAL DENSITY (PSD)	21
2.5	NEURAL NETWORKS FUNDAMENTALS	23
2.5.1	Neural Networks Description	24
2.5.2	Network Operation.....	27
2.5.3	Back-Propagation Network.....	28
2.5.3.a	Architecture:.....	29
2.5.3.b	Choices.....	30
2.5.3.c	Learning Algorithm:.....	33
2.5.3.d	Transfer Function.....	36
III.	FLIGHT TESTING	37
3.1	EXPERIMENTAL APPARATUS.....	37
3.1.1	Sensors and Accelerometers	37
3.1.2	Data Collection	42
3.1.2.a	Data Acquisition System.....	42
3.1.2.b	Testing Procedure	44
3.1.2.c	Testing Locations.....	44
IV.	POSTPROCESSING OF DATA	46
4.1	DADiSP	46
4.2	FLISEG.....	49
4.2.1	Theory	49
4.2.2	Exceedance Curves Plot - Cycle Counting.....	51
4.2.3	Fliseg Methodology for gust discrimination.....	52
4.3	Gust Discrimination.....	53
4.3.1	Smooth Air Time Domain Data.....	54
4.3.2	Smooth Air PSD Data.....	57
4.3.3	Time Domain for Gusty Conditions in the z-direction (Vertical Gust)..	60
4.3.4	PSD for Gusty Conditions in the z-direction (Vertical Gust).....	63
4.3.5	Time Domain for Gusty Conditions in the y-direction (Lateral Gust) ..	66
4.3.6	PSD for Gusty Conditions in the y-direction (Lateral Gust)	69
4.3.7	Time Domain for Maneuver Data.....	72

4.3.8	PSD for Maneuver Data.....	75
4.3.9	Gust Main Frequency Range	78
4.3.9.a	In the z-direction (Vertical Gust).....	78
4.3.9.b	In the y-direction (Lateral Gust).....	78
V.	NEURAL NETWORKS PROCEDURE	80
5.1	CHOICE OF THE NEURAL NETWORKS	80
5.2	NEURAL NETWORKS SETUP	82
5.2.1	Neural Networks Parameters	83
VI.	ANALYSIS OF RESULTS.....	85
6.1	PRELIMINARIES	85
6.1.1	Insignificant Stress Region and Tolerance Band.....	85
6.1.2	Strain and Stress Calculations.....	87
6.2	CURRENT RESEARCH RESULTS.....	91
6.2.1	Neural Networks Trained and Tested with the PSD Data	91
6.2.1.a	NN First Attempt: EDBD Rule and 5 PE.....	91
6.2.1.b	NN Second Attempt: Data Rescale.....	91
6.2.1.c	NN Third Attempt: Convergence Criterion Optimization	91
6.2.1.d	NN Fourth Attempt: Change in the Number of PE.....	92
6.2.1.e	NN Fifth Attempt: Change in Learning Rule.....	92
6.2.1.f	NN Sixth Attempt: Change in Learning Coefficients	92
6.2.2	Neural Networks Trained and Tested with the Time Data	93
6.2.3	Neural Networks Trained with the Maneuver Files.....	93
VII.	CONCLUSION AND RECOMMENDATIONS	95
7.1	IMPROVEMENT OF THE PREDICTIONS	95
7.2	LOW CORRELATION EXPLANATION	95
7.2.1	PSD vs. Time Domain	96
7.2.2	Fliseg Discrimination.....	97
7.3	RECOMMENDATIONS.....	98
	REFERENCES	99

LIST OF TABLES

Table 1.	Instruments Installed on-board the Testbed C-172.....	38
Table 2.	Maximum and Minimum Strain in $\mu\epsilon$ for Different Flight Conditions.....	89

LIST OF FIGURES

Figure 1. Vertical Gust Velocity [14].....	9
Figure 2. Head-on Gust Velocity [14].....	11
Figure 3. Gust Profile	14
Figure 4. Representation of an Idealized Gust	16
Figure 5. Gust Velocity and Airplane Vertical Velocity.....	17
Figure 6. Representation of a Processing Element.....	25
Figure 7. Architecture of a Network	26
Figure 8. Three-Layer Back Propagation Neural Network.....	30
Figure 9. A Single Neural Network Processing Element in Layer h	33
Figure 10. Instrumentation Setup on Board the Aircraft.....	39
Figure 11. Tail Accelerometers Location.....	40
Figure 12. Type of Strain Gages Mounted in the Aircraft	40
Figure 13. Running Wires Through the Back of the Airplane	40
Figure 14. Wires Through the Bulkhead.....	41
Figure 15. Centerline Gages.....	41
Figure 16. Daqbook 216 Diagram.....	42
Figure 17. Power Spectrum Density Analysis of the CG NZ Signal	48
Figure 18. Smooth Air Horizontal Tail Strain Gage Time Domain.....	54
Figure 19. Smooth Air CGNZ Accelerometer Time Domain.....	54
Figure 20. Smooth Air Horizontal Tail Accelerometer Time Domain	55
Figure 21. Smooth Air Vertical Tail Strain Gage Time Domain.....	55
Figure 22. Smooth Air CG NY Accelerometer Time Domain.....	56
Figure 23. Smooth Air Vertical Tail Accelerometer Time Domain.....	56
Figure 24. Smooth Air Horizontal Tail Strain Gage PSD.....	57
Figure 25. Smooth Air CG NZ Accelerometer PSD.....	57

Figure 26. Smooth Air Horizontal Tail Accelerometer PSD	58
Figure 27. Smooth Air Vertical Tail Strain Gage PSD	58
Figure 28. Smooth Air CG NY Accelerometer PSD.....	59
Figure 29. Smooth Air Vertical Tail Accelerometer PSD.....	59
Figure 30. Z-Gust Horizontal Tail Strain Gage Time Domain	60
Figure 31. Z-Gust CGNZ Accelerometer Time Domain	60
Figure 32. Z-Gust Horizontal Tail Accelerometer Time Domain.....	61
Figure 33. Z-Gust Vertical Tail Strain Gage Time Domain.....	61
Figure 34. Z-Gust CG NY Accelerometer Time Domain.....	62
Figure 35. Z-Gust Vertical Tail Accelerometer Time Domain.....	62
Figure 36. Z-Gust Horizontal Tail Strain Gage PSD	63
Figure 37. Z-Gust CG NZ Accelerometer PSD	63
Figure 38. Z-Gust Horizontal Tail Accelerometer PSD.....	64
Figure 39. Z-Gust Vertical Tail Strain Gage PSD.....	64
Figure 40. Z-Gust CG NY Accelerometer PSD.....	65
Figure 41. Z-Gust Vertical Tail Accelerometer PSD.....	65
Figure 42. Y-Gust Horizontal Tail Strain Gage Time Domain.....	66
Figure 43. Y-Gust CG NZ Accelerometer Time Domain.....	66
Figure 44. Y-Gust Horizontal Tail Accelerometer Time Domain	67
Figure 45. Y-Gust Vertical Tail Strain Gage Time Domain.....	67
Figure 46. Y-Gust CG NY Accelerometer Time Domain.....	68
Figure 47. Y-Gust Vertical Tail Accelerometer Time Domain.....	68
Figure 48. Y-Gust Horizontal Tail Strain Gage PSD.....	69
Figure 49. Y-Gust CG NZ Accelerometer PSD.....	69
Figure 50. Y-Gust Horizontal Tail Accelerometer PSD	70
Figure 51. Y-Gust Vertical Tail Strain Gage PSD	70
Figure 52. Y-Gust CG NY Accelerometer PSD.....	71
Figure 53. Y-Gust Vertical Tail Accelerometer PSD.....	71
Figure 54. Maneuver Horizontal Tail Strain Gage Time Domain	72
Figure 55. Maneuver CG NZ Accelerometer Time Domain.....	72
Figure 56. Maneuver Horizontal Tail Accelerometer Time Domain.....	73

Figure 57. Maneuver Vertical Tail Strain Gage Time Domain.....	73
Figure 58. Maneuver CG NY Accelerometer Time Domain.....	74
Figure 59. Maneuver Vertical Tail Accelerometer Time Domain.....	74
Figure 60. Maneuver Horizontal Tail Strain Gage PSD	75
Figure 61. Maneuver CG NZ Accelerometer PSD.....	75
Figure 62. Maneuver Horizontal Tail Accelerometer PSD.....	76
Figure 63. Maneuver Vertical Tail Strain Gage PSD.....	76
Figure 64. Maneuver CG NY Accelerometer PSD	77
Figure 65. Maneuver Vertical Tail Accelerometer PSD.....	77
Figure 66. S-N Curve of an AL2024-T3 Aluminum Sheet [28]	86
Figure 67. Tolerance Band and Insignificant Region.....	87

NOTATIONS

V = Airplane forward speed

$\frac{\rho}{2} \times V^2$ = Dynamic pressure

S = Reference wing area

$C_{l\alpha}$ = Lift curve slope (per rad)

$\Delta\alpha$ = Change in angle of attack due to gust

U = Gust speed

C_L = Lift coefficient

Δn = Incremental load factor

K_g = Factor to account for airplane motion and lag in buildup of lift

U_{de} = Derived equivalent gust velocity, fps

V_e = Airplane equivalent airspeed, knots

W = Airplane weight

μ_g = Airplane mass parameter

ρ = Air density

\bar{c} = Wing mean geometric chord

g = Acceleration due to gravity

E = Young modulus of Aluminum, $10 \times (10^6)$ p.s.i.

σ = Stress (p.s.i.)

ϵ = Strain ($\mu\epsilon$)

CHAPTER 1

INTRODUCTION

1.1 OVERVIEW

Both fatigue evaluation and detection has become an important safety consideration in aeronautics. Fatigue has been with aviation since the first flight of the Wright flyer in 1903. Since then, our knowledge and understanding of the fatigue phenomenon have greatly improved in such a way that now, we are able to design and build reliable structures. However, Federal Aviation Regulations (FARs) require that structural components critical to the safe operation of an aircraft must not fail within their expected life times due to damage caused by the repeated loads typical to daily operations. Consequently, knowledge of the types of loading acting on the structure is required.

The wing and empennage are the most critical structures during a flight. Fatigue life is determined using the Palmgren-Miner linear cumulative damage theory. However, this method requires the knowledge of the loading history or spectra of the aircraft, which is, nowadays, not always available.

The NASA VGH (velocity, load factor, altitude) program, which was one of the largest and longest running in-flight load monitoring program for General Aviation aircraft, permitted collection of information on flight loads (normal acceleration near aircraft center of gravity: CG NZ) and lead to a report that is still being used to determine the fatigue life of airplane wings [1]. Other research evaluated the fatigue life of vertical

aerodynamic surfaces such as fins, rudders or winglets [2] without establishing a correlation between the loads of the empennage and the CG accelerometers. But as far as only accelerations near the Center of Gravity (C.G.) were measured, the empennage structure fatigue loads stayed unexplored. A method to determine the empennage loads is consequently needed.

There is a wide range of aircraft operations, activities and usage such as flight training, aerobatics, commercial, agricultural, and others that result in significantly different fatigue design load spectra. Furthermore, the load history for a given aircraft often varies substantially from what was expected initially. An accumulated fatigue damage monitoring system would allow establishing a maintenance schedule more appropriate for each aircraft. The owner or operator would then keep records of the fatigue load spectra and the flight profile information of the aircraft. Technicians could use this database to better estimate loads and they could modify and improve their design to ensure airworthiness throughout the airframe life. This may provide significant economic advantages and improved safety for the owner, operator and the industry.

In order for General Aviation aircraft owners to be interested in such a system, it must be inexpensive, easy to install and maintain, and must not interfere with the normal operation of the airplane. The use of strain gages is consequently not recommended because of installation difficulties and associated costs. A better way to collect data would be to use a system similar to the NASA VGH recorder but one that is more robust and versatile that would provide loads on both the aircraft wing and empennage structure.

Previous research has demonstrated that from a load spectra database (load induced by maneuvers), an in-flight load monitoring method could be used to keep track of accumulated damage of an airframe [10 and 20]. Subsequently, a similar methodology to predict the fatigue induced by gust loads on the empennage structure is needed. Then, an empennage in-flight load database could be created, and a database of fatigue load spectra would be available and helpful in determining the entire aircraft fatigue life using the Palmgren-Miner linear cumulative damage theory thereby increasing aircraft safety.

1.2 PREVIOUS RESEARCH

Gust loads as well as maneuver loads, are of a stochastic nature. Their magnitude and frequency can only be predicted in a probabilistic sense. A relatively large amount of statistical data concerning vertical gusts is available in the format of CG vertical acceleration data (Δn_z) obtained during routine airline operations [3]. In 1962, at the request of the Federal Aviation Administration (FAA), and upon recommendation of the NASA Committee on Aircraft Operating Problems, the NASA VGH General Aviation Program was established. The purpose of this program was to define the gust and maneuver loads, airspeed practices, and altitude usage of General Aviation airplanes and to provide a data bank of information for use by airplane designers. In 1973, based on the data collected on thirty-six (36) airplanes flying approximately 12,400 hours, the FAA published Report No. AFS-120-73-02 [1] that describes the accepted method for fatigue evaluation of aircraft wings. Data collection was completed in 1981; at which time 42,155 hours of VGH data were accumulated on one hundred and five airplanes (105) airplanes. NASA evaluated the data for ninety-five (95) airplanes flying 35,286 hours and presented it in tabular forms in the Technical Memorandum 84660 in 1983 [4] (Final Report No DOT/FAAICT-91/20, 1993 [5]). The NASA VGH program measured normal (z-direction) accelerations near the C.G.. One of the recommendations in the report was that a similar program was needed for fatigue of vertical aerodynamic surfaces.

A database collected several years ago by the RAE (Royal Aircraft Establishment) contains fatiguemeter data in a wide variety of mainly piston-engine aircraft. The data, essentially consisting of acceleration counter readings together with speed and altitude, was recorded every ten minutes during flight. This database includes 10,697 flights. In this study, the range of mass, speed and altitude are fairly wide, and the accuracy of derived gust velocities is limited [6].

During a period of about ten (10) years, service load data have been retrieved from ACMS recordings made on Boeing 747 aircraft operated by the KSSU group-KLM, Swissair and SAS. These data were stored at NLR in the so-called ACMS Fatigue

Database. As indicated in the Technical Publication No. TP 89097 [7], the prediction of wing loads from the three previous databases is reasonably accurate but the loading of the tail structure includes a considerable amount of uncertainty. For this reason, the NLR carried out a service-tail load-recording program [8]. In this program, through the joint effort between NLR, the Fokker Company and the KLM, measurements were obtained during commercial operations of a Fokker F-100 over a period of one year. A strain load survey was performed to obtain tail load information using a 4-channel "Spectrapot" recorder. A reasonably large amount of data was collected, but for a fleet of aircraft, the method made it clear that using strain gages for measurements is not suitable as stated earlier in Overview. Thus, the problem of empennage fatigue load remained unaddressed until these past few years. Some research has been done to predict the empennage in-flight loads of General Aviation aircraft. The method used was the back propagation neural network. The study was limited to the prediction of fatigue loads induced by maneuvers. The problem of the prediction of gust load still remains.

Other previous works have defined design loads due to atmospheric turbulence using the Power Spectral Density (PSD) method. The design loads were calculated using linear transfer functions. This method was based on the assumptions that atmospheric turbulence could be described as a quasi-stationary Gaussian process. It was further assumed that the aircraft response to turbulence could be described with linear equations. Using theories about Gaussian processes, it was possible to define design loads based on number of exceedances of the design load level. However, for non-linear airplane motions or if other assumptions are no longer valid, the PSD method cannot be used [9].

The flight load prediction problem is being studied using Neural Networks at Embry-Riddle Aeronautical University, Florida. The research has demonstrated that it is possible to predict empennage strains resulting from maneuver loads in a Cessna 172P. The horizontal tail neural network was trained with CG NZ and x-, y-, and z-axis angular accelerometer signals and predicted 93% of all strains to within $50 \mu\epsilon$ of the measured value. The vertical tail neural network predicted 100% of all strains to within $50 \mu\epsilon$ of the measured value (Marciniak, M., "A Methodology for the Prediction of the Empennage

In-Flight Loads of a General Aviation Aircraft Using Back propagation Neural Networks” [10], Pechaud, L., “Improvement of a Methodology for the Prediction of the Empennage Maneuver In-Flight Loads of a General Aviation Aircraft Using Neural Networks” [16]).

Previous studies on empennage gust loads have been done at Embry-Riddle Aeronautical University. Veronique de Poitevin [21] and Nicolas Arcaute [23], both under the supervision of Dr. D. Kim, participated in these researches, but without success.

De Poitevin tried to train and test Neural Networks with the real time data filtered with DADiSP for the gust frequency range of interest. She focused on building a network for each tail (horizontal and vertical). The accuracy of the prediction was not sufficient, i.e. the correlation remained too low (well below 0.3 whereas 0.9 would be acceptable) and the R.M.S. (Root Mean Square) error too high (around 0.1 whereas 0.001 would be the target value). It was assumed that the gust quantity, gathered in flight was not significant enough for such a prediction. She also tried to train the network with the maneuver file and tested it with the gust file. The prediction was just slightly better without any real improvement.

Arcaute, however, concentrated on the PSD. As stated previously, feeding the network with the PSD data instead of time domain data would be more consistent and would lead to a significant gain of time. But he tried to predict the stress with only a single neural networks (for both horizontal and vertical tails) and the predictions were not as good as expected. Moreover, since this mean of load prediction is intended to be used on a regular basis on airliners as well as General Aviation airplanes, he decided to get rid of the expensive angular accelerometers as well as the very uneasy-to-install tail accelerometers for the Neural Network’s inputs. Like de Poitevin’s research, the correlation remained too low. Some optimization has been achieved but without any real improvement.

1.3 CURRENT APPROACH

The objective of this research is to find and develop a relationship between the data collected near the C.G and the strains at the empennage of General Aviation aircraft due to gust loads. More precisely, a method similar to the one used for the prediction of maneuver loads is desired for the prediction of gust loads. The research concentrates on finding:

- The minimum set of instrumentation sensors needed to accurately predict the strains due to gust loads
- The minimum threshold value of significant strains
- The correlation between sensor output and the empennage flight loads

Data recorded near the C.G. are used to determine loads induced on the empennage structure. It has already been found that there is only a weak linear relationship between normal acceleration in the z-direction (CG NZ) and strain experienced by the horizontal tail. The relationship between normal acceleration in the y-direction (CG NY) and strain experienced by the vertical tail is only slightly better [10]. However, there is no proof that other relationships cannot be found.

The test aircraft Cessna 172P is equipped with sensors: air data transducers (airspeed, altitude, angle of attack, sideslip), rate gyros (to provide the angular velocities around each of the aircraft axes), angular accelerometers (to determine the angular accelerations), linear accelerometers (for y- and z-axis accelerations near the C.G. of the aircraft and for the y- and z-axis accelerations in the tail section). A portable data acquisition system is used to collect data during the flight. But, one of the requirements for the successful implementation of this Data Monitoring System for General Aviation aircraft is low cost. Indeed if a useful flight load database is to be created, a large number of airplanes in a wide range of flight conditions and missions have to be monitored. Such a system should cost around \$2,000 but no more than \$3,000. One of the most expensive

instrumentation components is the angular accelerometer. Based on the previous research, it has been shown that the minimum set of instrumentation required for the prediction of maneuver loads consisted of only the linear accelerometers at the C.G. and the rate gyros (the angular accelerations can be derived by numerical differentiation of rate gyro signals). Consequently, in this research, it would be desired not to use the angular accelerometers as well as the tail accelerometers that are more difficult to install.

Unlike most of the previous research where predictions were based only on time domain, this work investigates the frequency domain using the Power Spectrum Density function (PSD). This approach was prompted by the need to separate gust and maneuver loads and by the fact that the PSD analysis is consistent with data needed for fatigue analysis, i.e., PSD gives the magnitude of the loads for each frequency of interest). The prediction of the strains on the empennage is realized with Neural Networks. Neural Networks analysis is a very powerful tool for modeling problems for which the explicit form of the relationship among certain variables is not known. Thus, this study consists of finding a network being able to predict the strains due to gust encountered during a flight. The basic architecture of the simplest possible neural networks consists of a layer with input units and a single output unit. For the prediction of gust loads, the inputs into the neural networks are provided by the PSD signals derived from the time domain data and collected in-flight from the above instruments. The necessary condition or the criteria used for testing the accuracy of the prediction is to evaluate the value of the correlation coefficient calculated between the strain predicted and the strain measured with a strain gage.

CHAPTER 2

BACKGROUND THEORY

2.1 AERODYNAMIC LOADING

2.1.1 INTRODUCTION

Two types of repeated flight loads are of principal significance to the fatigue of the aircraft structures: maneuver loads and gust loads. The pilot, in controlling the airplane, applies maneuver loads. Gust loads occur during flight due to the turbulence in the atmosphere. These are usually considered as being more frequent and larger than maneuver loads during normal airline operations. The same may or may not be true for General Aviation airplanes. The following discussions on gust loads are based on Reference [14], “Gust loads on Aircraft: Concepts and Applications”. For further details about gust theory, this reference should be consulted.

2.1.2 MECHANISM OF GUST LOADS GENERATION

Gust loads, whether due to discrete gusts or continuous turbulence, are ordinarily considered to be the result of a change in angle of attack due to a component of gust velocity at right angles to the flight path (Figure 1). Vertical and lateral gusts fall into this category. The change in angle of attack, in radians, is equal to the gust velocity divided by the forward speed.

2.1.2.a Vertical and Lateral Gust:

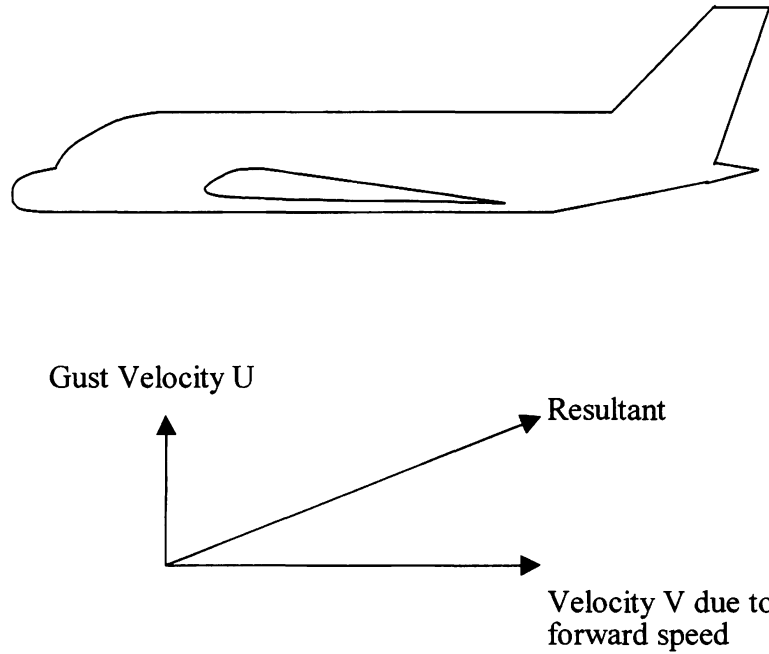


Figure 1. Vertical Gust Velocity [14]

Before gust, the lift of the airplane is equal to:

$$L = m \times g = \frac{\rho}{2} \times V^2 \times S \times C_{l\alpha} \times \alpha \quad (\text{Equation 1})$$

For a vertical gust, the change in lift due to the gust is:

$$\Delta L = \frac{\rho}{2} \times V^2 \times S \times C_{l\alpha} \times \Delta \alpha \quad (\text{Equation 2})$$

where:

V = Airplane forward speed

$\frac{\rho}{2} \times V^2$ = Dynamic pressure

S = Reference wing area

$C_{l\alpha}$ = Lift curve slope

$\Delta\alpha$ = Change in angle of attack due to gust

And $\Delta\alpha$ (in radians) $\approx \tan(\Delta\alpha) = \frac{U}{V}$ for $U \ll V$

where:

U = Gust speed

Then equation 2 becomes:

$$\Delta L = \frac{\rho}{2} \times V^2 \times S \times C_{l\alpha} \times \frac{U}{V} = \frac{\rho}{2} \times U \times V \times S \times C_{l\alpha} \quad (\text{Equation 3})$$

Dividing by W gives the incremental load factor Δn :

$$\Delta n = \frac{\Delta L}{W} = \frac{\frac{\rho}{2} \times U \times V \times C_{l\alpha}}{\frac{W}{S}} = \frac{\frac{\rho}{2} \times U \times V}{\frac{W}{S \times C_{l\alpha}}} \quad (\text{Equation 4})$$

Therefore, measuring the gust load can be done by the measurement of the load factor induced by it.

2.1.2.b Head-on Gust:

During a head-on gust, the angle of attack is equal to the pitch attitude of the airplane. The only noticeable change is the dynamic pressure (the angle of attack is simply the constant pitch attitude of the airplane).

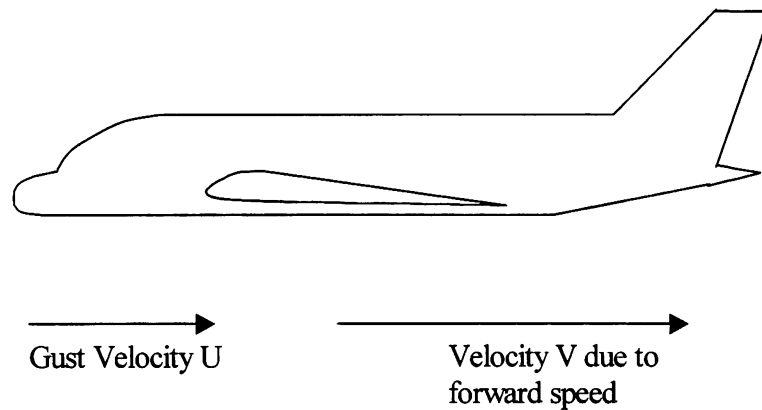


Figure 2. Head-on Gust Velocity [14]

Before gust, Equation 1 holds. For a horizontal gust, the change in lift due to the gust is:

$$\Delta L = \frac{\rho}{2} \times (V + U)^2 \times S \times C_L \quad (\text{Equation 5})$$

where:

C_L = Lift coefficient

and for $U \ll V$, $(U+V)^2 \approx V^2 + 2UV$.

Consequently, Equation 5 becomes:

$$\Delta L = \frac{\rho}{2} \times (2 \times U \times V) \times \left(1 + \frac{1}{2} \frac{U}{V}\right) S \times C_L \approx \frac{\rho}{2} \times (2 \times U \times V) \times S \times C_L \quad (\text{Equation 6})$$

Dividing by W gives the incremental load factor Δn :

$$\Delta n = \frac{\Delta L}{W} = \frac{\frac{\rho}{2} \times U \times V \times C_L}{\frac{W}{S}} = \frac{\frac{\rho}{2} \times U \times V}{\frac{W}{S \times C_L}} \quad (\text{Equation 7})$$

Substituting:

$$C_L = \frac{W}{\frac{\rho}{2} \times V^2 \times S} \quad (\text{Equation 8})$$

we finally end up with the following equation:

$$\Delta n = \frac{\frac{\rho}{2} \times (2 \times U \times V)}{\frac{\rho}{2} \times V^2} = \frac{2U}{V} \quad (\text{Equation 9})$$

Thus, a head-on gust produces only an additional lift but no side force.

2.1.2.c Effect of Airplane Motions:

The net change in angle of attack acting on the airplane depends not only on the gust velocity, but also on the airplane motion induced by the gust as the airplane traverses the gust profile. A gust does not reach its maximum velocity instantaneously; during the period of buildup, the airplane will have time to acquire motion. The pertinent airplane motions, in response to a vertical gust, are as follows:

Plunge: the airplane will translate vertically in the direction of the gust velocity, so that the net gust velocity felt is reduced.

Pitch: the airplane, because of its natural pitch stability, will tend to 'weathervane' so as to reduce the gust increment in angle of attack.

The equation of motion of a rigid airplane in response to a vertical gust can be written in terms of a single variable α . This variable is the increment in angle of attack

due to the airplane motions, $\theta + \frac{z}{V}$; it does not include the angle of attack $\alpha_g = \frac{U}{V}$

associated with the gust velocity, which appears in the equation of motion as the forcing function. This equation is a second-order linear differential equation, so the response is similar to that of a single-mass mass-spring damper system. Consequently, factors that affect the response of such a system also affect airplane response to gusts in much the same way. These would include, for example, damping, forcing-function "rise time," and resonant response to repeated load application. The forcing function, however, consists not only of the gust velocity itself, but also its first and second derivatives. Because the differential equation is of second order, the airplane motions can result in load alleviation or in load increase due to dynamic overshoot effect. Airplane motions in a manner comparable to that described for vertical gusts affect loads due to lateral gust.

For a head-on gust, the alleviation effect of the plunge motion is the same as for a vertical gust; the motion depends only on the lift produced, not on its source. The pitch motion is different, however, inasmuch as the increment in lift due to vertical gust acts at the airplane center of pressure, whereas the lift due to a head-on gust acts at the 1-g flight center of pressure, that is, the C.G. (these can differ substantially as a result of the difference between wing and tail angles of attack in 1-g flight; in fact, they must differ if the airplane is to be statically stable). In addition, in the case of a head-on gust, there is

probably some very small alleviating affect due to slowdown resulting from the drag increase associated with the increase in dynamic pressure.

2.1.3 CHARACTERISTICS OF TURBULENCE

2.1.3.a *Gust Profile*

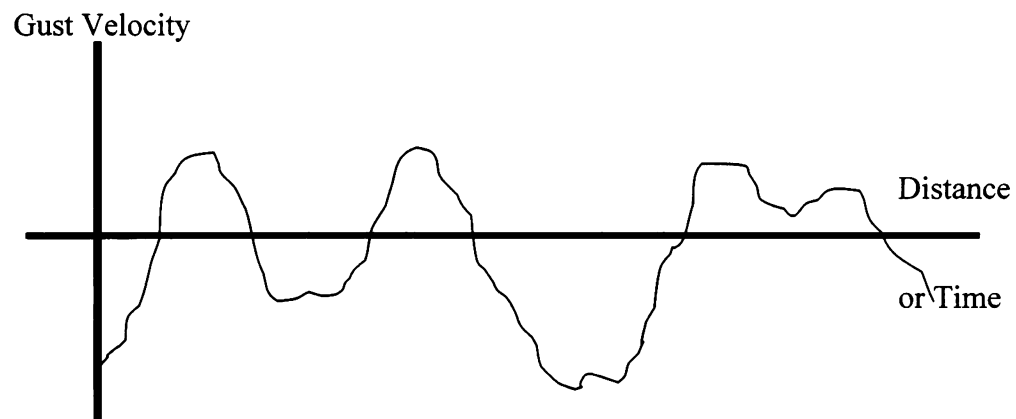


Figure 3. Gust Profile

A gust profile in space becomes a gust velocity time history when the distance scale is divided by the airplane forward speed to become a time scale. Typically, gust profiles tend to be continuous and irregular as illustrated in Figure 3. If the profile is continuous, the gust structure is referred to as turbulence. If the gust structure consists of more or less isolated pulses, a single pulse is referred to as a gust. In general, a continuous turbulence profile is thought of, loosely, as consisting of a series of gusts. Terms such as “gust structure”, “gust profile”, or “gust loads” refer equally to continuous turbulence and isolated gusts.

Isotropy:

Typically, atmospheric turbulence tends to be not only continuous, but also considered isotropic (same in all directions). Thus,

- 1) along a given path through a patch of turbulence, the lateral gust profile tends to have the same general characteristics as the vertical gust profile, including roughly the same peak values;
- 2) for traverse in various directions through the same patch of turbulence, the resulting profiles tend to have the same general characteristics; and
- 3) an individual gust is equally likely to be found in any direction of traverse (North-South, East-West, upwind, downwind, crosswind,...).

Sources of Turbulence:

The usual breakdown is as follows:

- 1) *Storm* (especially thunderstorm): the most common source of severe turbulence,
- 2) *Cumulus cloud*: the same mechanism as thunderstorm, but less severe,
- 3) *Clear air*: sources include wind shear, jet stream (can be severe due to high wind shear), wind over ground (wind shear in the Earth's boundary layer), wind over and between mountains (can be extremely severe close to the ground), and convection due to morning warming of air close to the ground, especially over the desert.

2.2 DISCRETE-GUST STATIC LOADS

2.2.1 GUST IDEALIZATION

The usual idealization of the gust structure consists of a one-minus-cosine pulse:

$$U = \frac{1}{2}U_0 \left(1 - \cos\left(\frac{2\pi x}{2H}\right) \right) \quad (\text{Equation 10})$$

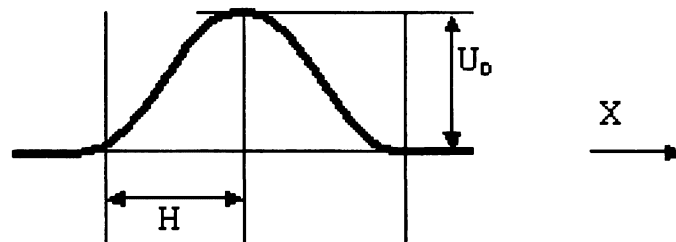


Figure 4. Representation of an Idealized Gust

2.2.2 FAR STATIC GUST REQUIREMENT

For the purpose of obtaining static gust loads, FAR specifies the one-minus-cosine shape and an airplane motion confined to plunge only.

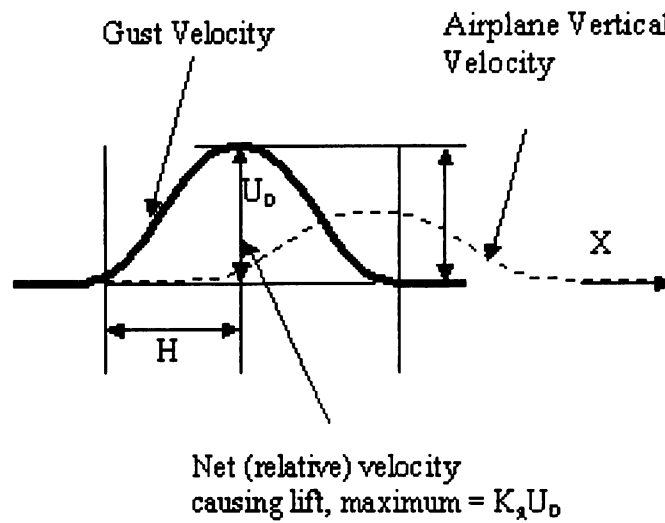


Figure 5. Gust Velocity and Airplane Vertical Velocity

The use of the coefficient K_g in the preceding figure is an over-simplification. It is used to include the lag in buildup of lift in response to gust entry and sudden changes in angle of attack.

2.2.3 FAR GUST LOAD FORMULA

For most vertical gusts, the FAR gust load formula is:

$$\Delta n = K_g \underbrace{\frac{U_{de} V_{eC_{L,\alpha}}}{498 \frac{W}{S}}}_{\text{“Sharp-edge-gust” response}} \quad (\text{Equation 11})$$

“Sharp-edge-gust” response

in combination with:

$$K_g = \frac{0.88\mu_g}{5.3 + \mu_g} \quad (\text{Equation 12})$$

$$\mu_g = \frac{2W}{\rho g S c C_{L\alpha}} \quad (\text{Equation 13})$$

where:

Δn = Incremental Load Factor

K_g = Factor to account for airplane motion and lag in buildup of lift

U_{de} = Derived equivalent gust velocity, fps

V_e = Airplane equivalent airspeed, knots

$C_{L\alpha}$ = Airplane lift curve slope (per rad)

$$498 = \frac{1}{\frac{\rho_0}{2} 1.689} \quad \text{where } \rho_0 \text{ is the sea-level air density and 1.689 converts } V_e \text{ in}$$

knots to fps

W = Airplane weight

S = Reference wing area

μ_g = “mass parameter” as defined by equation 13

ρ = Air density

\bar{c} = Wing mean geometric chord

g = Acceleration due to gravity

In Figure 5, U_0 corresponds to U_{de} , where “e” is the subscript for equivalent.

Hence, $U_{de} = U_0 \sqrt{\frac{\rho}{\rho_0}}$ (Equation 14). The subscript “d” means derived and

reflects the fact that values of U_{de} can be derived from accelerations recorded in flight.

U_{de} can be specified as function of altitude, from sea-level to 20,000 feet:

- at VB (design rough-air speed), $U_{de} = 66$ fps
- at VC (design cruise speed), $U_{de} = 50$ fps
- at VD (design dive speed), $U_{de} = 25$ fps

2.2.4 EFFECT OF STATIC AEROELASTIC DEFORMATION ON $C_{L\alpha}$

Whenever an airplane encounters a gust, its structure is subject to quasi-static deformation due to the forces encountered. This means that the aerodynamic forces are different from those for a rigid airplane. Thus, in using the gust loads formula, the appropriate $C_{L\alpha}$ must be used.

2.3 STRESSES AND STRAINS ACTING ON AN AIRCRAFT

One of the major concerns in aircraft design and operation is structural integrity. The airplane must withstand up to a certain amount of “load” without failure of its structure. Each airplane structure is subject to stresses. Stresses are present on the airplane whether on the ground or in flight. It is defined as a force applied to a unit area of material. Stress produces a deflection or deformation in the material called strain. Stress is always accompanied by strain and for uni-axial loading, it is:

$$\sigma = E\varepsilon \quad \text{(Equation 15)}$$

where:

E = Young Modulus = $10 \cdot (10^6)$ p.s.i.

σ = Stress in p.s.i.

ε = Strain in $\mu\varepsilon$

2.4 POWER SPECTRAL DENSITY (PSD)

The Power Spectral Density, PSD, describes how the power (or variance) of a time series is distributed with frequency. It is often used to define airplane design loads due to turbulence. The PSD of loads provide a measure of the flight-load intensity in terms of the standard deviation (root mean square) of the load distribution for an airplane in flight through rough air. In the expression “Power Spectral Density”,

- 1) *Spectral* indicates a measure of frequency content,
- 2) *Power* indicates, somewhat by analogy, that the quantity to which the various frequency components contribute is the mean square value of the variable and
- 3) *Density* indicates that the frequencies are not discrete but continuously distributed, so one cannot speak of the contribution of a single frequency ω but only of the contribution of a band of frequencies between ω and $\omega+d\omega$.

Mathematically, it is defined as the Fourier Transform of the autocorrelation sequence of the time series:

The Fourier transform $X(f)$ of the signal $x(t)$ is given by:

$$X(f) = \int_{-\infty}^{+\infty} x(t)e^{-2j\pi ft} dt \quad -\infty < f < \infty \quad (\text{Equation 16})$$

$X(f)$ contains all the information of the original signal, and $x(t)$ can be obtained from $X(f)$ by the inverse Fourier transformation:

$$x(t) = \int_{-\infty}^{+\infty} X(f)e^{2j\pi ft} df \quad -\infty < t < \infty \quad (\text{Equation 17})$$

For discrete time-series $x(n)$, the discrete-time Fourier Transform is used:

$$X(e^{j\omega}) = \sum_{n=-\infty}^{+\infty} x(n)e^{-j\omega n} \quad (\text{Equation 18})$$

The inverse transform is:

$$x(t) = \frac{1}{2\pi} \int_{-\pi}^{+\pi} X(e^{j\omega}) e^{j\omega n} d\omega \quad (\text{Equation 19})$$

An equivalent definition of PSD is the squared modulus of the Fourier transform of the time series scaled by a proper constant term. Since this is power per unit of frequency, the dimensions are those of a power divided by Hertz.

In order to apply the PSD to determine the airplane design loads due to turbulence, some assumptions must be made:

- The airplane is described as a linear system,
- The turbulence is stationary.

2.5 NEURAL NETWORKS FUNDAMENTALS

Neural Networks represent an attempt to imitate the human brain and simulate what goes through nervous systems, with the hope of capturing some of the computing power of these biological systems. Whereas a computer is simply programmed to execute instructions written by a programmer, the human nervous system, due to its billions of interconnected cells, can perform some computations without the benefit of a programmer.

Neural computing, in general, builds models based on historical data. It is applicable in any situation where there is an unknown relationship between a set of input factors and an outcome, and for which a representative set of historical examples of this unknown mapping is available. The objective of building a model is to find a formula or a program that facilitates predicting the outcome from the input factors.

An artificial neural network is information processing that has certain performance characteristics in common with biological neural networks and consequently has the ability to learn through training. Artificial neural networks have been developed as generalizations of mathematical models of human cognition or neural biology, based on the assumptions that:

- 1) Information processing occurs at many simple elements called neurons,
- 2) Signals are passed between neurons over connection links,
- 3) Each connection link has an associated weight, which, in a typical neural net, multiplies the signal transmitted,
- 4) Each neuron applies an activation function (usually nonlinear) to its net input (sum of weighted input signals) to determine its output signal.

A neural network is characterized by:

- The arrangement of neurons into layers and the connection patterns within and between layers (architecture),
- Its method of determining the weights on the connections (training, or learning, or algorithm) and
- An activation function.

What makes a network useful in the analysis of complex systems is the ability to modify its connectivity through experience. There are three types of modifications to a network:

- The development of new connections,
- The loss of existing connections and
- The modifications of the strengths of connections that already exist in the network.

2.5.1 NEURAL NETWORKS DESCRIPTION

A Neural Network (NN) consists of a large number of simple processing elements called neurons, units, cells, or nodes. There are three types of processing units in a neural network model:

- The *input units* which receive data from sources external to the model,
- One or more layers of *hidden units* which are internal to the model only,
- One or more *output units* which send signals out of the model to influence other external systems.

Each neuron is connected to other neurons by means of directed communication links, each with an associated weight. The weights represent information being used by the net to solve a problem. A neuron has an internal state, called its activation or activity level, that is a function of the inputs it has received. Typically, a neuron sends its

activation signal to several other neurons. It is important to note that a neuron can send only one signal at a time, but that signal is broadcast to several other neurons. Each neuron first calculates a weighted sum of the input signals, then applies a transfer function to this sum and outputs the result (Figure 6). Transfer functions are generally nonlinear. Nonlinear functions are required to achieve the advantages of multi-layer nets. The following drawing represents the basic architecture of a processing element (PE).

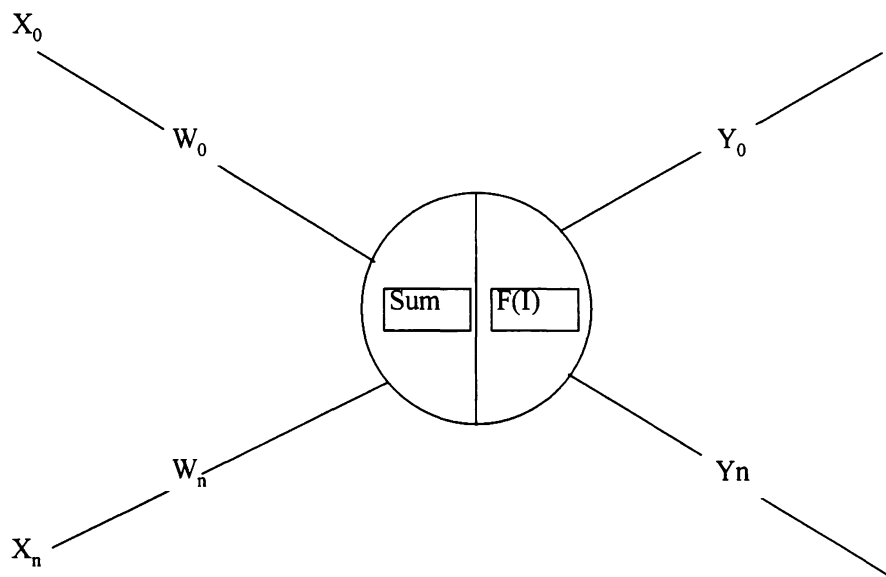
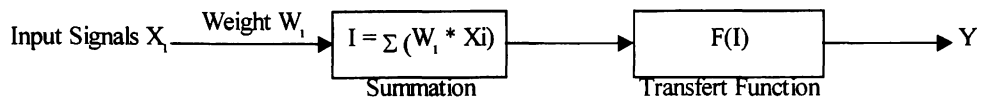


Figure 6. Representation of a Processing Element

Neurons are arranged in layers. Neurons in the same layer behave in the same manner. Within each layer, neurons usually have the same activation function and the same pattern of connections to other neurons. To be more specific, in many NN, the neurons within a layer are either fully interconnected or not interconnected at all.

Neural nets are often classified as single layer or multi-layer. There are typically two layers with connections to the outside world: an input buffer where data is presented to the network, and an output buffer which holds the response of the network to a given input. Layers distinct from the input and output buffers are called hidden layers (Figure 7). A single-layer net has one layer (or level) of connection weights. A multi-layer net is a net with one or more layers of nodes (the so-called hidden units) between the units and the output units. Typically, there is a layer of weights between two adjacent levels of units (input, hidden, or output). Multi-layer nets can solve more complicated problems than can single-layer nets, but training may be more difficult. However, in some cases, training may be more successful because it is possible to solve a problem that a single-layer net cannot be trained to perform correctly at all.

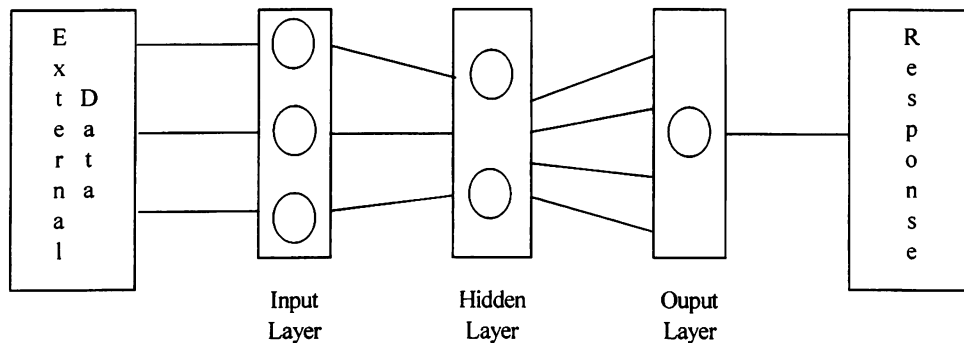


Figure 7. Architecture of a Network

There are a number of procedures for training a network and adjusting the weights. Many learning algorithms have been derived over the last two decades. In choosing a learning algorithm for a system, we must realize the function that we want to specify is initially unknown to us because of the myriad possible fault situations. We can impose an unspecific function on the network as long as we can supply a set of examples of the desired input/output pairs. The network is then trained until it performs the input to output transformation desired.

2.5.2 NETWORK OPERATION

There are two main phases in the operation of a network: learning and recall. In most networks, these are distinct.

Learning is the process of adapting or modifying the connection weights in response to stimuli being presented at the input buffer and optionally the output buffer. A stimulus presented at the output buffer corresponds to a desired response to a given input; a knowledgeable 'teacher' must provide this desired response. In such a case, the learning is referred to as "supervised learning". If the desired output is different from the input, the trained network is referred to as a hetero-associative network. If, for all training examples, the desired output vector is equal to the input vector, the trained network is called auto-associative. If no desired output is shown, the learning is called unsupervised learning. A third kind of learning, falling between supervised and unsupervised learning, is reinforcement learning where an external teacher indicates only whether the response to an input is good or bad. In some instances, the network may only be graded after the network has processed several inputs. Whatever kind of learning is used, an essential characteristic of any network is its learning rule. The learning rule specifies how weights adapt in response to a learning example. Learning may require showing a network many examples, many thousands of times, or only once. The parameters governing a learning rule may change over time as the network progresses in its learning. The long-term control of the learning parameters is referred to as a learning schedule.

Recall refers to how the network processes a stimulus presented at its input buffer and creates a response at the output buffer. Often a recall is an integral part of the learning process such as when a desired response of the network must be compared to the actual output of the network to create an error signal. The simplest form of a network has no feedback connections from one layer to another or to itself. Such a network is called a “feed-forward network”. In this case, information is passed from the input buffer, through intermediate layers to the output layer, in a straightforward manner, using the summation and transfer function characteristics of the particular network. In some feed-forward networks, a certain amount of feedback is used to create time-sensitivity in the network. These are called recurrent networks or “feedback networks”.

2.5.3 BACK-PROPAGATION NETWORK

For a prediction problem, back-propagation network seems to be the best choice. As it is the case with most NN, the aim is to train the network to achieve a balance between the ability to respond correctly to the input patterns that are used for training (memorization) and the ability to give reasonable (good) responses to input that is similar, but not identical, to that used in training (generalization). Back-propagation assumes that all processing elements and connections are somewhat to blame for an erroneous response. Responsibility for the error is affixed by propagating the output error backward through the connections to the previous layer. This process is repeated until the input layer is reached. The name “back-propagation” (or generalized delta rule) derives from this method of distributing the blame for errors.

The training of a network by back-propagation involves three stages:

- The *feed-forward* of the input training pattern,
- The *calculation and backpropagation* of the associated error,
- The *adjustment of the weights*.

After training, application of the network involves only the computations of the feed-forward phase. Even if training is slow, a trained net can produce its output very rapidly.

2.5.3.a Architecture:

The typical back-propagation network (see Figure 6) always consists of:

- Input layer (denoted “X”),
- Output layer (denoted “Y”) and
- Hidden layer (denoted “H”).

The number of hidden layers is not limited but typically there will be one or two. Each layer is fully connected to the succeeding layer. The arrows indicate flow of information during recall. During learning, information is also propagated back through the network and used to update the connection weights. The weights of the connections between the input and the hidden layer are denoted by “v” and “w” for those between the hidden and the output layer.

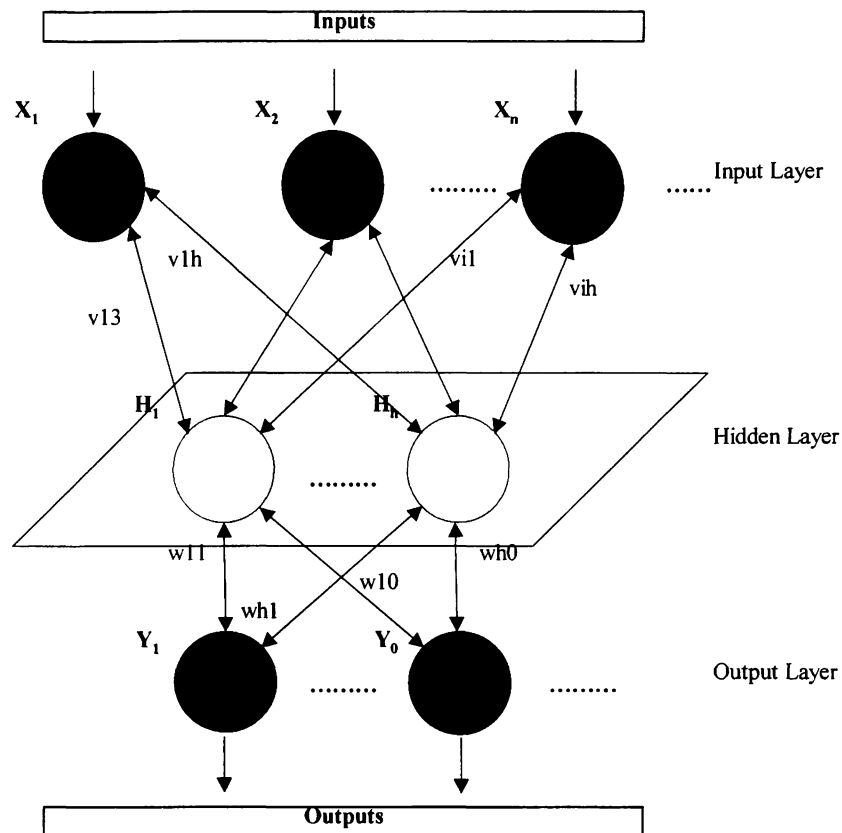


Figure 8. Three-Layer Back Propagation Neural Network

2.5.3.b Choices

Before creating a back-propagation network, some choices have to be made in order to improve the quality of the net.

- Number of Inputs:

The input layer must have the same number of processing elements than the number of inputs.

- Choice of Initial Weights:

The choice of the initial weights will influence whether the net reaches a global (or only a local) minimum of the error and, if so, how quickly it converges. The values for the initial weights must not be too large, or the initial input signals to each hidden or output unit will be likely to fall in the region where the derivative of the transfer function has a very small value (the so-called saturation region). On the other hand, if the initial weights are too small, the net input to a hidden or output unit will be close to zero, which also causes extremely slow learning. A common procedure is to initialize the weights to random values between -0.5 and 0.5 (or between -1 and 1 or some other suitable interval).

- Data Representation:

If input vectors and output vectors have components in the same range of values, because one factor in the weight correction expression is the activation of the lower unit, units whose activations are zero will not learn. Therefore, learning can be improved if the input is represented in bipolar form and the hyperbolic tangent is used for the activation function.

- Number of Hidden Layers and Number of Neurons:

Up to three hidden layers can be chosen. A linear problem requires only one hidden layer whereas more complex problems need more. One hidden layer is sufficient for a back-propagation network to approximate any continuous mapping from the input patterns to the output patterns to an arbitrary degree of accuracy. However, two hidden layers make training easier in some situations.

The number of neurons in the hidden layer is much more difficult to establish; it is found by trial and error. An arbitrary number of neurons is chosen until the maximum one is found after analysis of the results.

- Number of Training Pairs:

The question to be answered is “Under what circumstances can I be assured that a net which is trained to predict correctly a given percentage of the training patterns will also predict testing patterns drawn from the same sample space?” The answer is that if the training set contains a very large pattern of possible values of inputs and outputs and that they appear in the same proportion as in the testing set, then the network will be able to generalize as desired (predict unknown testing patterns correctly). For prediction problems, like the one addressed here, there is no rule available to determine this number of training patterns. Therefore, some trial and error is required, remembering that if the training fails, the number of training pairs must be increase.

- Number of Outputs:

For the output layer, the number of neurons is the same than the number of predicted variables for a prediction problem. In the case of a classification problem, the number of neurons must be equal to the number of classification.

- Training Duration:

Since the main motivation for applying a back-propagation net is to achieve a balance between memorization and generalization, it is not necessarily advantageous to continue training until the total squared error actually reaches a minimum. A current approach is to use two sets of data during training: a set of training patterns and a set of

testing patterns. These two sets must be disjoint. Weight adjustments are based on the training patterns; however, at intervals during training, the error is computed using the testing set. Training is terminated when the error for the testing patterns starts to increase; the net is beginning to memorize the training set too specifically (loss of its ability to generalize).

2.5.3.c Learning Algorithm:

Let us suppose a processing element in layer h:

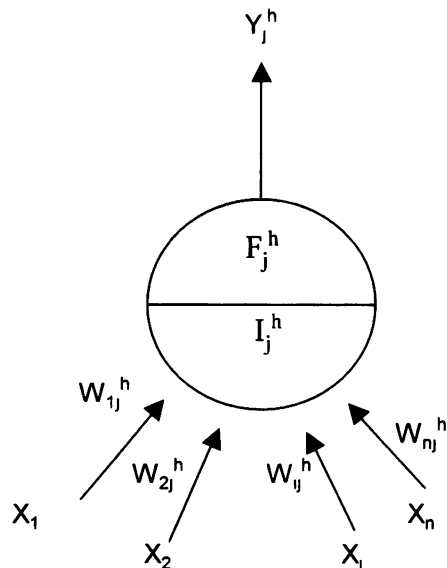


Figure 9. A Single Neural Network Processing Element in Layer h

with:

$$X_i^h = (X_1, X_2, \dots, X_i, \dots, X_n)$$

$$I_j^h = \sum_{i=1}^n W_{ij}^h X_i : \text{Summation} \quad (\text{Equation 20})$$

$$F_i^h = f(I_i^h): \text{Transfer} \quad (\text{Equation 21})$$

In this figure:

- Y_j^h is the current output of neuron j in layer h
- W_{ij}^h is the connection weight between neuron i and layer $(h-1)$ and the neuron j in layer h
- I_j^h is the weighted sum of inputs to neuron j in layer h

The function f is a transfer function (or activation function); it can be linear, non-linear or a sigmoid. For sigmoid, it is given by:

$$f(z) = \frac{1}{1 + e^{-z}} \quad (\text{Equation 22})$$

For each processing element in the output layer, the scaled local error ε_k is calculated as:

$$\varepsilon_k = (t_k - o_k) \cdot f'(I_k) \quad (\text{Equation 23})$$

The raw local error is given by: $(t_k - o_k)$ (Equation 24)

and the Delta Weight by: $\Delta W_{ij}^h = \eta \delta_j X_i$, (Equation 25)

where δ_j is the term used to back-propagate errors in the hidden layer, and η is the learning coefficient. The δ_j term is given by:

$$\delta_j^h = f'(I_j^h) \sum_k \delta_k^{(h+1)} W_{kj}^{(h+1)} \quad (\text{Equation 26})$$

In the previous equation, there is a layer above h , therefore, this equation can only be used for non-outputs layers.

If f is the sigmoid function, then its derivative can be expressed as a simple function of itself as follows:

$$f'(z) = f(z) \cdot (1 - f(z)) \quad (\text{Equation 27})$$

Therefore, the δ_j^h term becomes:

$$\delta_j^h = X_j^h (1 - X_j^h) \sum_k \delta_k^{(h+1)} W_{kj}^{(h+1)} \quad (\text{Equation 28})$$

provided the transfer function is a sigmoid.

If for an input I , the desired output vector is t , and the actual output vector produced by the network is o , then the global error E is calculated as:

$$E = \sqrt{\left(\sum_{k=1}^M (t_k - o_k)^2 \right)} \quad (\text{Equation 29})$$

where M is the number of output nodes present in the network. The learning procedure for a standard back-propagation model can now be summarized as follows:

- (i) Present an input vector I to the input layer
- (ii) Calculate the summation value I using equation (20)
- (iii) Calculate the output value F using equation (21)
- (iv) For each node in the output layer calculate the local errors and the delta weights using equations (22) and (26)
- (v) For each node in the hidden layer calculate the local errors and the delta weights using equations (22) and (26)
- (vi) Finally, update all weights in the network by adding the current delta weights to the previous weights

The process of forward feeding the input and back-propagating the error continues until the error at the output node is zero or is within an acceptable range. At this point the network is said to be converged. The converged network is used to predict the empennage in-flight loads due to gust of a General Aviation aircraft.

2.5.3.d Transfer Function

A transfer function is the component of a processing element through which the sum is passed (transformed) to create net output. For a back-propagation network the activation function should have several important characteristics:

- Continuous
- Differentiable
- Monotonically non-decreasing

Furthermore, for computational efficiency, it is desirable that its derivative be easy to compute. Instead of the sigmoid function, any smooth function can be used as the transfer function for a processing element. The hyperbolic tangent and the sine function are an alternative. The hyperbolic tangent function is just a bipolar version of the sigmoid function: the sigmoid is a smooth version of a $[0,1]$ step function whereas the hyperbolic tangent is a smooth version of a $[-1,1]$ step function.

CHAPTER 3

FLIGHT TESTING

3.1 EXPERIMENTAL APPARATUS

Sets of data containing gust in sufficient quantity are needed for the purpose of the study. Data were collected during flight tests aboard the Embry-Riddle Aeronautical University test aircraft Cessna 172P. The flight test parameters were collected using an IOtech DaqBook 216 portable data acquisition system.

3.1.1 SENSORS AND ACCELEROMETERS

The aircraft is equipped with sensors and accelerometers to collect data (Table 1). Among those is an air data transducer (or digital air data system), which provides information about total temperature, density altitude, pressure altitude, static air temperature, vertical speed, computed airspeed and true airspeed. This system is completely independent from the aircraft's navigational system, deriving data from a pressure transducer assembly and a temperature probe.

Table 1

Instruments Installed on-board the Testbed C-172

Type	Qty	Model	Manufacturer	Price
Air Data Transducer	1	Unknown	Unknown	\$2,000
Linear Accelerometer	4	Columbia Research SA-107BHP	Columbia Research Laboratories, Inc.	
Rate Gyroscope	3	Gyrostar ENV-05H-02	Murata Mfg. Co. Ltd.	\$300
Angular Accelerometer	3	Shaevitz, Inc.	Shaevitz, Inc.	\$1,700
Instrumentation Boom	1	Unknown	E.R.A.U. Student	
Portable Computer	1	PC	Toshiba	
Portable Data Acquisition System	1	Daqbook 216	IOTech, Inc.	
Strain Sensors	6	Columbia Research Model 2681	Columbia Research Laboratories, Inc.	

One of the objectives of this research is to determine the minimum set of instruments needed to analyze gust loads. Consequently, not all the sensors were needed to obtain the results. Just the next one were used:

- Four linear accelerometers, used to measure the acceleration in terms of g-loads. Two are installed in the cabin of the aircraft, in the vicinity of the aircraft C.G., and the two others are located in the tail.
- Three rate gyroscopes and three angular accelerometers installed in the baggage area of the aircraft on a removable instrument pallet and
- Six temperature compensated strain gages mounted on the front spar of the horizontal and vertical stabilizer, and on the wing front spar.

The following figure indicates the location of those different sensors on board the aircraft.

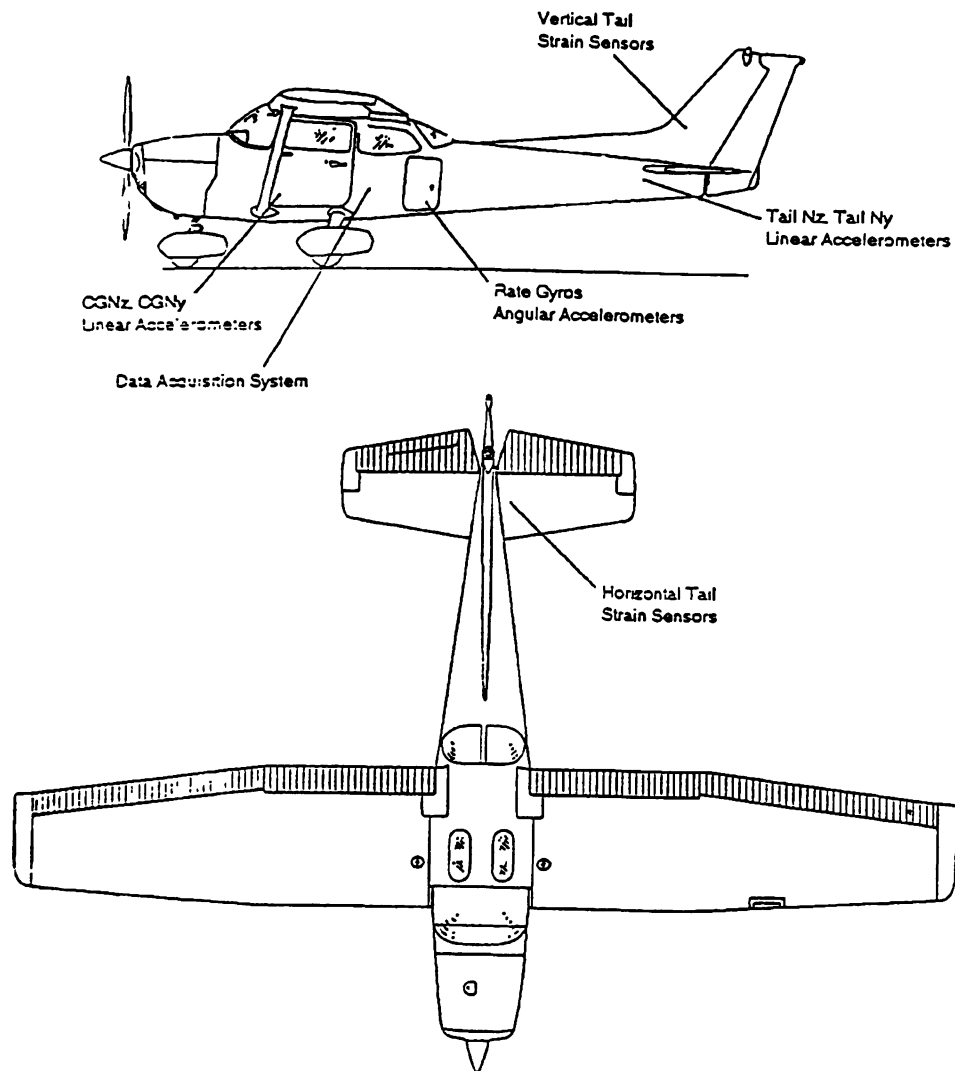


Figure 10. Instrumentation Setup on Board the Aircraft

The following pictures were taken during the installation of the instruments:



The accelerometers are placed
inside the bulkhead

Figure 11. Tail Accelerometers Location

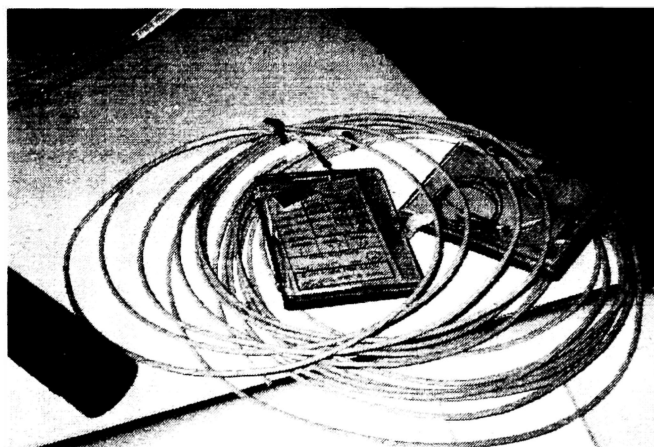


Figure 12. Type of Strain Gages Mounted in the
Aircraft

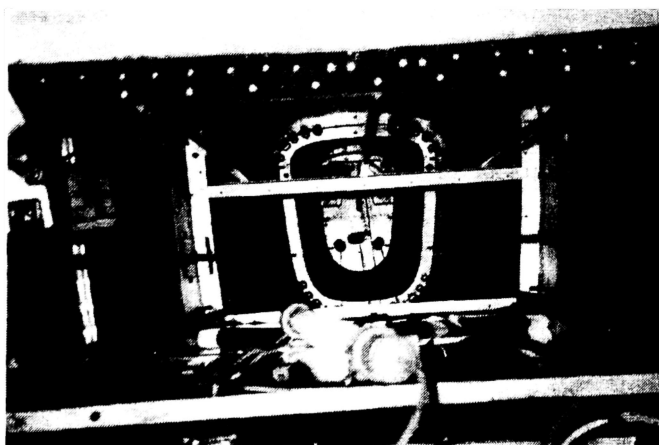


Figure 13. Running Wires Through the Back of the Airplane

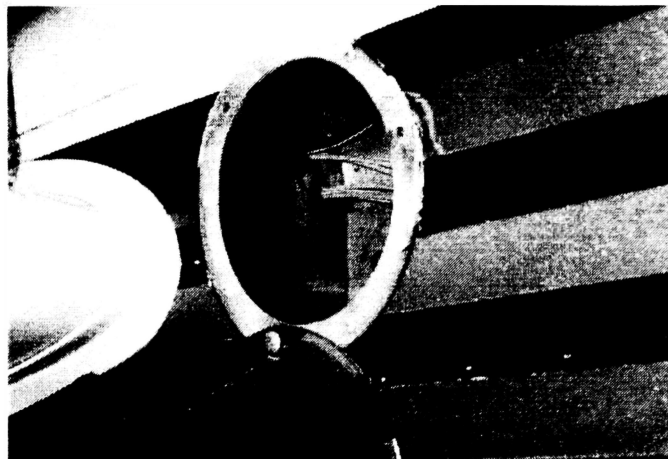


Figure 14. Wires Through the Bulkhead

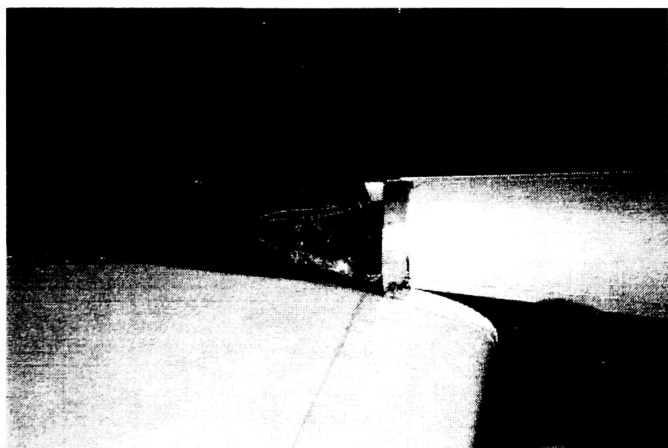


Figure 15. Centerline Gages

3.1.2 DATA COLLECTION

3.1.2.a Data Acquisition System

DaqBook is a data acquisition system capable of high-speed multi-function I/O to notebook PC's for portable test applications. The Daqbook Unit is directly connected to the PC's parallel port and provides a second parallel connector for attaching a parallel printer. This acquisition system is powered with a portable battery. The DaqBook 216 model provides 256 analog inputs and 2 analog outputs and scan 16 digital inputs in the same sequence used for analog inputs (Figure 16). The DaqBook model has broad-ranging software support, two Windows programs:

- DaqView4.2, a set-up and data acquisition package
- PostView, a post-acquisition waveform-display package

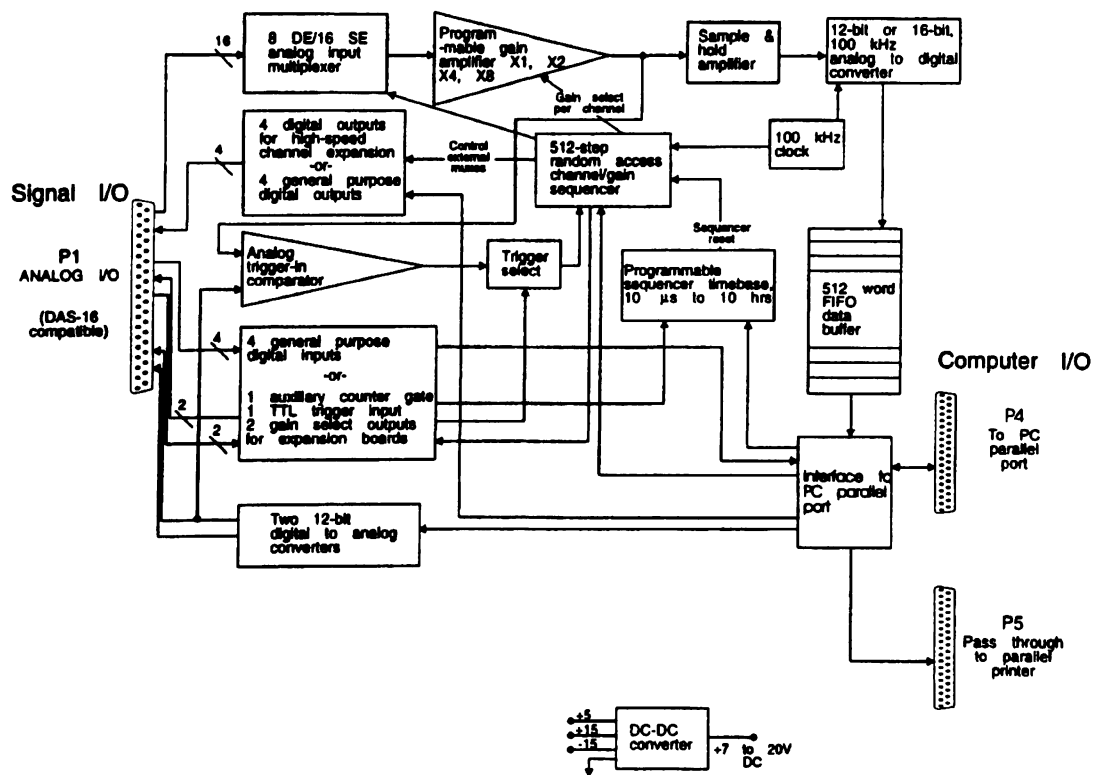


Figure 16. Daqbook 216 Diagram

DaqView 4.2 allows the selection of the desired channels and their gain settings. It also permits to stream data to disk and display them in either numerical or graphical formats. PostView is a post-acquisition waveform-viewing package, permitting the simultaneous viewing of up to 16 channels of acquired data.

The DaqBook 216 acquisition system was equipped with an IOTech DBK 15 Universal Current/Voltage Input card and an IOTech DBK43 Eight-Channel Strain Gage module. The DBK15 features a 16-channel multiplexer and a programmable gain input amplifier. Its component sockets accept resistors that configure each channel for either current-to-voltage conversion or for voltage attenuation. The DBK15 can measure voltages up to 200 VDC or currents up to 1 AMP by scaling these parameters to the 0-5 VDC DaqBook input range. Therefore, for the problem addressed here, this card is used to collect data from linear and angular accelerometers and rate gyros. The DBK43 eight-channel strain gage expansion module accommodates the connection of most strain-gages types, from single element quarter bridges to 4-element full bridges. The DBK43 also includes provisions for bridge completion resistors and provides four adjustments on each of its eight channels, including excitation voltage, input gain, offset nulling and output scaling. The DBK43's 0 to 5 VDC offset adjustment range and output gain scaling nulling of large quiescent loads and expansion of dynamic range for maximum resolution. This is an important feature because strain gages typically exhibit pre-load or quiescent output, leading to a non-zero output prior to the application of the load to be measured. The DBK43's offset adjustments are used to null these pre-load conditions. The remaining signal can then be expanded by the DBK43's output scaling amplifiers to increase the resolution. Therefore, the DBK43's card is used to collect data from strain gages. Connected with the DaqBook data acquisition system, a laptop computer was used to record the data during the flight.

3.1.2.b Testing Procedure

The pilot alone could acquire the data. However, safety considerations required a second crewmember to be present. Data were acquired at several altitudes, airspeeds and engine power settings to capture maximum gust loads without compromising safety. The data were recorded only during VFR (Visual Flight Rules) flights. Indeed FAA does not permit the usage of electrical devices while operating under IFR (Instrument Flight Rules) unless those electrical equipments are FAA certified. This data acquisition methodology is applicable to any flight condition and flight envelope. However, for safety reasons, the aircraft was flown only at or below its maneuvering speed.

These data were collected for a time period varying from three to five minutes in order to have samples of gust loads in sufficient quantity. Detailed descriptions of the data acquisition system and testing procedure can be found in Reference [10]. The data-sampling rate was set to 200 Hz (for a three minutes flight, 36,000 records were collected and for a five minutes flight, 60,000 records).

Before start recording, the pilot performed some maneuvers (push-pull, rolls, constant-rate turns, sideslips, etc.) to check that all channels were correctly connected and were fully functional. The data collection was then started manually once the airplane was flying in a straight-and-level attitude. The data file was saved in a binary format.

Several files were recorded during a flight, and flights were flown during several days at different geographic locations.

3.1.2.c Testing Locations

For this research, several flights have been carried out especially during gusty conditions. Most of the flights were local flights in the vicinity of Daytona Beach (DAB), Florida. Data showed that the turbulence in this area and other parts of Florida was primarily in the z-direction caused by thermals activities. Flights in the southern part of

Florida showed similar results. In contrast, flights in the Appalachian Mountain region, north of Greenville International airport (GSP), showed that the turbulence was predominantly in the y-direction caused by mountain waves from strong horizontal surface winds.

CHAPTER 4

POSTPROCESSING OF DATA

Once the data were recorded, they were converted from binary into ASCII format. Prior to using the data to train or to test a network, they were checked for integrity and content. The data files must contain gust information in a sufficient quantity to be useful. DADiSP was used to verify those files. DADiSP is an interactive graphics worksheet and a visually oriented software package for the display, management, analysis and presentation of scientific and technical data. DADiSP can be used to edit, filter, and process the data. In addition, to confirm the presence of gust (using a modified FAA two second gust separation method), a software developed in-house, Fliseg, was also used.

4.1 DADISP

Using DADiSP, a Power Spectrum Density (PSD) is constructed to identify gust loads. This analysis shows that several noises have been recorded in the same time as the gust. Those noises are characteristic of those encountered in a General Aviation airplane. According to a study conducted by Howard V.L. Patrick on a two-bladed propeller powered Cessna 172 airplane some significant different noises can be distinguished [25 and 26].

Those noises are:

- The firing frequency:

Considering a four-stroke engine, each piston fires every two revolutions. Depending on the rotational speed of the engine, it results in a fundamental firing frequency, f , equal to:

$$f = \frac{1}{4} \times \frac{\text{Cycles}(RPM)}{60} \times \text{Number of Blades}$$

For example, for a rotational speed of 2400 RPM (Revolution Per Minute) or 40 RPS (Revolution Per Second), the fundamental firing frequency will be equal to 20 Hz, i.e. half of 40. Moreover, the engine has four cylinders resulting in a primary engine firing frequency (EFF) of four times f , equal to 80 Hz.

- The structural resonance frequencies:

They occur at the harmonics of f , which are at $2f$, $3f$, $4f$, $5f$, etc. Higher harmonic frequencies are present but they are beyond the range studied. The most intense tone occurs at primary engine frequency. The propeller blade passing frequency (BPF) for a two-bladed propeller is twice the engine rotational speed, which is in fact identical to EFF. Consequently, this identity between BPF and EFF means that tones of both as well as multiples obscure each other.

- The Avionics Noise Frequency:

Previous PSD studies have shown that it occurs around 69 – 70 Hz.

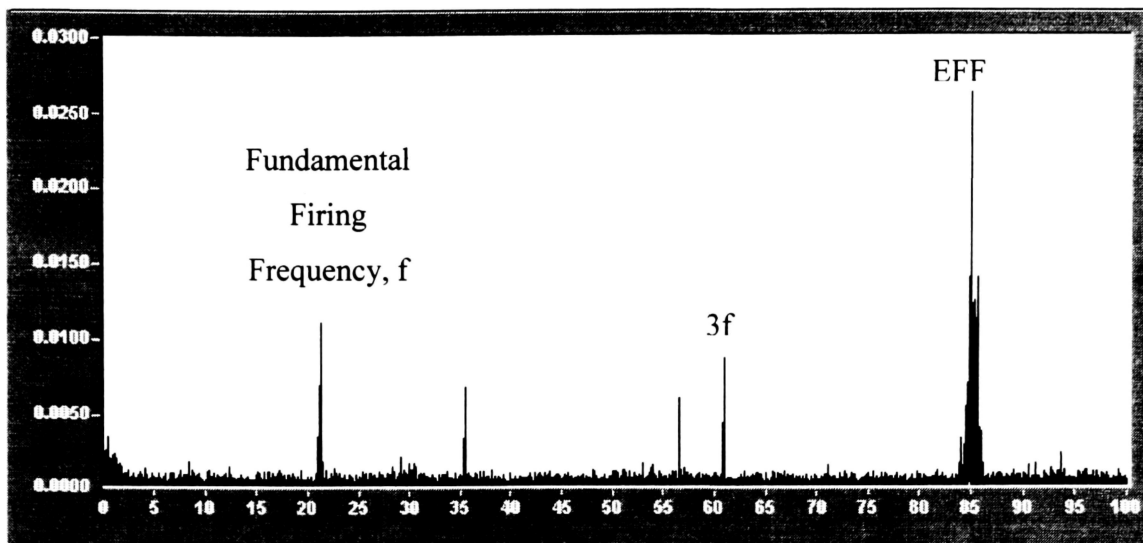


Figure 17. Power Spectrum Density Analysis of the CG NZ Signal

All those preceding features show the necessity to record data at a high RPM setting (at least above 2,400 RPM) so that f is not included into the frequency range of interest (i.e. below 20 Hz for gust consideration). Then, since during the flights a lot of noise induced by the aircraft is recorded with the gust load data, the files must be filtered. Indeed, in order to train properly a neural network, one must get rid of all that noise. For the previous research, a digital band pass filter had been applied to the real-time collected gust data. Another way to do it would consist of considering the frequencies of interest once the PSD of the signal has been applied. However this method has to be validated. The second solution was adopted for this study for a much less time consuming reason and accounting that the PSD had to be calculated anyway.

4.2 FLISEG

4.2.1 THEORY

Fliseg has been developed and written at ERAU for the purpose of establishing Gust Load Spectra for General Aviation aircraft using a modified FAA two-second rule method. Presently, only wing loading spectra have been published and are available in Report No. AFS-120-73-2, "Fatigue Evaluation of Wing and Associated Structure on Small Airplanes" [1]. ACE-100, "Fatigue Evaluation of Empennage, Forward Wing, and Winglets/Tip Fins on Part 23 Airplanes" [2] provides an accepted method for estimating the fatigue life of empennage structures based on AFS-120 normal acceleration data, but this method is yet to be substantiated. These data are central to considering the "safe-life" or "fail-safe" concepts.

Fliseg calculates the acceleration fraction $\left(\frac{a_n}{a_{nLLF}}\right)$. The cumulative number of occurrences of each value of the acceleration fraction is also plotted either per unit of time or per nautical miles. Initially, this program was written to derive the gust exceedance curves from data downloaded from the cumulative fatigue data recorder installed on Embry-Riddle Aeronautical University fleet airplanes. According to previous research it has been determined that a gust appears to occur above 2 Hz, depending on the airplane. This result allows the identification of the gust-induced loads from the maneuver loads. This is based on the acceleration near the C.G. only. The acceleration fraction $\left(\frac{a_n}{a_{nLLF}}\right)$ is the recorded incremental normal limit load factor (airplane limit load factor minus 1g). The airplane limit gust load factor is determined using the appropriate certification regulation (F.A.R. Part. 23).

Those values are:

- For a utility aircraft:

- -1.76 g for the negative load factors
- +4.4 g for the positive load factors

- For a normal aircraft:

- -1.52 g for the negative load factors
- +3.8 g for the positive load factors

This acceleration fraction, $\left(\frac{a_n}{a_{nLLF}}\right)$, relates both the recorded gust accelerations to the airplane limit gust load factor and the recorded maneuver accelerations to the airplane's limit maneuver load factor. Consequently when the aircraft is in level flight, the acceleration equals zero. An acceleration fraction of 1 or greater indicates that the limit gust load factor has been reached or exceeded. Using this fraction results in the possibility of comparing the data for airplanes of different design limit gust load factors.

The limit gust load factor is determined from the certification regulation but Amendment 23-7 in Section 23.341 of the FAR is used to calculate a_{nLLF} . The incremental gust limit load factor calculation is based on the following equations:

$$a_{nLLF} = \frac{K \times U \times V \times m}{\left(\frac{\rho_0}{2} \times 1.689\right) \times \frac{W}{S}} \quad \text{(Equation 30)}$$

Where:

U = the nominal gust velocity

V = the airplane design cruise speed

m = the wing lift curve slope

ρ_0 = the density at Sea-Level, i.e. 0.0023769 slugs/ft³

$\frac{W}{S}$ = the wing loading at maximum weight (lb/ft²)

K = has two different values depending on the value of the wing loading:

$$\text{If } \frac{W}{S} < 16 \text{ psf}, K = \frac{1}{2} \times \left(\frac{W}{S} \right)^{\frac{1}{4}} \quad (\text{Equation 31})$$

$$\text{Otherwise, } K = 1.33 - \frac{2.67}{\left(\frac{W}{S} \right)^{\frac{3}{4}}} \quad (\text{Equation 32})$$

At a given point of the flight, the normal acceleration is equal to (n_z-1) ; the acceleration fraction can therefore be determined since the value of the load factor (n_z) recorded at the C.G. is known.

4.2.2 EXCEEDANCE CURVES PLOT - CYCLE COUNTING

As shown above, the value of the acceleration fraction is determined for each recorded point of the flight quite easily. From there, different methods of cycle counting may be used to determine the number of occurrences of the normal acceleration fraction during a given flight. A standard way of counting described in ASTM Standards, *Cycle Counting in Fatigue Analysis – Designation E 1049-85* [28], is used. Three different methods are offered: Level-Crossing Counting, Peak Counting and Simple-Range Counting. The method used is the peak counting. It identifies the occurrence of a relative maximum or minimum load value. Peaks above the reference load level are counted, and valleys below the reference load level are counted. The results for peaks and valleys are usually reported separately. The FAA uses this counting method.

4.2.3 FLISEG METHODOLOGY FOR GUST DISCRIMINATION

In order to process the real-time data with Fliseg and ensure that gust is present in a sufficient quantity, the frequency threshold in order to discriminate gusts and maneuvers is set to 2 Hz, meaning that if a change in CG occurs below 2 Hz, this part of the flight is considered as maneuvers (pilot response or pilot control/maneuver). And for the part of the flight where a change in CG occurs in more than 2 Hz, it is considered as gusts. Then, the program discriminates the flight into two files, maneuver and gust. The exceedance curves can be plotted. An analysis of both the acceleration at the C.G. and at the tail revealed that Fliseg is able to discriminate for either acceleration data. An important remark is that the file's result for both the acceleration at the C.G. and at the tail is nearly the same, meaning that a relation between the acceleration at the C.G. and the one at the tail can be drawn. However, studies for the Tail PSD's acceleration may show some peaks but those one are damped compared to one issued from the CG PSD.

4.3 GUST DISCRIMINATION

First, a study of the time domain data was undertaken. It consisted of comparing the data collected during smooth and gusty conditions as well as maneuvering conditions. The following figures present data recorded during some smooth, gusty and maneuver conditions. The smooth air data were the baseline reference. The time domain data allowed the determination of the amplitude for the different channels concerned. The most important ones, i.e. the ones that were the most likely of influencing the NN are presented below.

Secondly, the PSD of each channel has been studied. The PSD, primary, permitted the determination of the gust amplitude.

Time domain and PSD data are drawn below in order to show the magnitude of the “gust” occurring during the flights. The x-axis is in seconds⁻¹ (or Hertz) and the y-axis is in Seconds*Volts². The maneuver flight consists of push-pulls and rolls.

4.3.1 SMOOTH AIR TIME DOMAIN DATA

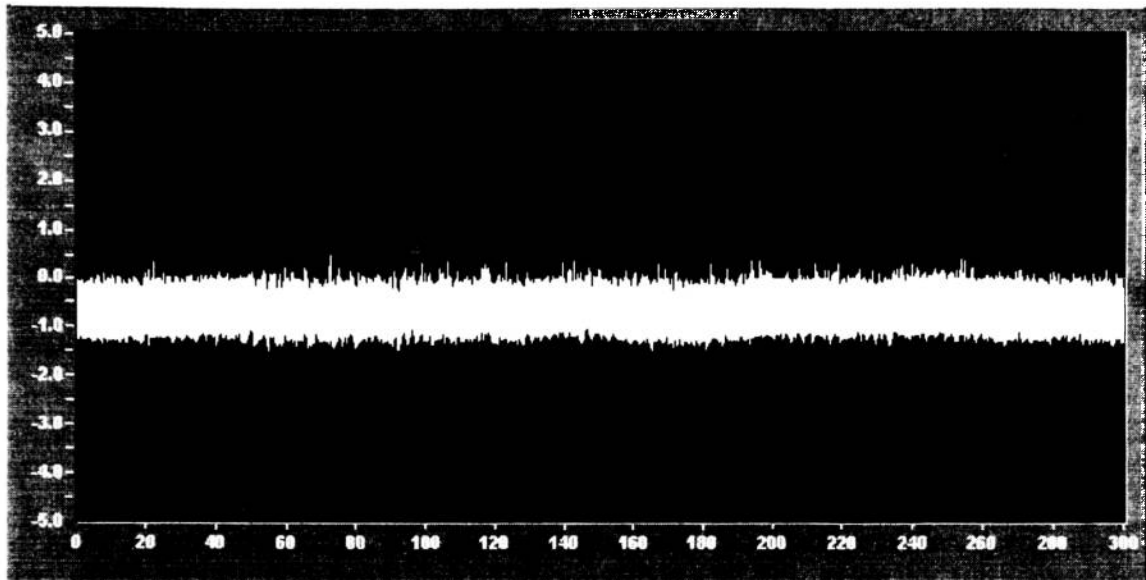


Figure 18. Smooth Air Horizontal Tail Strain Gage Time Domain

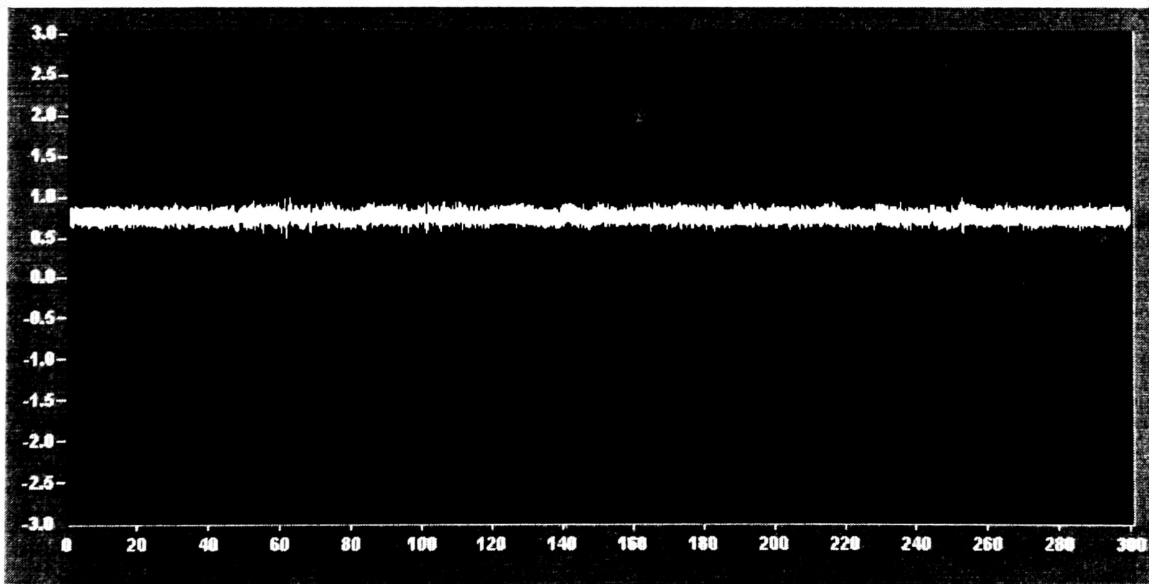


Figure 19. Smooth Air CG NZ Accelerometer Time Domain

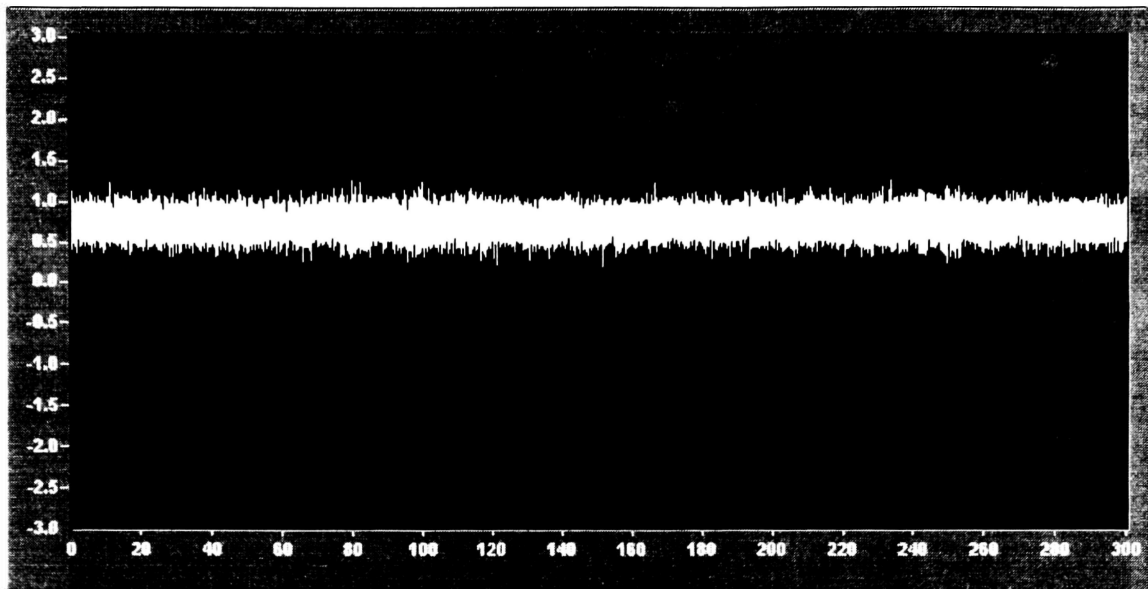


Figure 20. Smooth Air Horizontal Tail Accelerometer Time Domain

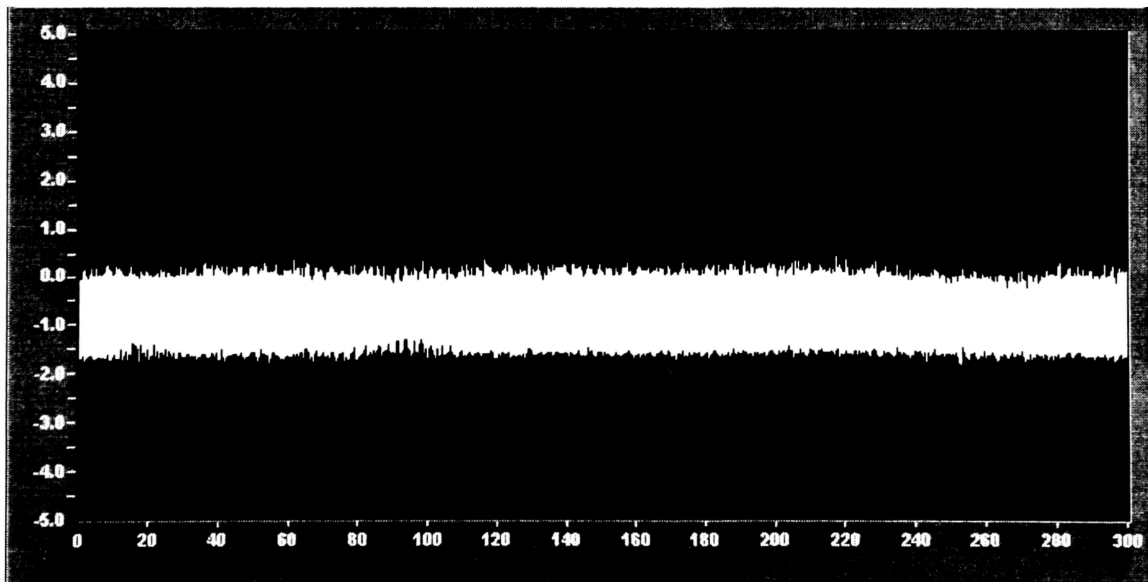


Figure 21. Smooth Air Vertical Tail Strain Gage Time Domain

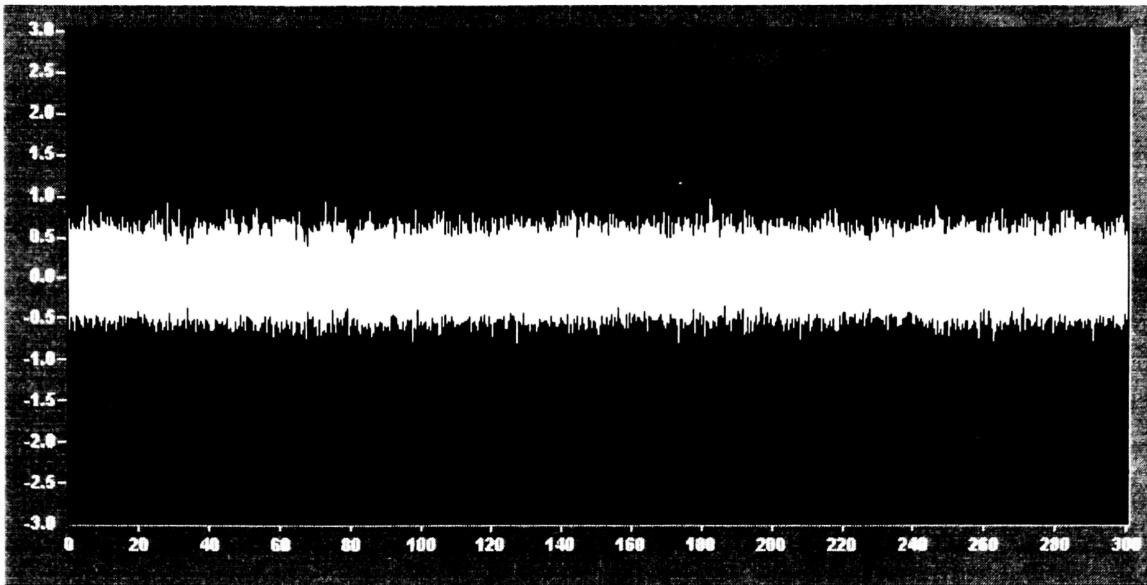


Figure 22. Smooth Air CG NY Accelerometer Time Domain

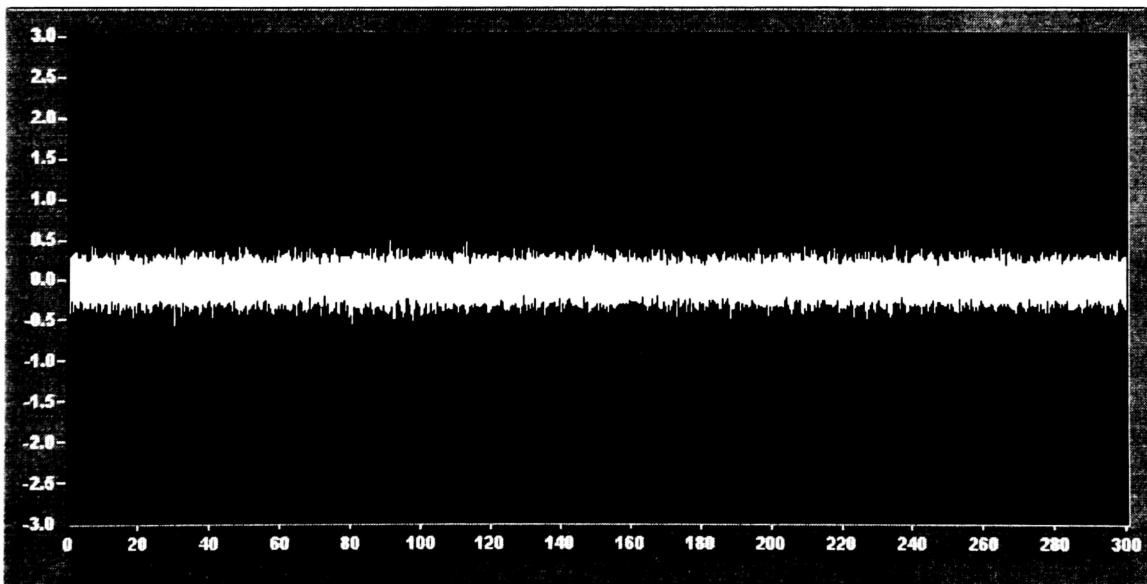


Figure 23. Smooth Air Vertical Tail Accelerometer Time Domain

4.3.2 SMOOTH AIR PSD DATA

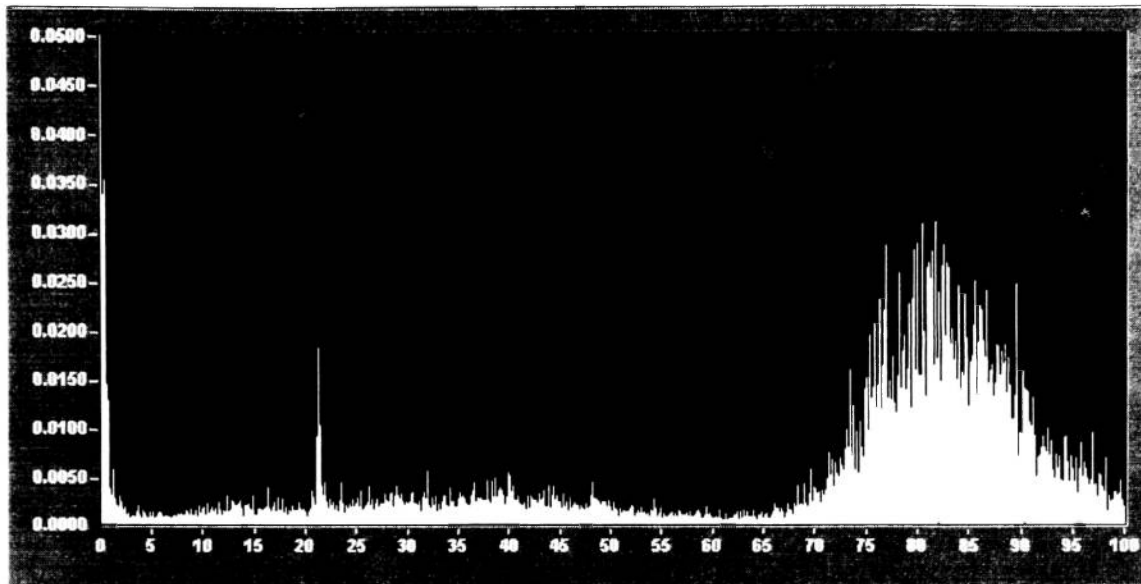


Figure 24. Smooth Air Horizontal Tail Strain Gage PSD

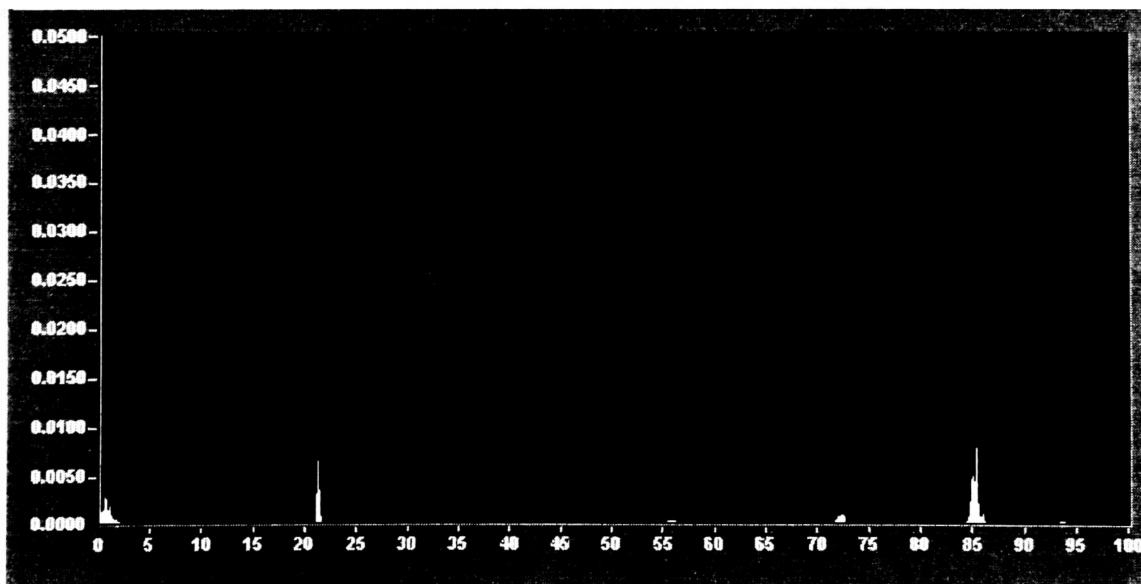


Figure 25. Smooth Air CG NZ Accelerometer PSD

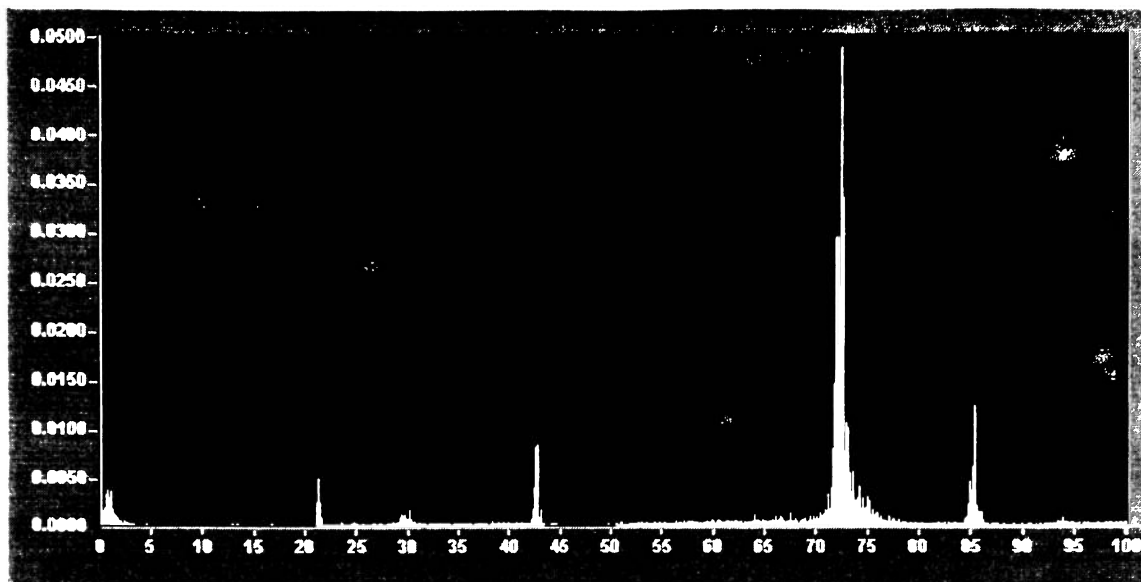


Figure 26. Smooth Air Horizontal Tail Accelerometer PSD

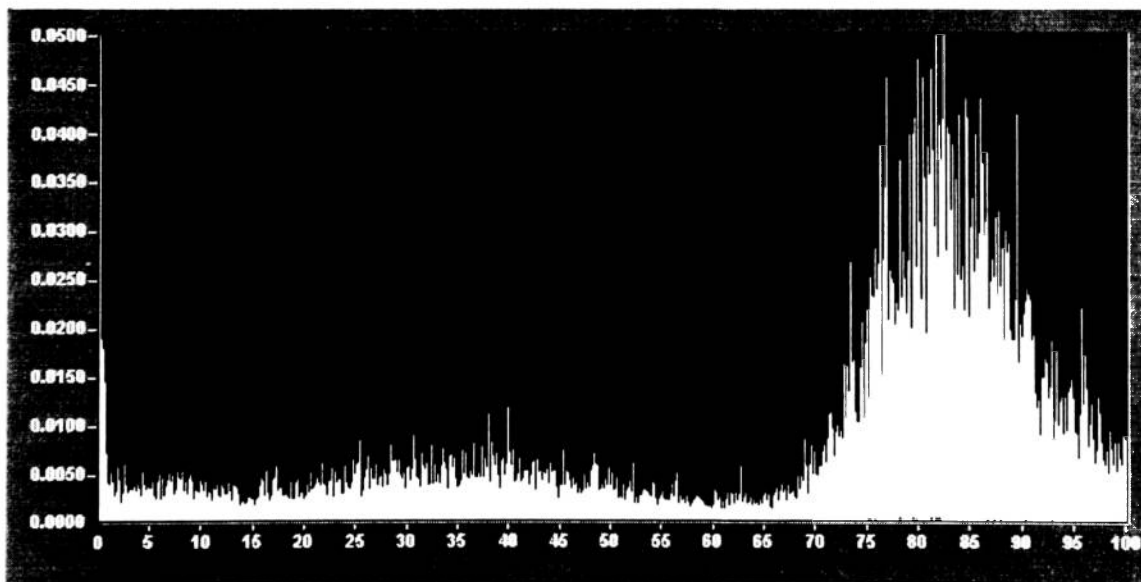


Figure 27. Smooth Air Vertical Tail Strain Gage PSD

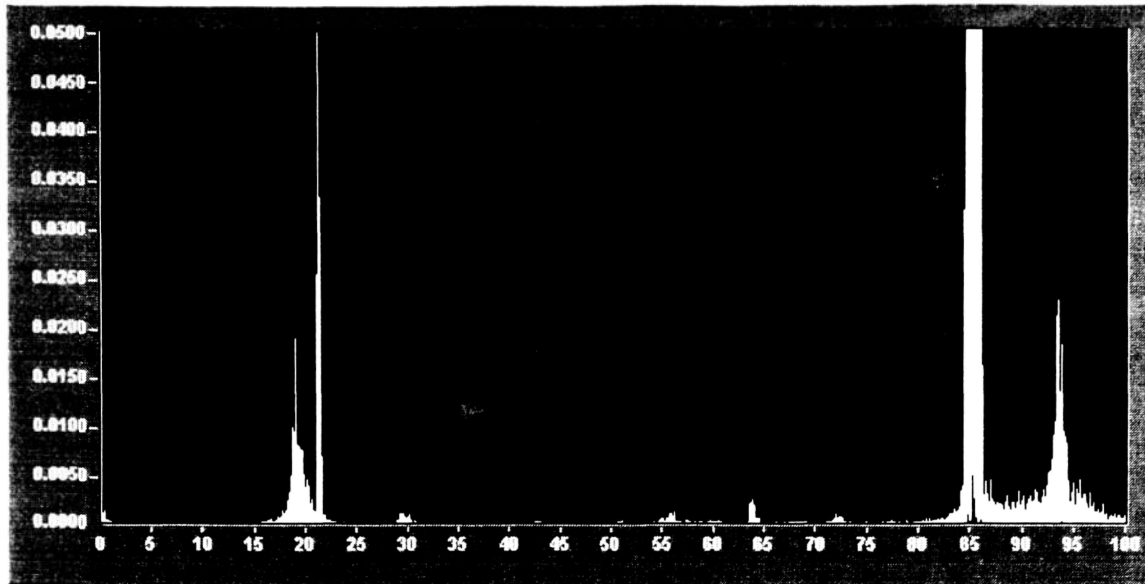


Figure 28. Smooth Air CG NY Accelerometer PSD

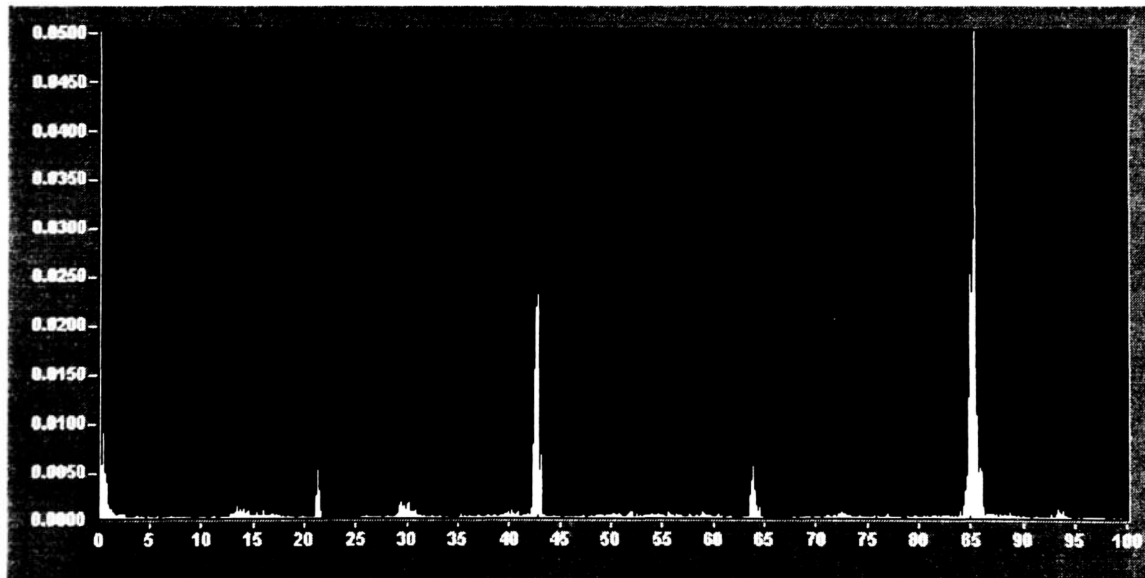


Figure 29. Smooth Air Vertical Tail Accelerometer PSD

4.3.3 TIME DOMAIN FOR GUSTY CONDITIONS IN THE Z-DIRECTION (VERTICAL GUST)

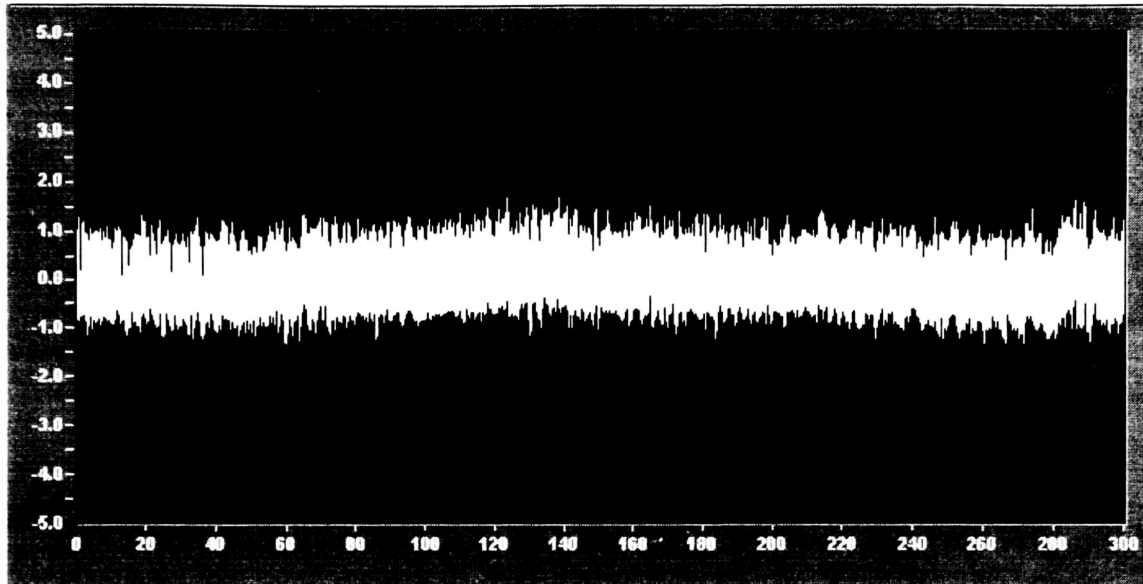


Figure 30. Z-Gust Horizontal Tail Strain Gage Time Domain

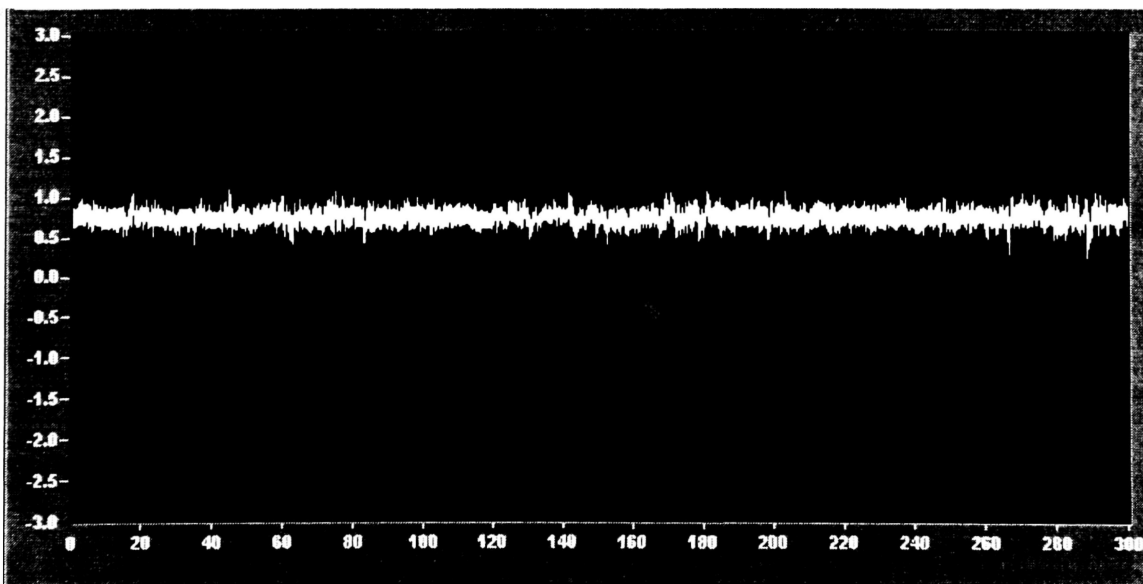


Figure 31. Z-Gust CG NZ Accelerometer Time Domain

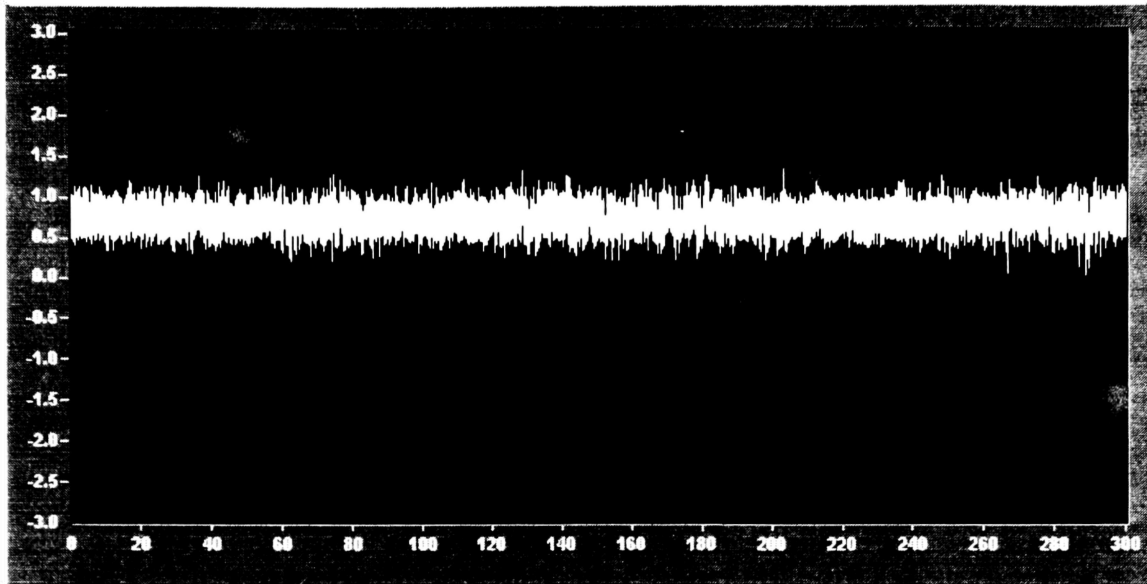


Figure 32. Z-Gust Horizontal Tail Accelerometer Time Domain

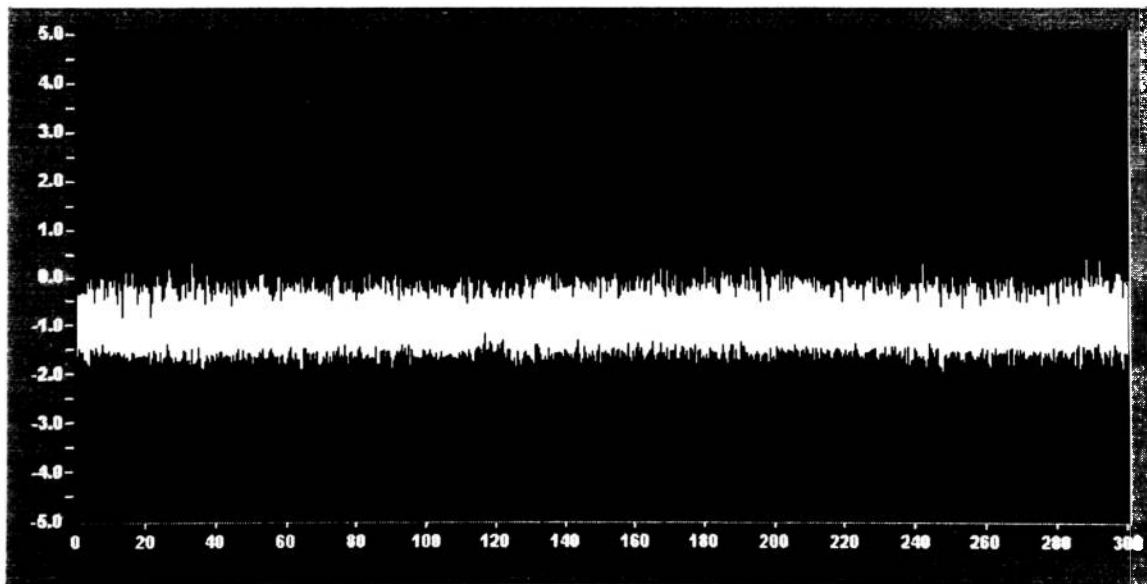


Figure 33. Z-Gust Vertical Tail Strain Gage Time Domain

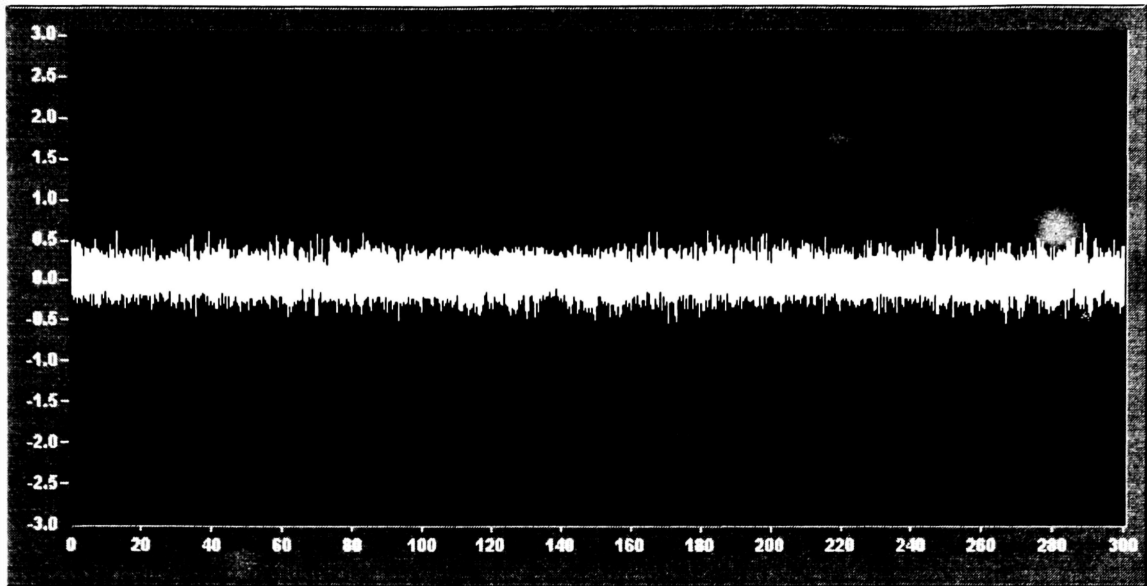


Figure 34. Z-Gust CG NY Accelerometer Time Domain

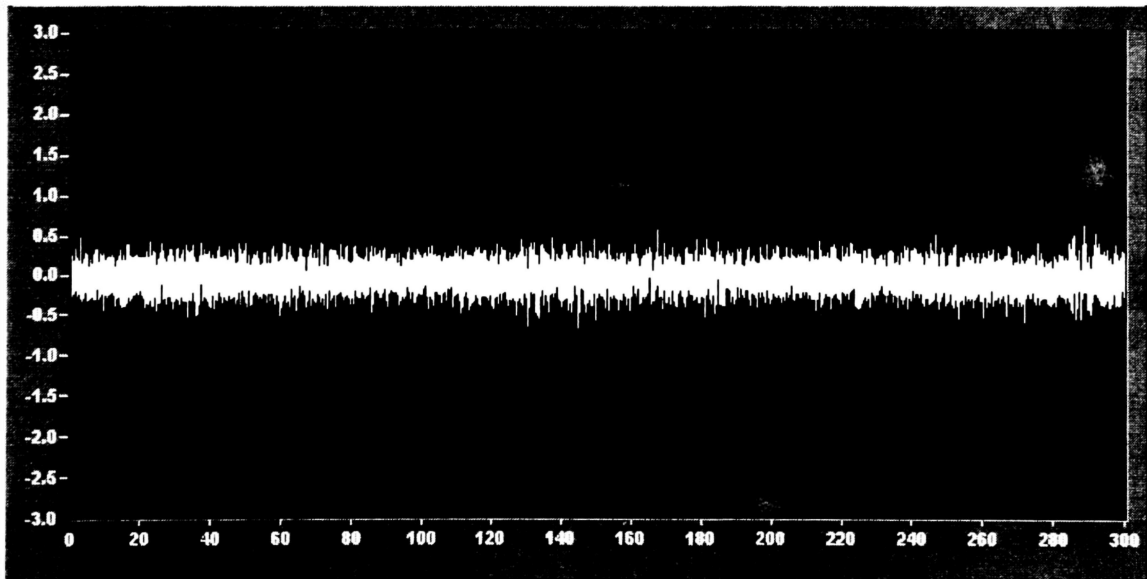


Figure 35. Z-Gust Vertical Tail Accelerometer Time Domain

4.3.4 PSD FOR GUSTY CONDITIONS IN THE Z-DIRECTION (VERTICAL GUST)

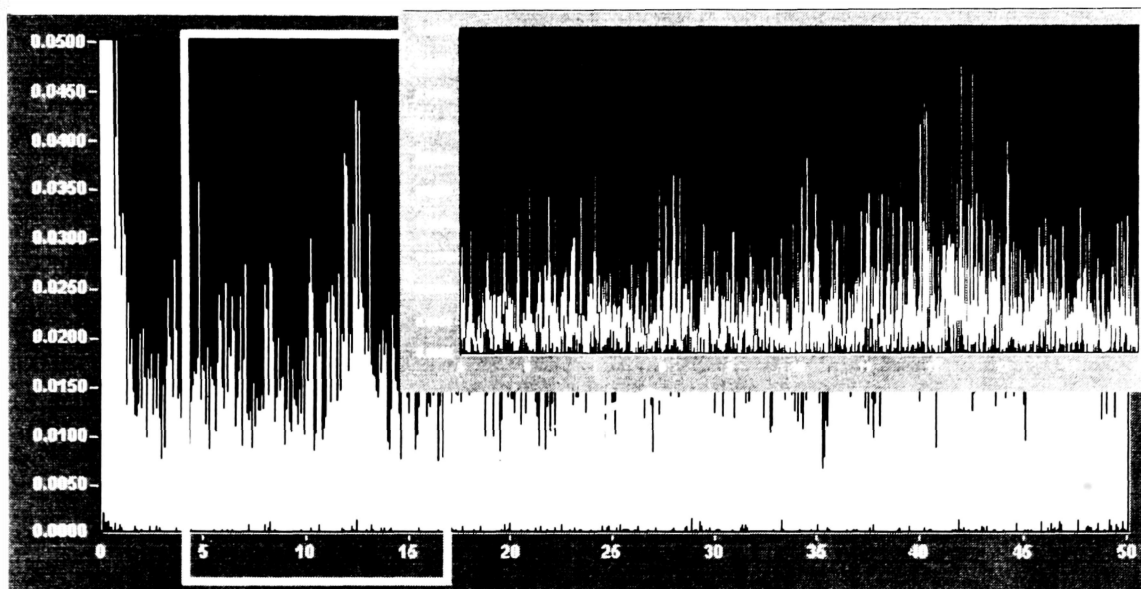


Figure 36. Z-Gust Horizontal Tail Strain Gage PSD

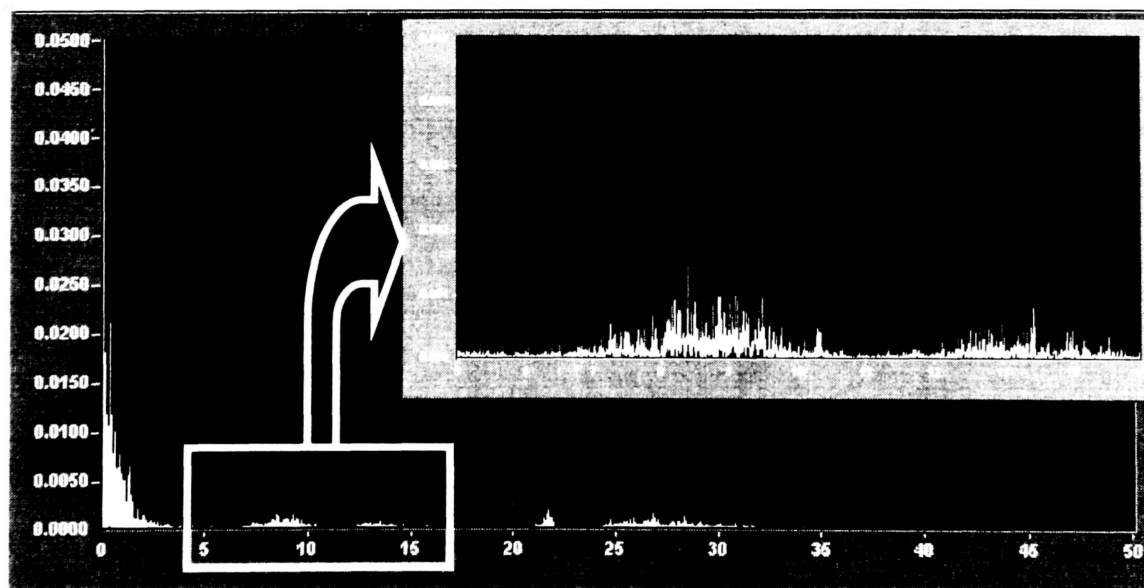


Figure 37. Z-Gust CG NZ Accelerometer PSD

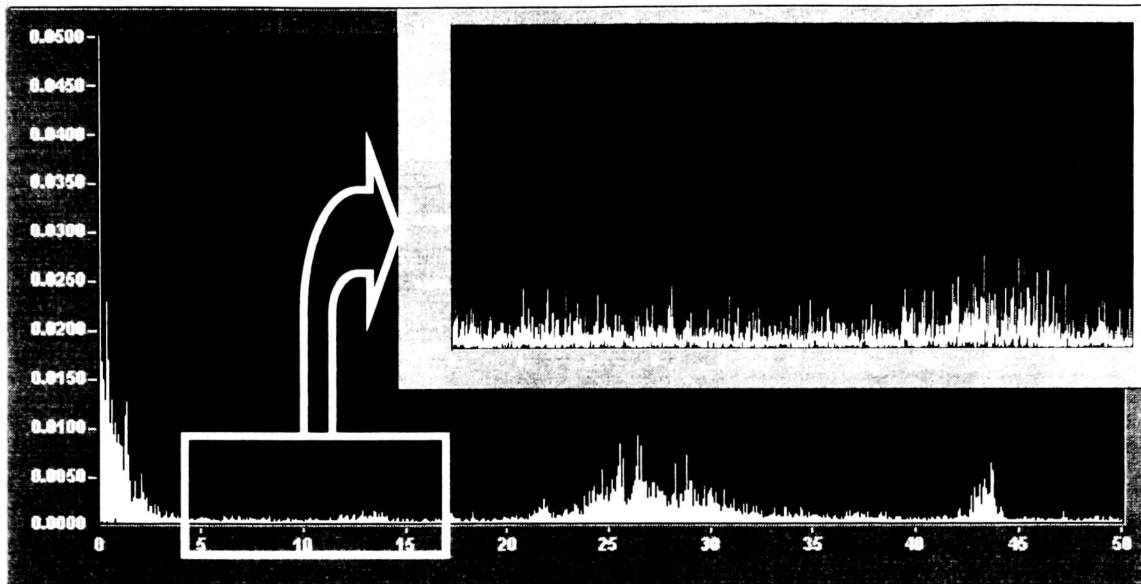


Figure 38. Z-Gust Horizontal Tail Accelerometer PSD

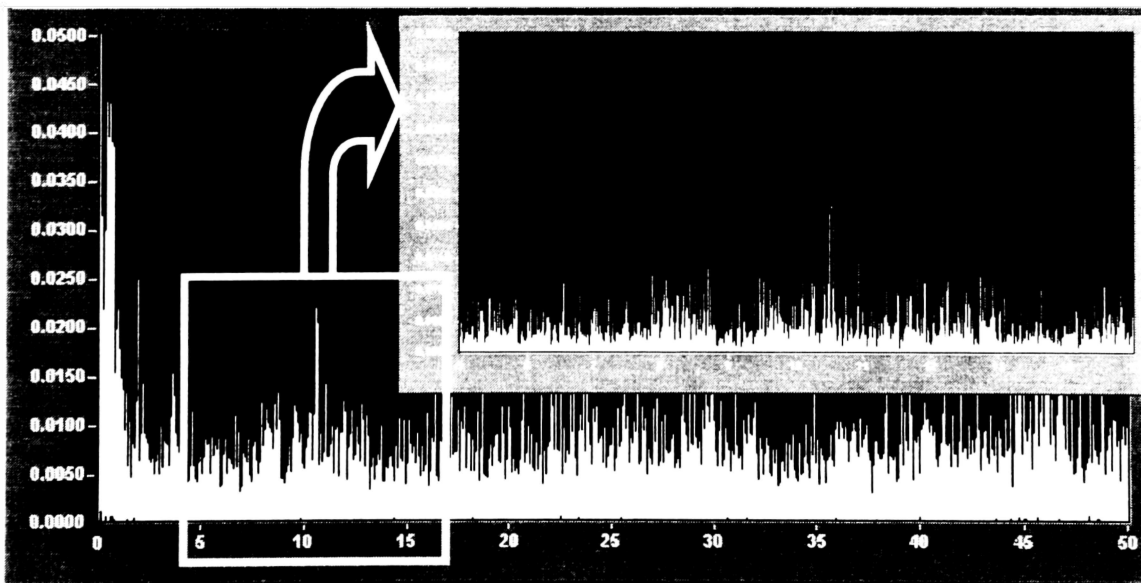


Figure 39. Z-Gust Vertical Tail Strain Gage PSD

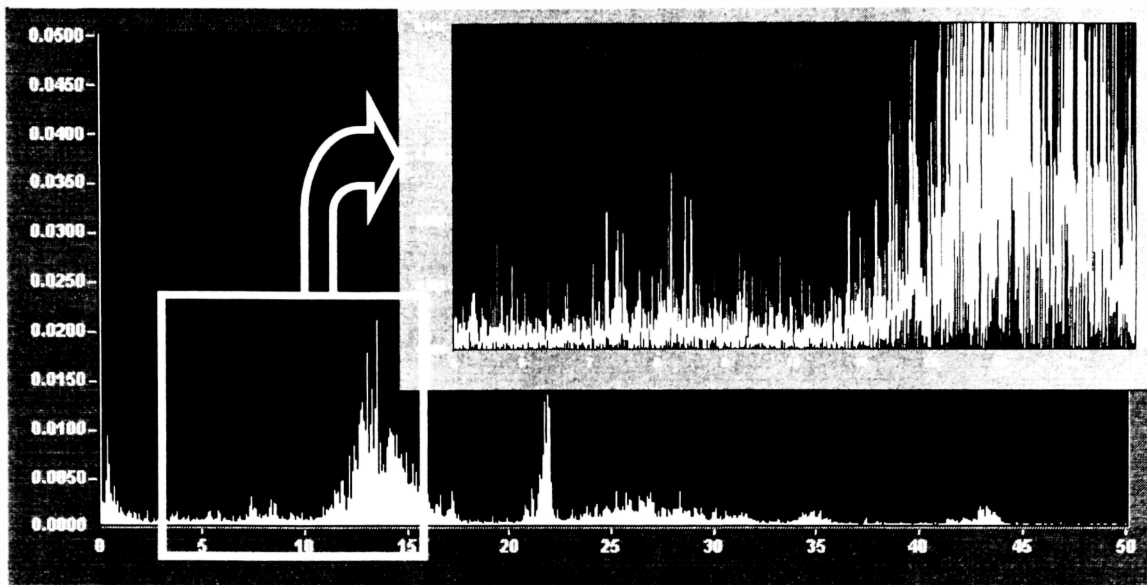


Figure 40. Z-Gust CG NY Accelerometer PSD

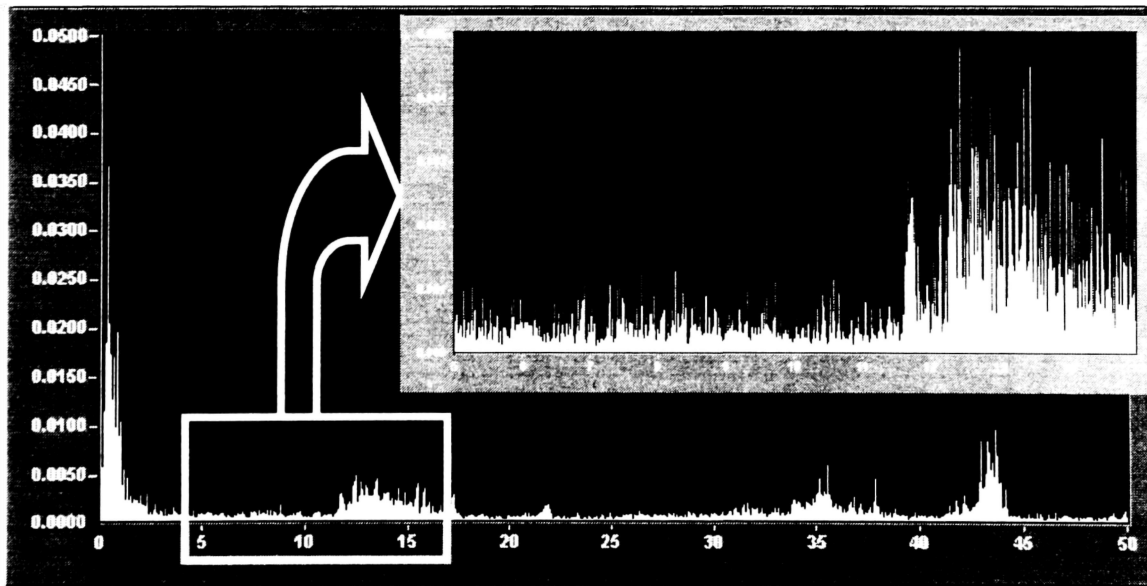


Figure 41. Z-Gust Vertical Tail Accelerometer PSD

4.3.5 TIME DOMAIN FOR GUSTY CONDITIONS IN THE Y-DIRECTION (LATERAL GUST)

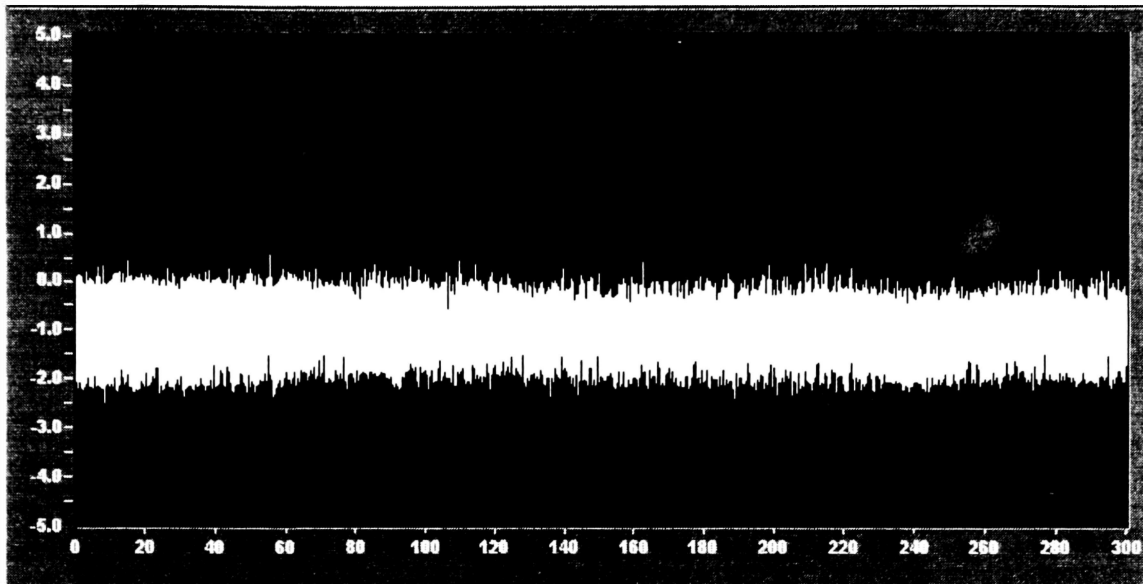


Figure 42. Y-Gust Horizontal Tail Strain Gage Time Domain

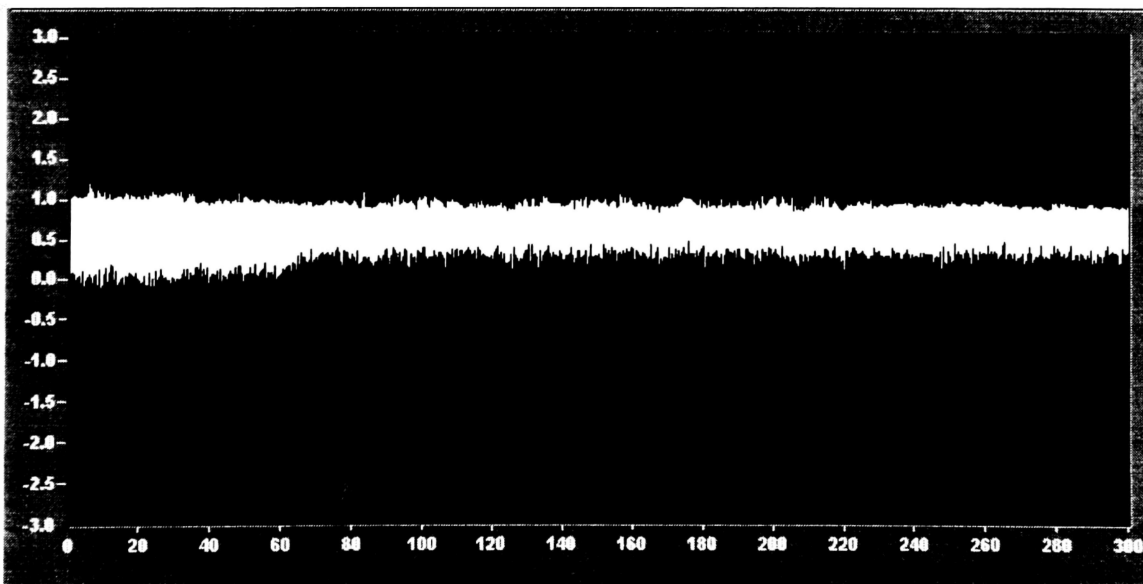


Figure 43. Y-Gust CG NZ Accelerometer Time Domain

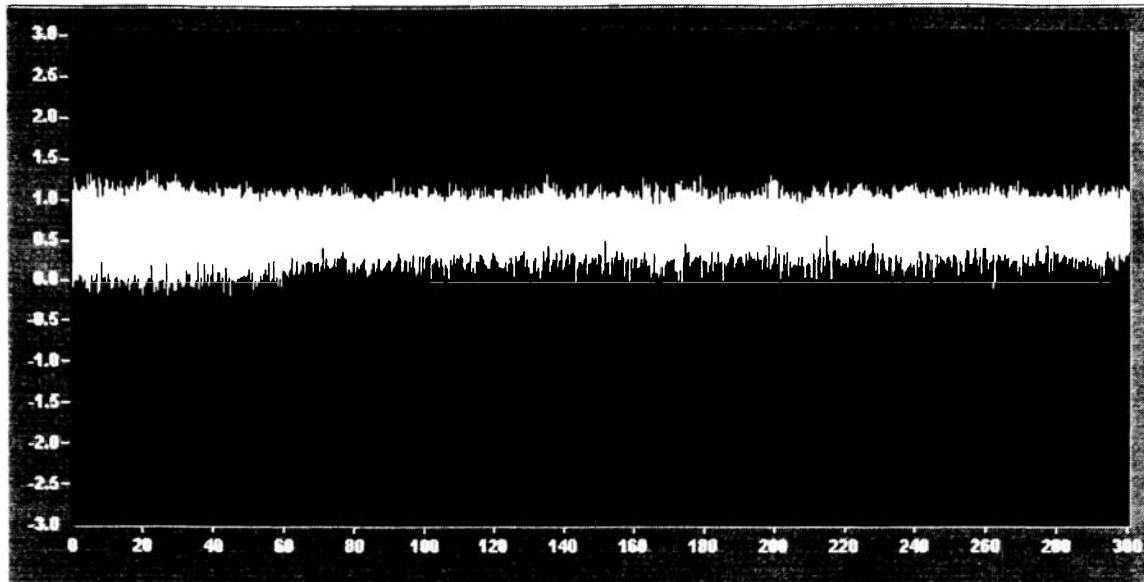


Figure 44. Y-Gust Horizontal Tail Accelerometer Time Domain

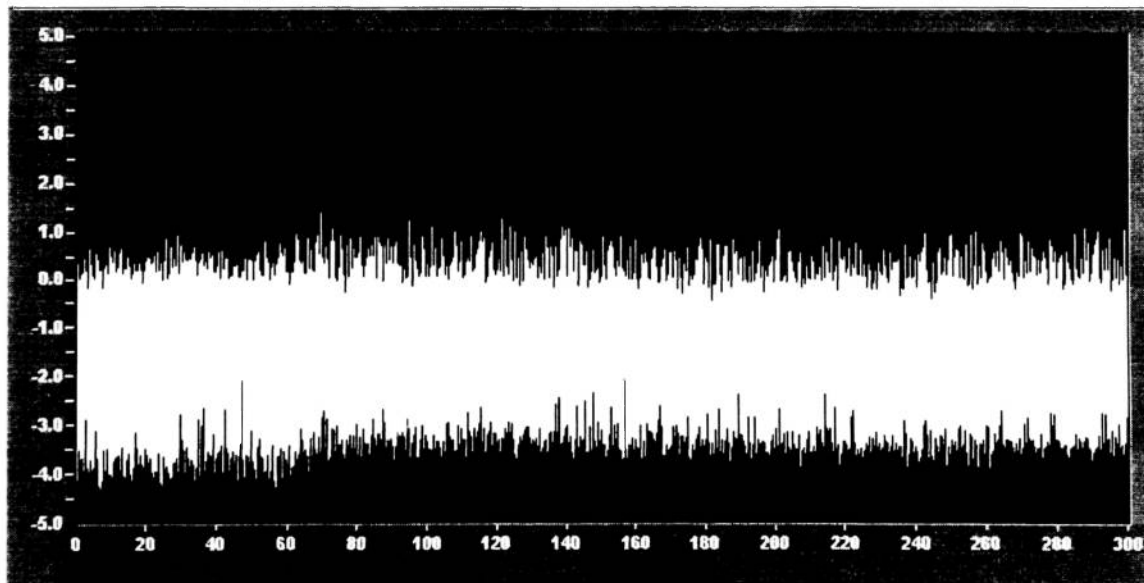


Figure 45. Y-Gust Vertical Tail Strain Gage Time Domain

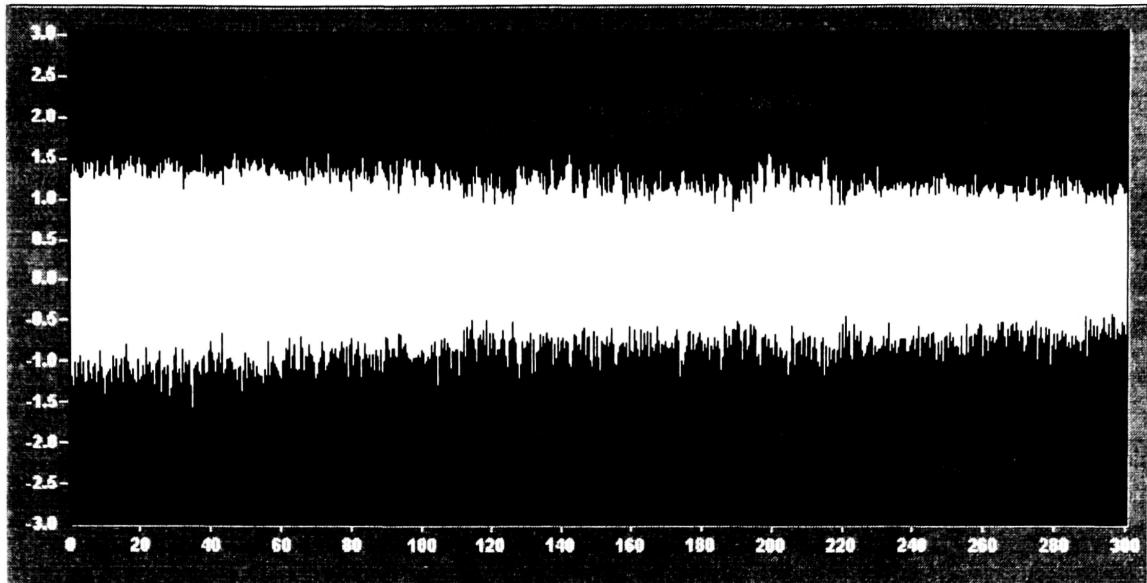


Figure 46. Y-Gust CG NY Accelerometer Time Domain

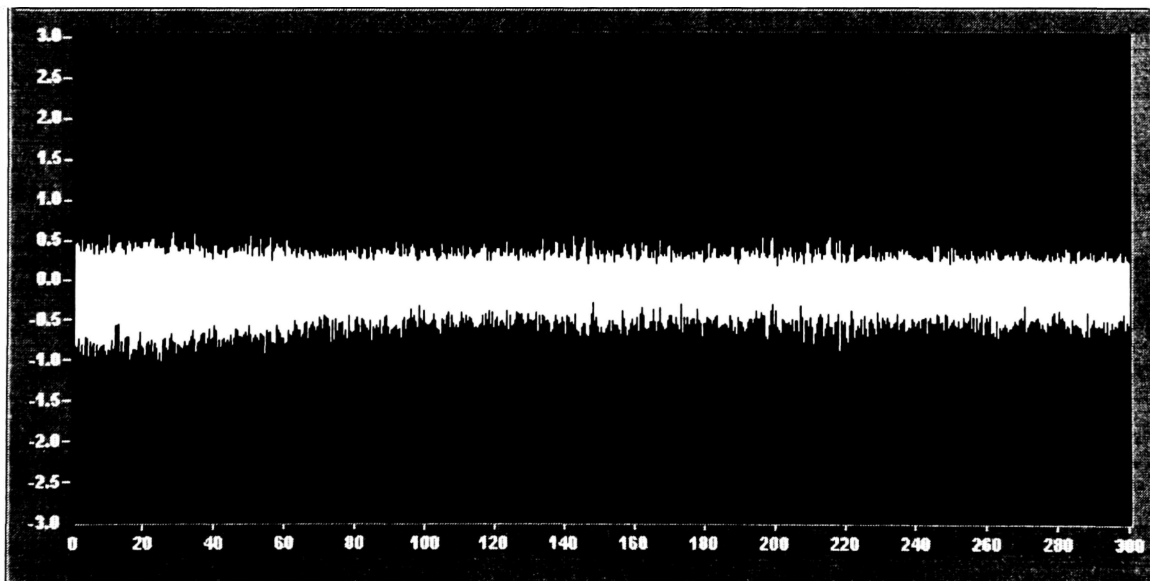


Figure 47. Y-Gust Vertical Tail Accelerometer Time Domain

4.3.6 PSD FOR GUSTY CONDITIONS IN THE Y-DIRECTION (LATERAL GUST)

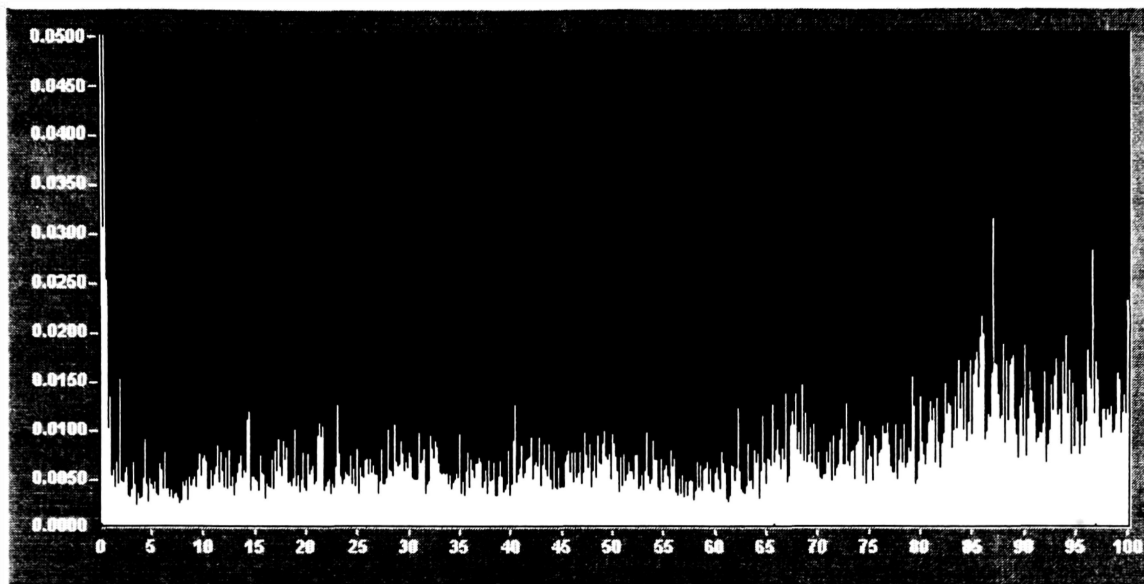


Figure 48. Y-Gust Horizontal Tail Strain Gage PSD

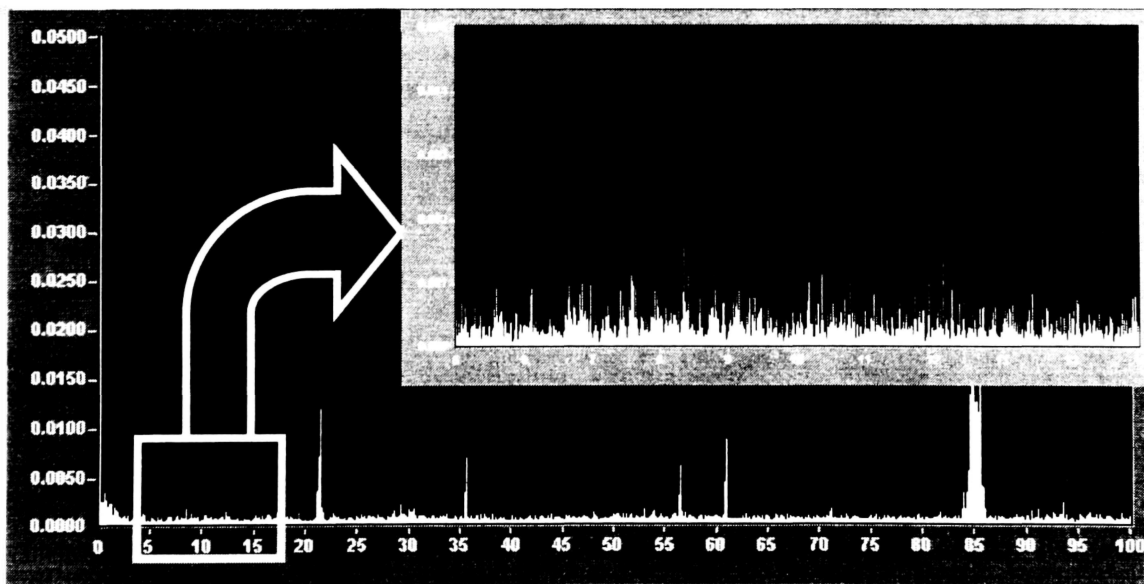


Figure 49. Y-Gust CG NZ Accelerometer PSD

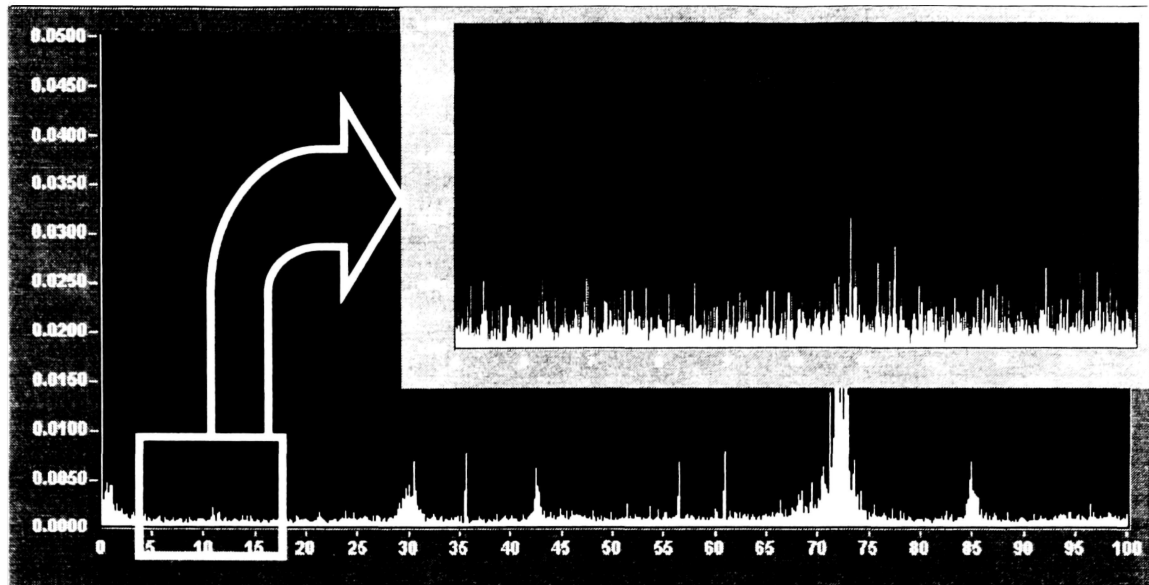


Figure 50. Y-Gust Horizontal Tail Accelerometer PSD

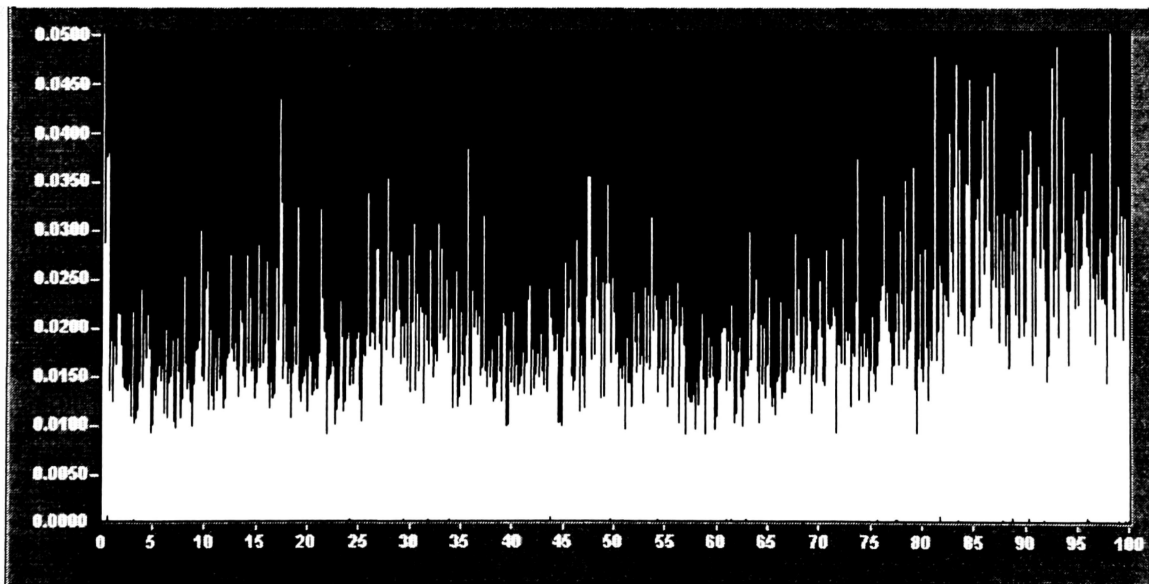


Figure 51. Y-Gust Vertical Tail Strain Gage PSD

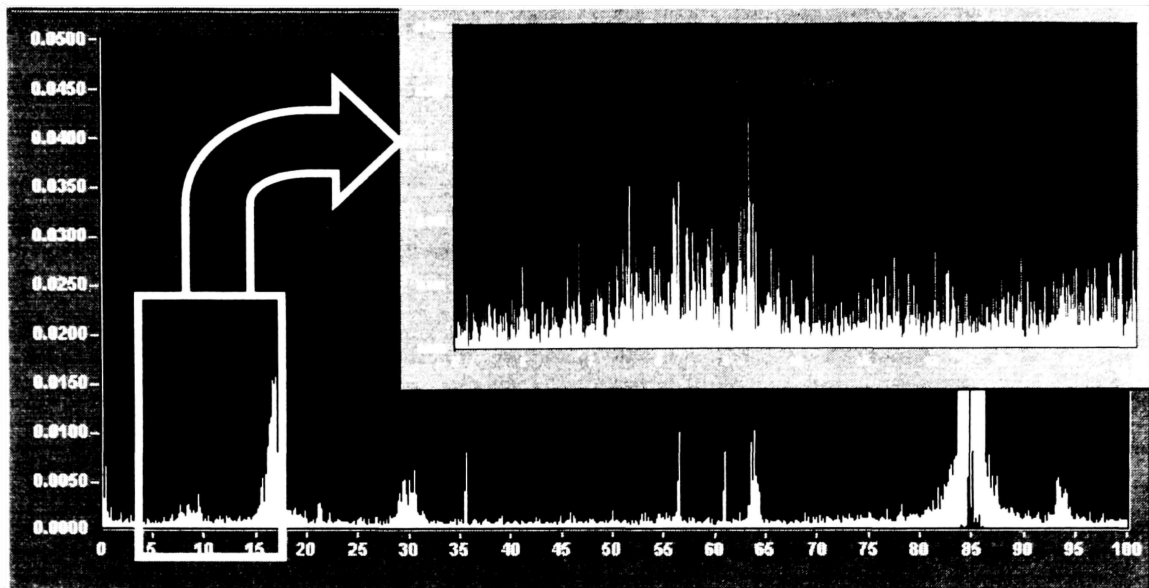


Figure 52. Y-Gust CG NY Accelerometer PSD

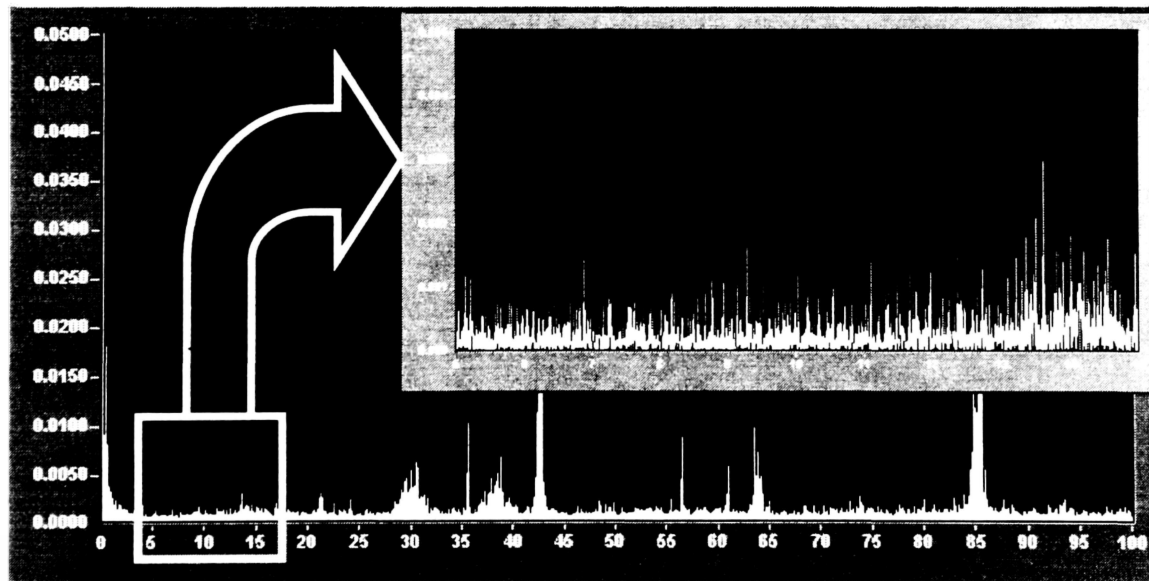


Figure 53. Y-Gust Vertical Tail Accelerometer PSD

4.3.7 TIME DOMAIN FOR MANEUVER DATA

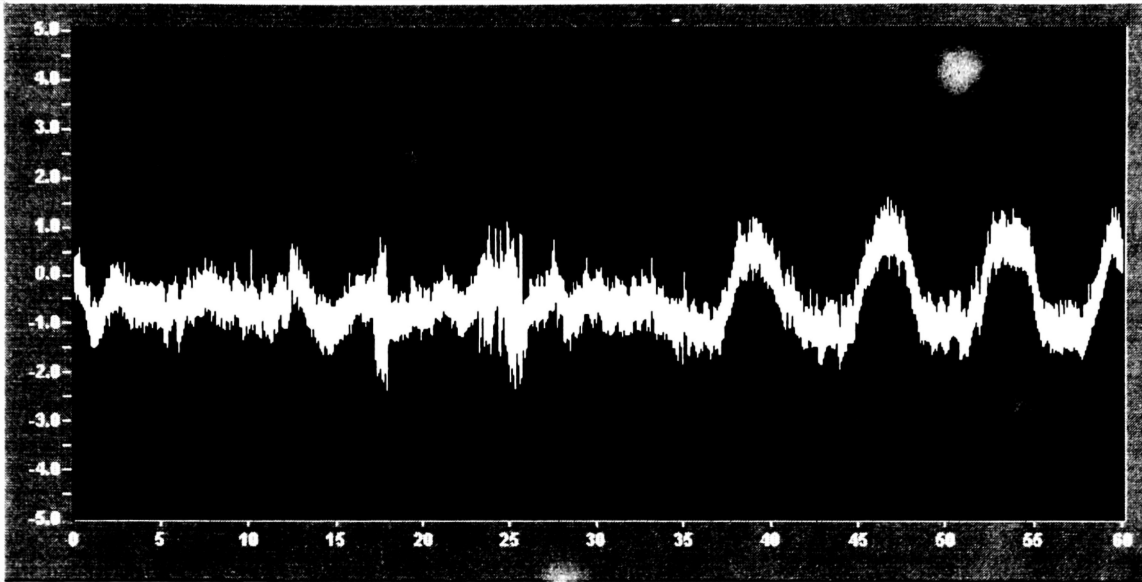


Figure 54. Maneuver Horizontal Tail Strain Gage Time Domain

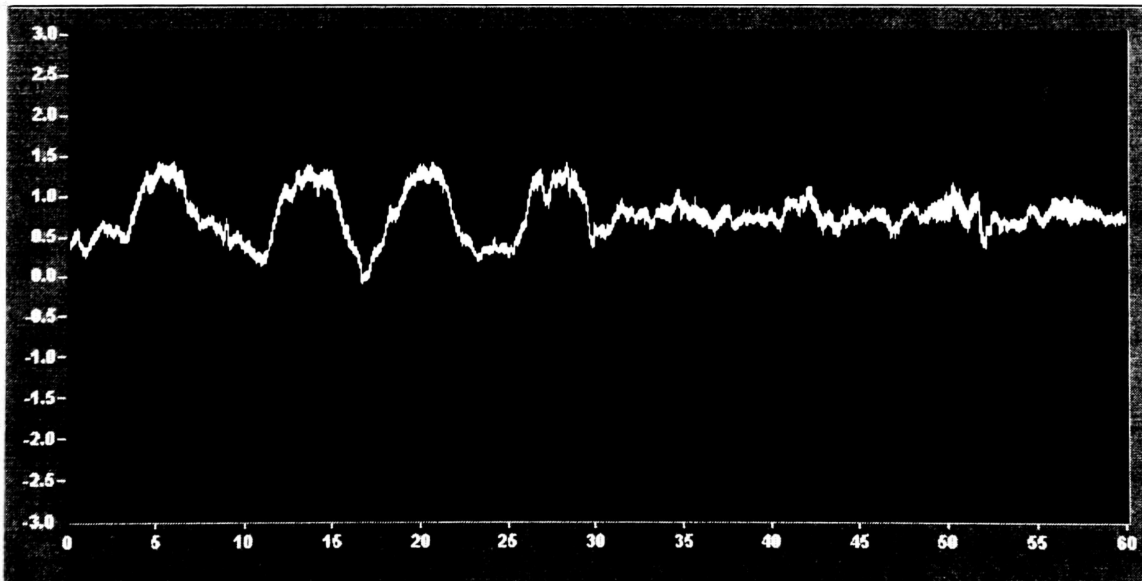


Figure 55. Maneuver CG NZ Accelerometer Time Domain

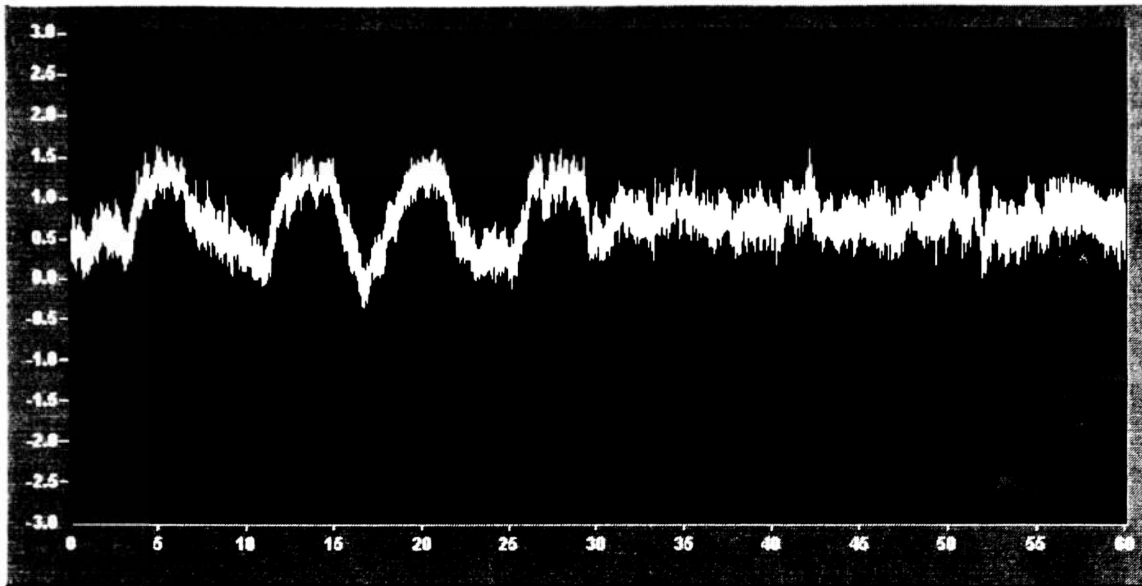


Figure 56. Maneuver Horizontal Tail Accelerometer Time Domain

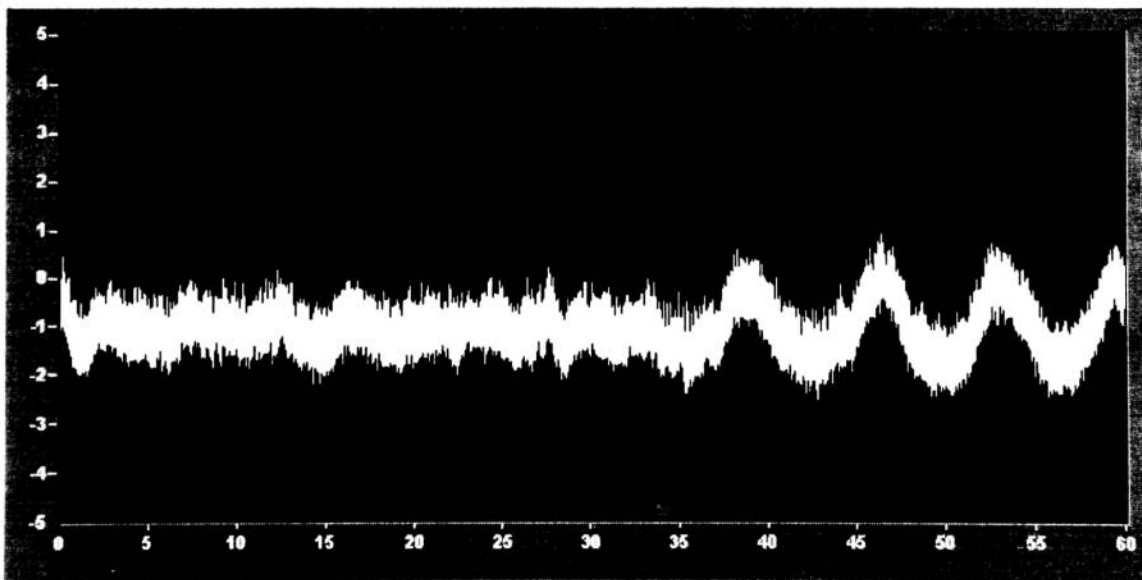


Figure 57. Maneuver Vertical Tail Strain Gage Time Domain

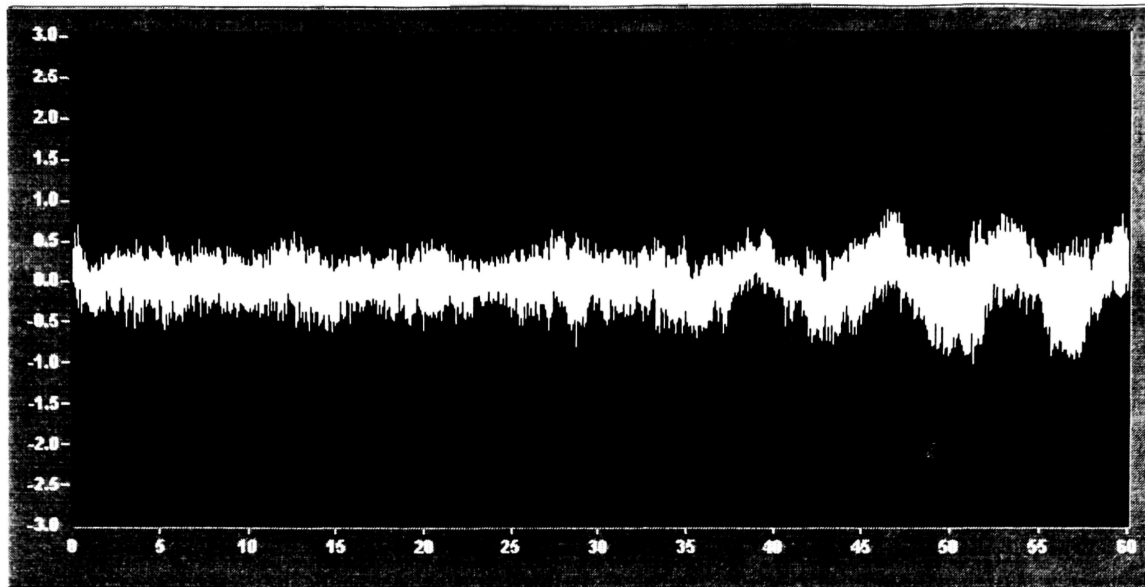


Figure 58. Maneuver CG NY Accelerometer Time Domain

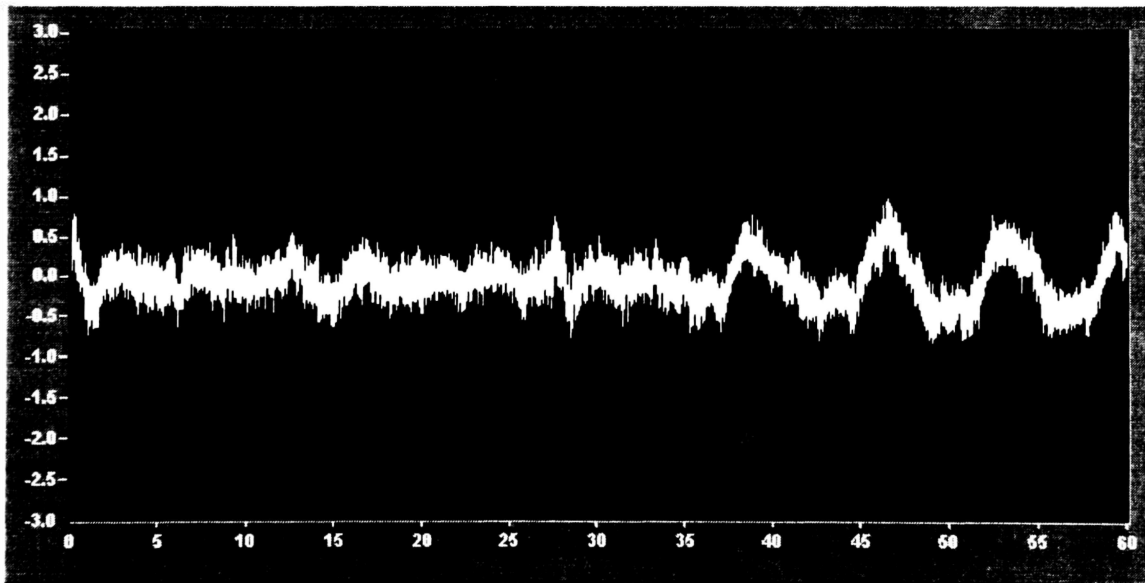


Figure 59. Maneuver Vertical Tail Accelerometer Time Domain

4.3.8 PSD FOR MANEUVER DATA

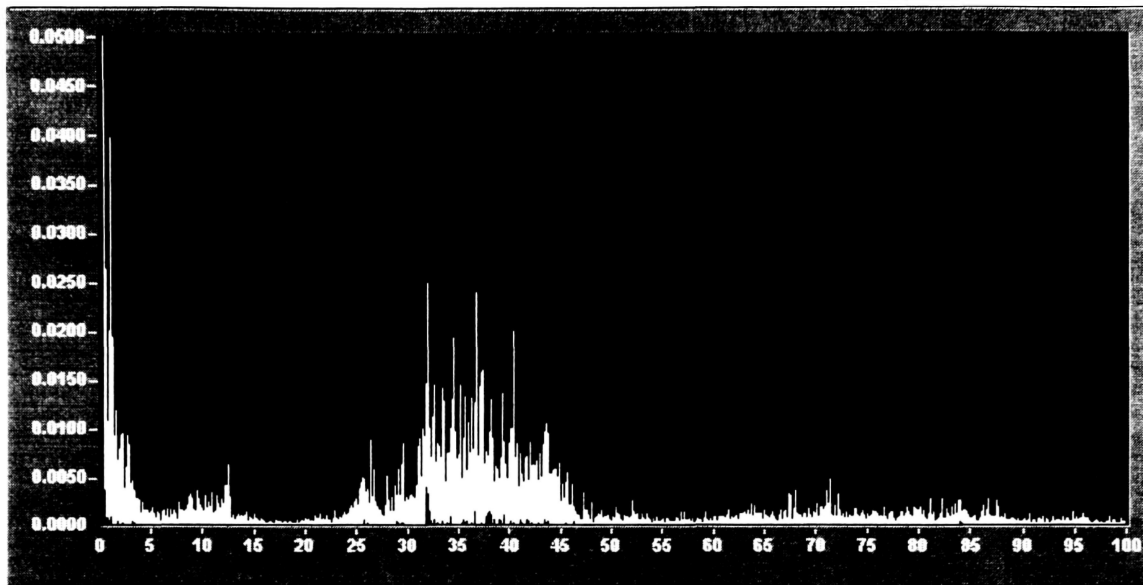


Figure 60. Maneuver Horizontal Tail Strain Gage PSD

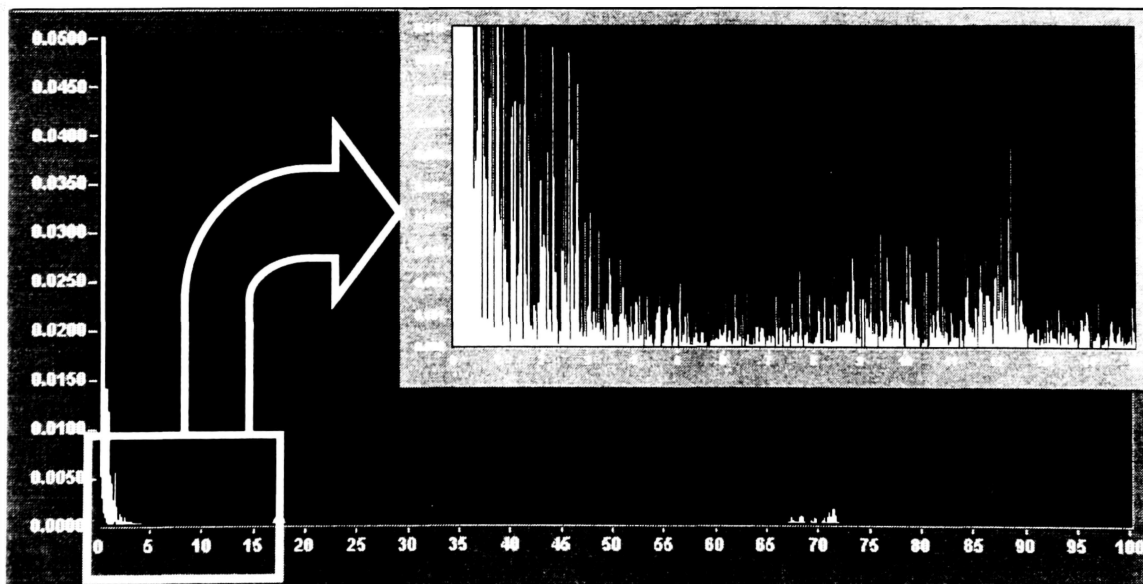


Figure 61. Maneuver CG NZ Accelerometer PSD

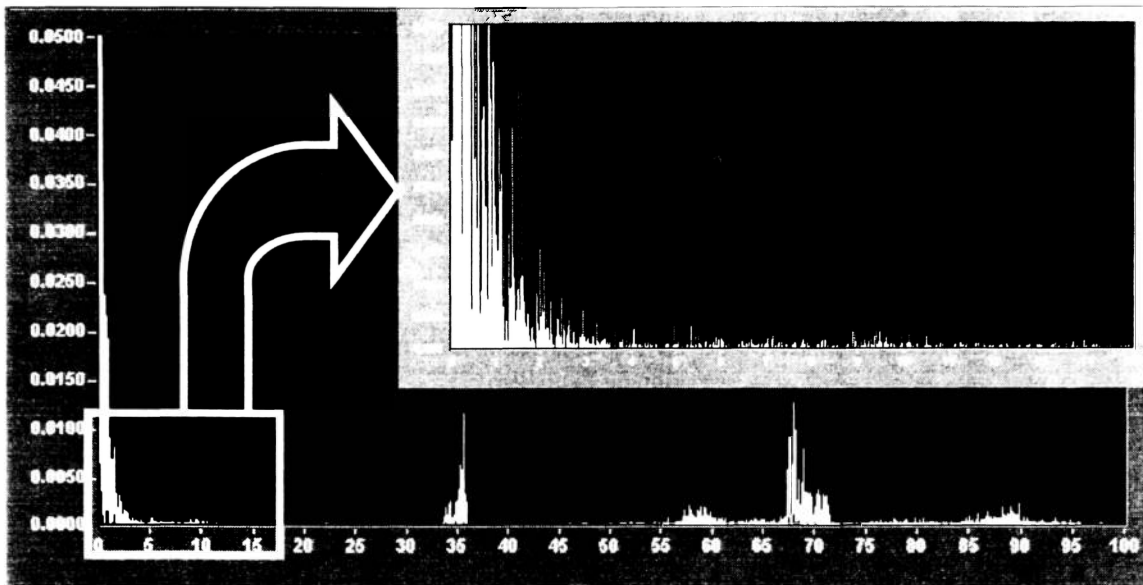


Figure 62. Maneuver Horizontal Tail Accelerometer PSD

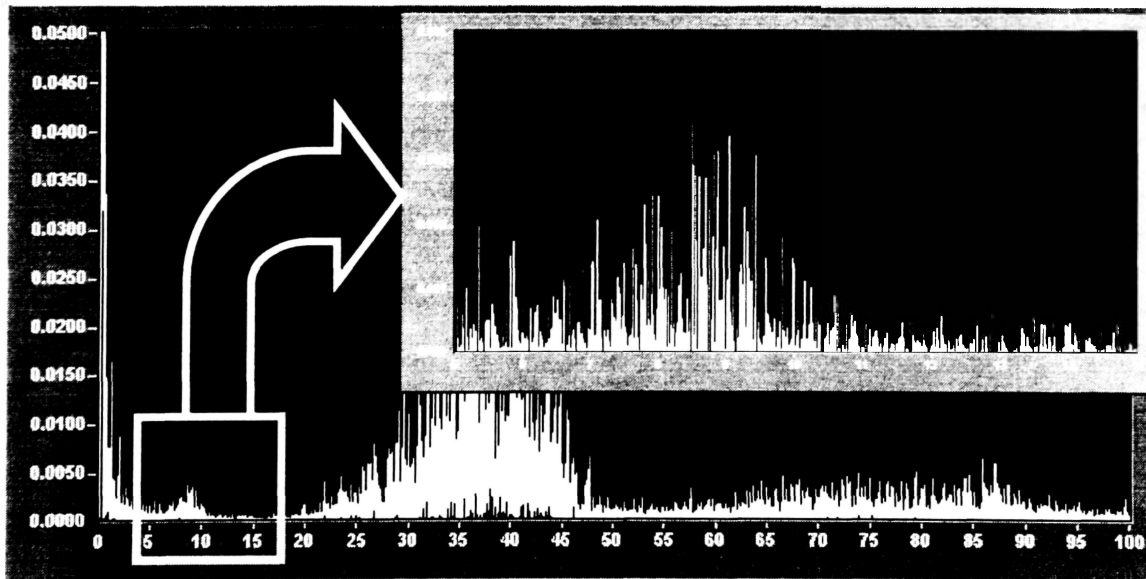


Figure 63. Maneuver Vertical Tail Strain Gage PSD

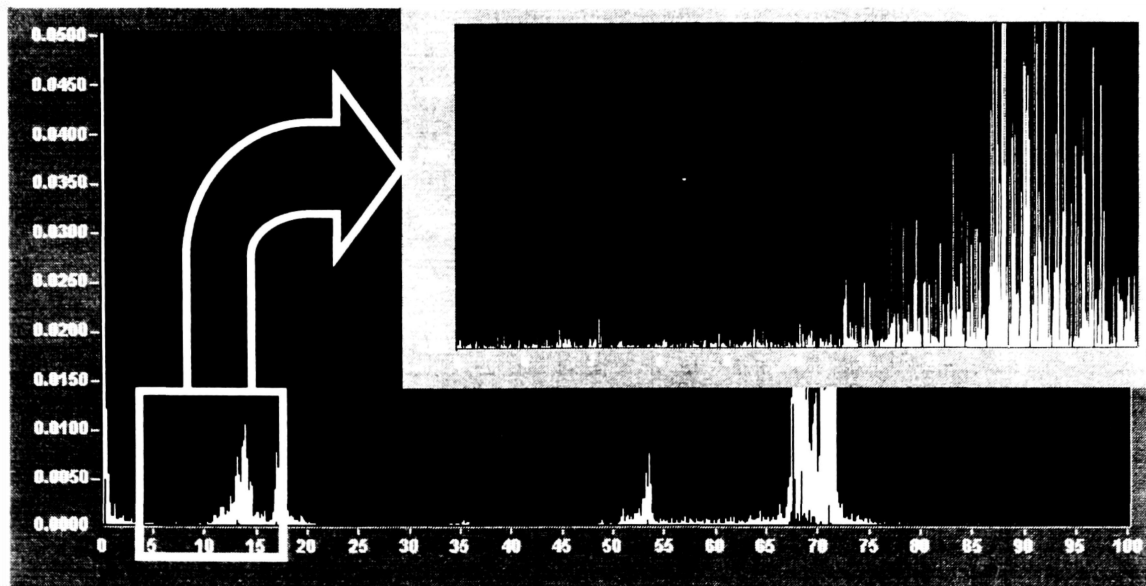


Figure 64. Maneuver CG NY Accelerometer PSD

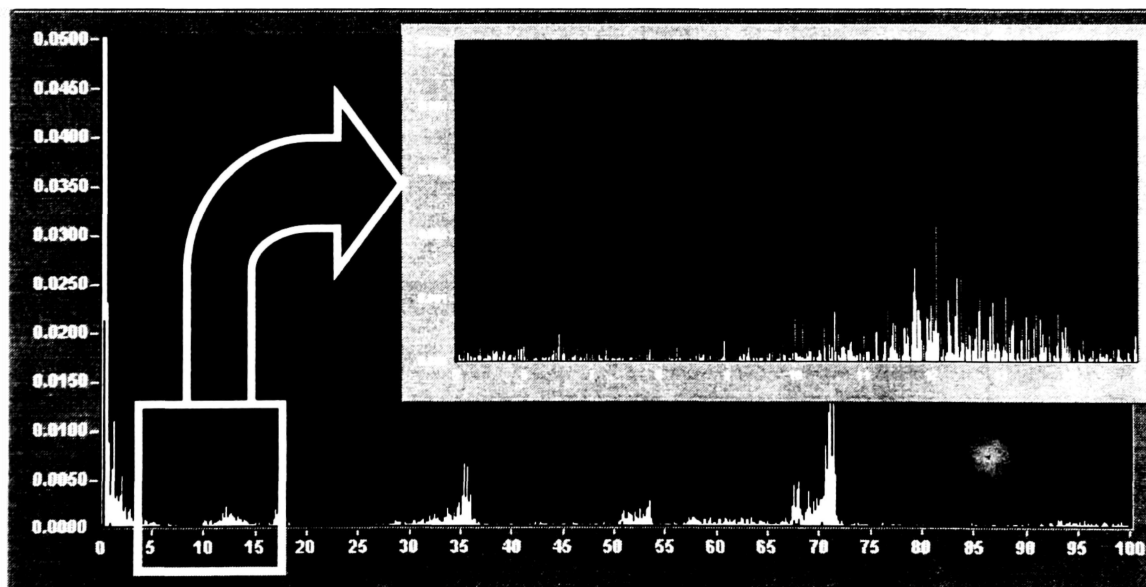


Figure 65. Maneuver Vertical Tail Accelerometer PSD

The research for gust was not limited to the above figures only. Many other PSD analyses were accomplished. Both gust in the z- and y- directions were studied.

4.3.9 GUST MAIN FREQUENCY RANGE

The PSD figures for the smooth air tend to be linear, with no particular fluctuations (except for the peaks characteristic of noise as stated earlier in this research). The gusty conditions, however, reveal some peaks located between 4 and 18 Hz, especially around 10 Hz. Without any doubt, and remembering the fact that the data were gathered during very gusty conditions, it can be said that those peaks are representative of gust.

4.3.9.a In the z-direction (Vertical Gust)

The above figures characteristic of turbulence in the z-direction (due to thermals) demonstrate the presence of gust around 8 to 10 Hz. This is much more noticeable on the CG NZ PSD signals. Indeed, a “Gaussian shape”, typical of gust, is clearly identifiable on the recorded CG NZ signal (figure 37), but is not as clearly apparent on the strain gage signal and horizontal Tail accelerometers and (figure 36 and 38). In the meantime, studies of the PSD for the y-channels (CG NY, Vertical Tail and Vertical Tail Strain gages) depict some peaks located between 7 and 8 Hz. Those peaks may be considered carefully since gust was recorded in Florida (z-direction). However, it may have been some structural resonance frequencies of the airplane.

4.3.9.b In the y-direction (Lateral Gust)

This previously stated frequency range is similar for gust in the y-direction. It confirms the hypothesis that gust is present within that range. Similarly, even if gust is recorded for one particular turbulence condition (y- for that case), some peaks are however noticeable on the z-direction, confirming the isotropy of a gust.

The “feeding” of the neural network requires that only the frequencies of interest be selected. Consequently, some macros were written in Visual Basic to facilitate this process. Those macros enabled a frequency cut-off (or a frequency band-pass cut). To ensure that the entire gust frequency range was selected, the band-pass frequency was initially set to 2-20 Hz. But, the lower limit was raised to 5 Hz due to some unexplained “noise” that can be seen on the figures of interest. And since it was initially thought that the gust may excite the first structural resonance and that this frequency may be included in the band pass used to predict the gust induced loads, the upper limit of the band pass frequency was lowered from 20 to 15 Hz. Moreover, on the CG NY PSD signal for z-gust conditions, the Blade Passage Frequency can be noticed around 21 Hz (for 2520 RPM), but another peak is clearly identifiable near 15 Hz (figure 40). This peak is also present on all other PSD channels relative to the y-direction. After a thorough study, it has been concluded that this peak is not induced by either gust or maneuver. It is most likely due to aircraft structural excitations. The fact that this peak is not present on the z-direction channels allowed us to think that it might come from spiraling slipstream (asymmetric buffet) induced by the propeller that envelops the entire aircraft and hits the left side of the vertical empennage. Nevertheless, this hypothesis needs to be validated but is beyond the scope of the current work.

Finally, the frequency range of interest was set to 5 – 15 Hz in order to get rid of the noise and for better predictions.

CHAPTER 5

NEURAL NETWORKS PROCEDURE

5.1 CHOICE OF THE NEURAL NETWORKS

The previous research, conducted for the prediction of loads induced by maneuvers, suggested that two different neural networks should be used for accurate predictions. In other words, one network for the horizontal tail and another one for the vertical tail were necessary to predict strains in the empennage structures. Consequently, the same procedure will be conducted for the prediction of gust loads in the vertical and horizontal tails

The decomposition in two neural networks required a separation between the signals collected. The first set contained the signals that were used in the prediction of the strain in the vertical tail while the second set included the signals used in the prediction of the strain in the horizontal tail. It was initially decided to train and test NN with the PSD files and depending on the accuracy of the results, i.e., the correlation, the usage of the time domain would be considered. The PSD analysis of the angular accelerometers was much clearer than the one for the rate gyroscopes, i.e. a gust peak was much more noticeable and the channel was much less noisy. Consequently, for the feeding of the NN, the angular accelerometer values (pitch, roll and yaw) would serve to ‘feed’ the network. If successful, rate gyro signals would be differentiated to obtain accelerations (actually angular accelerometers are expensive, not easy to install and Pechaud has already demonstrated the feasibility of this technique, as well as its advantages).

The following PSD signals were used as inputs for the prediction of the strains in the vertical tail:

- Frequency,
- CG NY,
- Tail NY
- Pitch Angular Acceleration
- Roll Angular Acceleration
- Yaw Angular Acceleration

Similarly, the same quantities were used for the strains' prediction in the horizontal tail:

- Frequency,
- CG NZ,
- Tail NZ
- Pitch Angular Acceleration
- Roll Angular Acceleration
- Yaw Angular Acceleration

The output signals were, respectively, the Vertical Tail Strain Gages and the Horizontal Strain Gages. Special care was taken to ensure that the full range of measured strains was represented within the training files, so that, the networks were able to well predict the testing files.

A second set of NN tests were performed, but this time using the time domain data. These values were initially filtered with a bandpass filter using DADiSP. The inputs for the NN were the same as the one mentioned previously but without the frequency.

The choice of a neural network type was driven by the fact that the relationship between the kinematical variables and the strains was unknown.

5.2 NEURAL NETWORKS SETUP

NeuralWorks Professional II+ (NW2) version 5.20 software was used for this research. This program could automatically generate a modular neural network from the specified parameters. For each 'bump' (or gust file) a file with seven (7) columns, six (6) for input and one (1) for the output, was defined to feed the NN. These files were built from the single channel PSD files obtained previously. Neural Networks Architecture requires a special configuration so that it will be able to identify the inputs and desired outputs (measured data). To avoid saturation of the Processing Elements (PE) the input data were scaled between some given values depending on the Transfer Function. In the case of back propagation applications, the hyperbolic tangent (TanH) function was recommended. Consequently, TanH was used in the following part of this research, but it required the data to be scaled between -1 and 1 . NW2 offers the possibility to scale automatically the data using the min-max table. This function was tested in previous research but appeared unsatisfactory since it was normalizing each column independently. Indeed, if normalization is conducted in this manner, the relative effect of the data is then changed. This would have lead to inappropriate results in term of flight dynamics.

It had been initially decided to study signals within the 5 - 15 Hz range. This interval selection was appropriate considering that gust loads seemed to be located around that range.

For the first part of this study, the input data-files did not have to be normalized since the PSD's between 5 and 15 Hz were already distributed between -1 and 1 (actually between 0 and 1 the PSD's being positive).

5.2.1 NEURAL NETWORKS PARAMETERS

The number of input layer neurons was initially set to 6. Further trials were needed to determine the minimum set of inputs required to accurately predict the strains. The number of neurons in the hidden layers was arbitrarily set to 5. However, most back propagation networks will have one or two layers. It has been decided to start with one hidden layer. A dichotomy method was used to define the best number of PE's when the performances start declining.

The Extended Delta-Bar-Delta (EDBD) learning rule was selected. This learning rule consists of a weight update rule and a learning rate update rule minimizing the convergence time. It automatically selects and adjusts the learning coefficient, coefficient ratio, the learning coefficient transition and the momentum term.

The epoch was set to 15 for the horizontal tail and 20 for the vertical tail (number based on previous research). Epoch is the number of sets of training data presented to the network (learning cycle) between weight updates. If the epoch checked box is selected, values gathered by the probe are combined across the probe component and over the number of cycles set by the epoch.

The F'offset has been set to 0.3 for a TANH activation function, as suggested by the NeuralWorks User's Guide and by previous research [17]. This value is a constant added to the value of the derivative of the neuron activation function (TANH for our case) during training in order to prevent neuron saturation.

- Monitoring instruments:

The root mean square error criterion calculates the RMS error between the target outputs. It adds up the squares of the errors for each node in the output layer, divides by the number of nodes in the output layer to obtain an average, and then takes the square root of that average. The confusion matrix is the square matrix whose rows and columns represent the sub-range for the target and model outputs respectively. The idea is to develop a network with a value of 1 on the diagonal running from lower left to upper right, and 0 elsewhere.

CHAPTER 6

ANALYSIS OF RESULTS

6.1 PRELIMINARIES

The ideal networks would allow the prediction of gust loads with very good accuracy. However, “accuracy” must be defined in term of structural analysis. The main idea of this research was to determine the stresses on the empennage due to the accelerations (linear and angular) at a remote location such as the C.G.. This chapter states the criteria used to evaluate such predictions. Then the results obtained with NN are presented and analyzed.

6.1.1 INSIGNIFICANT STRESS REGION AND TOLERANCE BAND

The insignificant stress region is defined as the stress domain at which a material can withstand up to 10^7 cycles (for a given stress ratio) of stress reversal (repetition of loads or stresses or strains) without any failure. If any failure occurs after 10^7 cycles, the stress would then be considered as fatigue-stress (i.e. the stress causing fatigue). Empennage structures of the C-172 airplane are fabricated with 2024-T3 aluminum. Accordingly, based on the S-N curves (alternating or maximum stress versus number of cycles to failure) shown in figure 66, all stresses (or strains) lower than or equal to 1,000 p.s.i. (or $100 \mu\epsilon$, since $\sigma \text{ (p.s.i.)} = E \cdot \epsilon$, with $E = 10 \cdot 10^6 \text{ p.s.i.}$) are considered to be insignificant. Actually, the value of the minimum stress that causes fatigue damage is

5,000 p.s.i. for a full stress reversal [28]. However, since the strain gages are not located where the stresses are maximum and because the aircraft was not flown during extreme gust conditions (for safety reasons), a lower value of 1,000 p.s.i. (or $100 \mu\epsilon$) was chosen as the threshold value.

A second prediction criterion must be defined for the expected accuracy of the gust load predictions. The loads should be predicted at least within the tolerance of the 2024-T3 aluminum S-N curves since this data is used to evaluate the fatigue life of the horizontal and vertical tails (figure 66). The S-N curve of an AL2024-T3 Aluminum sheet is presented in figure 66. According to the MILITARY-HANDBOOK-5E [28], the S-N curves are plotted within 1,000 p.s.i. (or $100 \mu\epsilon$), therefore a tolerance band of ± 500 p.s.i. (or $50 \mu\epsilon$) was selected. Figure 67 presents the tolerance band and insignificant region based on the criteria.

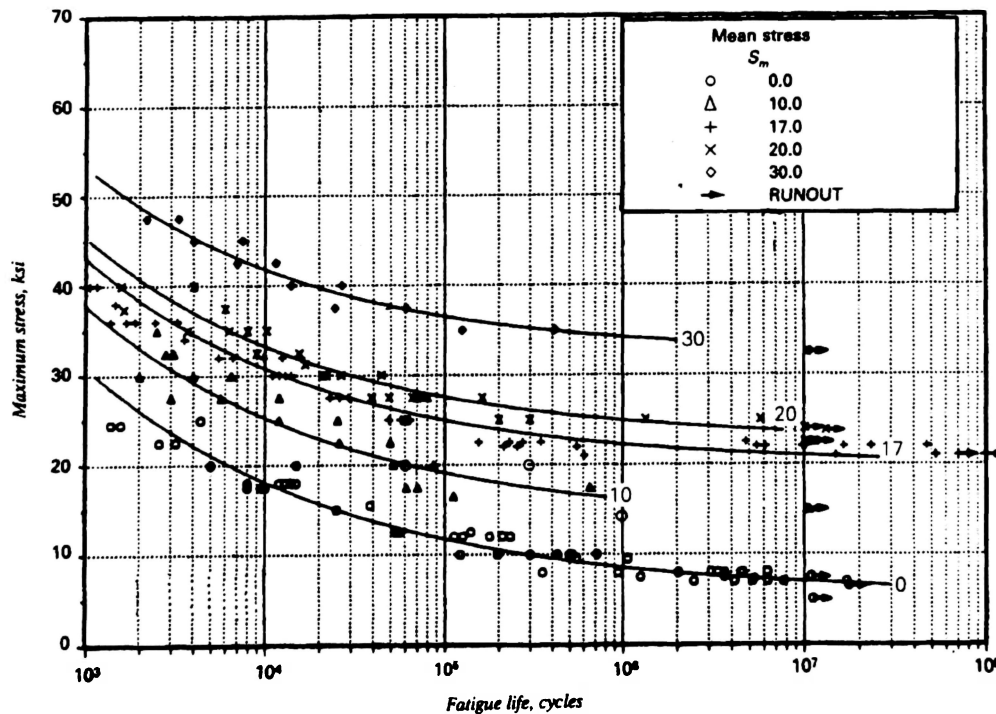


Figure 66. S-N Curve of an AL2024-T3 Aluminum Sheet [28]

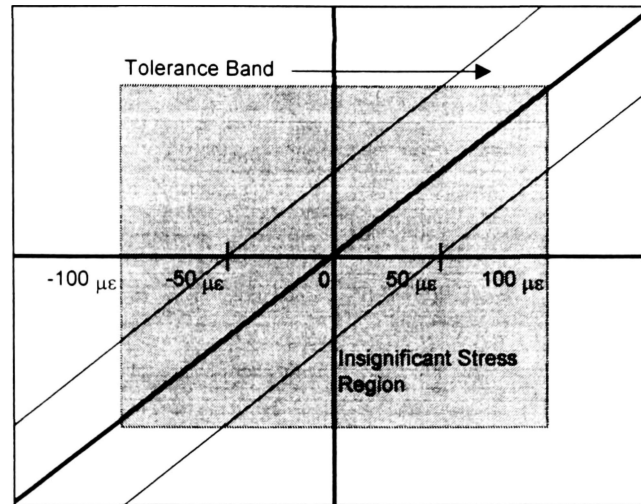


Figure 67. Tolerance Band and Insignificant Region

6.1.2 STRAIN AND STRESS CALCULATIONS

As previously mentioned, Daqbook was used to measure and record the flight parameters in volts. But in order to compare the predicted and measured strains together, one must first be able to calculate the different strains that are acting on the empennage. A conversion factor must then be applied to the data recorded from the strain gages. The gages have the following conversion factor:

$$(10.25 \text{ mV} / \text{V}) / 1000 \Rightarrow 97.560976 \mu\epsilon / \text{mV}$$

For example, for an input of 1 V, the output will be equal to 10.25 mV or 1000 $\mu\epsilon$.

The conversion factor to apply is the following:

$$X(\mu\epsilon) = \frac{V_{input}(\text{Volts}) \times 97.560976(\mu\epsilon)}{10^{-3}(\text{Volts})} \quad (\text{Equation 33})$$

But, the gain added by the data acquisition system between the inputs and the outputs must also be taken into account, they are:

- Gain for HT: 1430 (From Input in mV to Output in mV)
- Gain for VT: 1782 (From Input in mV to Output in mV)

In order to compare the magnitude of the gust and consequently the load induced on the empennage, the maximum and minimum stress values occurring during a flight were computed. Those values belonged to the 5-15 Hz range, accounting that this was the only frequency domain of interest for gust occurrence. Those results were not typical or just arbitrary. They were carefully considered. They are presented below:

Table 2

Maximum and Minimum Strain in $\mu\epsilon$ for Different Flight Conditions

	Horizontal Tail Strain			Vertical Tail Strain		
	Maximum	Minimum	Difference	Maximum	Minimum	Difference
Smooth Air	36	-102	138	20	-97	117
Bump A (z-direction)	84	-84	168	47	-68	115
Bump B (z-direction)	79	-72	151	43	-55	98
Bump C (z-direction)	62	-76	138	37	-68	105
Bump D (y-direction)	38	-169	207	75	-235	310
Bump E (y-direction)	54	-157	211	26	-140	166
Maneuver A	133	-160	293	66	-146	212
Maneuver B	133	-148	281	67	-146	213

The smooth air data have been recorded in October while flying in very smooth air condition in the southern part of Florida. Bumps A, B and C have been gathered in Florida during gusty conditions and are mostly in the z-direction certainly due to convective activities. Bumps D and E have been recorded in the Appalachian Mountains region where most of the gusts encountered were in the y-direction. There were strong surface winds over rough terrain. Maneuver A consists of push-pull and rolls whereas Maneuver B consists of left/right side-slip, rolls and stabilized g-turns.

Those values of stress and strains were very consistent with the type of gust encountered. Moreover, a thorough comparison between the loads induced by the maneuvers on the horizontal tail and the one induced by gust shows that the ratio between both ranged between 0.47 and 0.63 for the maximum values and between 0.45 and 0.52 for the minimum values. In other words, the airplane was subjected to more stress during maneuvers than when it encountered gusts during these flights.

6.2 CURRENT RESEARCH RESULTS

6.2.1 NEURAL NETWORKS TRAINED AND TESTED WITH THE PSD DATA

6.2.1.a *NN First Attempt: EDBD Rule and 5 PE*

A NN was developed for each horizontal and vertical tail. The first attempt (consisting of using the EDBD rule) was nearly as expected and confirmed de Poitevin's results. The correlation remained low and the RMS error high. Both networks revealed poor results. Neither horizontal or vertical tails were satisfactory. However, accounting that the gust's amplitude differs between all flights, additional files have been tested through the network, but without any further improvement. It has then been hypothesized that the too low order of magnitude of the data might have been a reason why.

6.2.1.b *NN Second Attempt: Data Rescale*

The data were therefore rescaled. They were multiplied by a corrective factor. A multiplication per one hundred (100) was considered but most of the data would have been greater than 1, which would have lead to the PE's saturation. Consequently, a multiplication factor of ten (10) was then applied. Unfortunately the results were still unsatisfactory because of a too high and constant RMS and a too low correlation coefficient.

6.2.1.c *NN Third Attempt: Convergence Criterion Optimization*

Then the convergence criterion has been changed from 0.001 to 0.0001 in order to see if a longer training phase would allow the decrease of the RMS and the increase of the correlation coefficient. But the RMS error remained around 0.1 even after 50,000 training samples with a still meaningless correlation coefficient.

6.2.1.d NN Fourth Attempt: Change in the Number of PE

The next step consisted of increasing the number of Processing Elements (PE), in the hidden layer, from 5 to 40. The goal was to apply a dichotomy method to find the best number of PE. Still no real improvement was observed.

6.2.1.e NN Fifth Attempt: Change in Learning Rule

Following this failure to predict accurately the strains, a more radical approach was taken. The learning rule was changed from EDBD to the Delta Rule. This learning rule was chosen since it allows the learning coefficient's adjustment, which is difficult with the EDBD rule. This rule permits the minimization of the squares of the difference between the net input to the output units and the target values. Moreover, the local error is reduced more rapidly by adjusting the weights. With this network, the number of PE's was maintained at 40 and the default learning weights were used. A small improvement was observed since the RMS error decreased below 0.01 (which is still too high when the order of magnitude of the data is considered). The correlation slightly increased but stayed below 0.2. One possible reason of this poor prediction could have been the saturation of one or several PE's. However, it was found that no saturation was occurring during the training of the NN (Contrarily to the EDBD rule, the Delta Rule is not influenced by the change of the Epoch number).

6.2.1.f NN Sixth Attempt: Change in Learning Coefficients

The last step of this optimization consisted of changing the learning weights. This modification was performed as suggested in the NeuralWare manual (UN-55). The main idea was to allow the adjustment of the learning weights during the training phase to help the convergence and speed it up. The other purpose of the learning weight adjustment was to avoid local minimums.

This change of the learning weights induced a decrease of the RMS below 0.005 that is acceptable, but the correlation coefficient still remained well below 1.

6.2.2 NEURAL NETWORKS TRAINED AND TESTED WITH THE TIME DATA

The use of the PSD for loads prediction on the empennage still needs to be validated. Previous studies have demonstrated that maneuver loads on the empennage could be predicted using time domain data and this with very good accuracy [10 + 16]. And, since the use of the PSD for loads prediction has not been validated yet, it was thought that the low correlation value was a consequence. Therefore, it has been decided to check the accuracy of the predictions by using time domain data to feed the network. A comparison between PSD results and time domain results would then be possible.

The same technique used in de Poitevin's research was utilized, i.e. filtering the gust data with a band pass filter. The frequency of interest remained unchanged, i.e. the 5 - 15 Hz range.

Neural Networks did not predict better, but the correlation however increased to 0.25.

6.2.3 NEURAL NETWORKS TRAINED WITH THE MANEUVER FILES

As a result of these poor predictions, training the network with a maneuver file was considered. It has indeed been thought that it might improve the correlation. Two different methods were followed.

First, a network was created and trained with the filtered maneuver file's time domain. This idea was based on a time domain study revealing that the maneuver loads' and gust loads' amplitudes were similar. Indeed, the CG NZ time domain graphs showed

that the acceleration data gathered by the accelerometers had nearly the same range of voltage, meaning that the load induced by gust might have been as significant as the one induced by a maneuver. In the meantime, the study of the stress induced by the maneuvers and the gusts (table 2) reinforced that hypothesis, even if the maneuver amplitude is slightly larger than the gust one. In order to run the network, and as stated previously, the EDBD rule was initially used then the Delta-Bar and finally the learning weight coefficient's adjustment. Moreover, different transfer functions were tried in order to improve the network.

The best correlation reached only a low value of 0.31.

Secondly, the PSD has been considered. The PSD of the maneuver data has been computed to permit the training of the network. The same technique used for gust files was used (Macros to setup DADiSP files). The net has therefore been tested with the gust's PSD.

Unfortunately, the correlation did not increase.

CHAPTER 7

CONCLUSION AND RECOMMENDATIONS

7.1 IMPROVEMENT OF THE PREDICTIONS

The results, though not as good as expected, showed a slight improvement compared to Arcaute's and de Poitevin's work. The correlation increased to about 0.31 even if the RMS remained quite constant and high.

7.2 LOW CORRELATION EXPLANATION

Whereas the network was able to predict 93% of the stress induced by a maneuver for the horizontal tail and 100% for the vertical one [16], it seemed incomprehensible that it could not perform the same computation for gust. Though there was a significant presence of gust on the PSD files, i.e. in the 5 - 15 Hz frequency range, it seemed, however, that "gust" was much more pronounced on the CG accelerometers than on the tail accelerometers or even the strain gages. This fact is really explicit on figures 36 and 37. In addition, the PSD of the strain gages appeared to be very "noisy" when analyzed with DADiSP (figure 35). The time domain signals seemed to be filled with noise too. Whenever the strain gage PSD for a maneuver was visualized, the curve trend was clear

and representative of the kind of maneuver. But for a gust, no conclusion could be drawn with certainty.

7.2.1 PSD VS. TIME DOMAIN

One of the objectives of this research was the validation of the use of PSD for gust loads prediction. The feasibility of predicting maneuver loads using time domain data had already been proved. It was thought that the use of the PSD as inputs for the network would help in predicting gust loads.

Unfortunately, it did not. Trying to use the PSD might have been too ambitious and could have been the reason of such poor predictions, even if the cause was unknown. Unfortunately, networks fed with time domain data did not improve the correlation nor decrease the RMS error. The presence and the magnitude of gust were then questioned.

Moreover, an important fact was that the maneuver's PSD revealed some peaks on all of the y-direction. A sharp shape can be distinguished between 11 and 17 Hz, whereas no gusty conditions were encountered during the record of these maneuvers. Of course a gust is a very sudden and unpredictable phenomena with a very short lifetime. But even if its intensity fluctuates, its frequency range should remain quite constant. That is why the PSD was used, to make sure that the magnitude was significant enough. But those results were inconsistent with the previous hypothesis that gust was located between 5 and 15 Hz. The period at which those maneuvers were experienced did not imply turbulence at all.

7.2.2 FLISEG DISCRIMINATION

In the meantime, Fliseg did confirm the fact that gust was present. Based on previous theories and research, a correlation should have consequently been found. But nothing significant happened.

Fliseg discriminated the flight between maneuver and gust, with a threshold value of 2 Hz. If the threshold was changed to 10 or even 25 Hz, Fliseg found some 'gust'. But it was not sufficient enough to be correctly predicted by the network. Perhaps its magnitude was not big enough. Referring to table 2 (Maximum and Minimum Stress in μg for different flight conditions), it can be noticed that the maneuver induced load is much more significant than the gust induced one. As strange as it may appear, this means that the airplane was much more subject to stress while performing maneuvers such as side-slip, rolls and stabilized g-turns than while encountering gust.

Actually, the method used in Fliseg for gust discrimination was based on the modified FAA two-second rule. This counting method was developed for wing loading based on normal acceleration and should be applicable to any airplane. However, it appeared that the C172 airplane damped the oscillations at the empennage, meaning that if a gust was encountered at the C.G., the acceleration was damped by the structure and/or aircraft rigid body rotation and nothing significant was observed at the tail. A bigger airplane should be used for this kind of research to confirm that hypothesis (such as a T-Tail).

7.3 RECOMMENDATIONS

This research did not lead to the anticipated results of predicting the load induced by a gust, but the findings opened even more questions as to the structural (empennage) response of the airplane in turbulence.

The minimum sets of instruments to be used may however be defined, even though the accuracy of the predictions was less than expected. Indeed, it appeared that the tail accelerometers were fully needed for the prediction of the loads induced by a gust. If its signal was suppressed from the network's inputs, the correlation decreased significantly. The angular accelerometers can therefore be suppressed and the derivative values of the rate gyroscopes be used.

Another consideration is that gust might not have been acquired in sufficient quantity. The gust conditions might have been too "smooth". More thorough flight-testing must be accomplished in much more gusty conditions to validate this hypothesis, but Embry-Riddle flight operations guidelines make this practically impossible.

The strain gage channels should be examined more carefully to see if they can be isolated better to reduce noise that might negatively affect NN predictions. Moreover, the airplane's installation is quite old now and the accuracy of those strain gages should be confirmed. The option of using the PSD is still unanswered and needs to be validated. However, even though the predictions were unsatisfactory, the slight improvement of the correlation still leaves some hope of predicting the stress induced by a gust on the aircraft's empennage.

REFERENCES

1. Anonymous, "Fatigue Evaluation of Wing and Associated Structure on Small Airplanes", Report No. AFS-120-73-2, Federal Aviation Administration, Washington, D.C., 1973.
2. Anonymous, "Fatigue Evaluation of Empennage, Forward Wing, and Winglets/Tip Fins on Part 23 Airplanes", Report No. ACE-100-01, Federal Aviation Administration, Kansas City, MO, 1974.
3. De Jonge, J.B., van de Wekken, A.J.P. and Noback, R., "Acquisition of Gust Statistics from AIDS-Recorded Data", AGARD Report 734, 1987.
4. J.W. Jewel Jr., "Tabulation of Recorded Gust and Maneuver Accelerations and Derived Gust Velocities for Airplanes in the NASA VGH General Aviation Program", NASA TM 84660, Langley Research Center, Hampton, Virginia, September 1983.
5. Locke, J.E., and Smith, Howard, W., FRL, Edward, A., Gabriel, ACE-111, and Thomas, Le Flore, ACD-220, "General Aviation Aircraft-Normal Acceleration Data Analysis and Collection Project", University of Kansas Flight Research Laboratory, February 1993.
6. De Jonge, J.B., Hol, P.A., and van Gelder, P.A., "Re-Analysis of European Flight Load Data", NLR TP 93535 L.
7. De Jonge, J.B., "12th Plantema Memorial Lecture Assessment of Service Load Experience", NLR TP 89097 L, 1989.

8. van Gelder, P.A., "In-Flight Tailload Measurements", Proceedings of the 18th ICAS Congress, pp. 1058-1066, 1992.
9. Noback, R., "Definition of P.S.D.–Design Loads for Non-Linear Aircraft", NLR TP 89016 U.
10. Marciniak, M., "A Methodology for the Prediction of the Empennage In-Flight Loads of a General Aviation Aircraft Using Back propagation Neural Networks", Thesis, Embry-Riddle Aeronautical University, FL, Fall 1996.
11. Hoffman, M.E., "Neural Network Prototype for Individual Aircraft Tracking", NAWCADWAR, Warminster, PA 18974-0591, 1993.
12. Haas, D.J., Milano, J., and Flitter, L., "Prediction of Helicopter Component Load Using Neural Networks", AIAA-93-1301-CP, Department of the Navy, Bethesda, Maryland, 1993.
13. Cook, A.B., Fuller, C.R., O'Brien, W.F., Cabell, R.H., "Artificial Neural Networks for Predicting Non-Linear Dynamic Helicopter Loads", AIAA Journal, Vol. 32, No. 5, May 1994.
14. Frederic M. Hoblit, "Gust Loads on Aircrafts: Concepts and Applications", AIAA Education Series, 1998.
15. Pidaparti, R.M.V., and Palakal, M., "Fatigue Crack Growth Prediction for Spectrum Loadings Using Neural Networks", AIAA-93-1609-CP, Purdue University, Indianapolis, 1993.
16. Pechaud, L., "Improvement of a Methodology for the Prediction of the Empennage Maneuver In-Flight Loads of a General Aviation Aircraft Using Neural Networks", Thesis, Embry-Riddle Aeronautical University, FL, Fall 1997.

17. NeuralWare, Inc. Technical Publications Group, "A Technology Handbook for Professional II+ and NeuralWorks Explorer", pp.235-237, 1995.
18. Gabriel, E.A., et. al., "General Aviation Aircraft - Normal Acceleration Data Analysis and Collection Project, Final Report", Report No. DOT/FAA/CT-91/20, Department of Transportation, Federal Aviation Administration, Washington, D.C., 1993.
19. ASTM Standards – Designation E 1049-85: "Standard Practices for Cycle Counting in Fatigue Analysis"
20. Kim, D. "General Aviation Aircraft Empennage Flight Loads", SAE, 1999.
21. de Poitevin, V., Unpublished notes.
22. Anonymous, "Daqbook/Daqboard User's Manual", Part #232-0920, Revision 3.2, Iotech, Inc., Ohio, March 1995.
23. Arcaute, N., Unpublished Notes.
24. Tom DeFiore and Terence Barnes, "The FAA Regional/Commuter Aircraft Flight Loads Data Collection Program", SAE,1993.
25. Patrick, H.V.L., Marchand, P., Louvel, B., Villoteau, I., "General Aviation Piston Engine Noise Test Facility", ERAU, 2000.
26. Patrick, H.V.L., Lobo, K.W., Tada, H., "General Aviation Engine Noise Measurement Experiment", ERAU, Spring 2000.

27. ASTM Standards-Designation E 1049-8, "Standard Practices for Cycle Counting in Fatigue Analysis".
28. U.S. Government, Military Handbook. MIL-HDBK-5D, "Metallic Materials and Elements for Flight Vehicle Structures", Washington D.C., 1986.